



**SYNTHESIS AND APPLICATION OF GRAPHENE NANORIBBON DECORATED
WITH TiO₂ TOWARDS THE SIMULTANEOUS DETECTION OF NEVIRAPINE AND
GLUCOSE**

BY

DANIEL APATH

R158049E

**Submitted in partial fulfillment of the requirements for the degree of Bachelor of Science
Honours in Chemical Technology Department of Chemical Technology in the Faculty of
Science and Technology at the Midlands State University**

Supervisors: Prof. M. Moyo

Dr M. Shumba

May 2019

DEDICATION

This research is dedicated to my parents who laid the foundation of my destiny and the government of South Sudan who stood by me against all odds during the course of this degree.

ACKNOWLEDGEMENTS

Praise be unto the lord Jesus Christ. My profound gratitude goes to my supervisor Prof M. Moyo and Dr M. Shumba who provided me with invaluable advice and insight throughout my studies. Sincere gratitude also goes to my parents and work-related learning mentors, Mr. Mambanda and Mrs. Mambanda for the endless support. Special thanks to all my classmates for their endless support. Finally, but as importantly I would like to thank the MSU department of chemical technology laboratory staff for their contributions in making this research possible.

ABSTRACT

Graphene nanoribbons (GNRs), titanium dioxide (TiO₂), and their composites Graphene nanoribbons/titanium dioxide (GNRs/TiO₂) were employed towards the simultaneous detection of nevirapine (NVP) and glucose (GLC). The nanomaterials were characterized Fourier-transform infrared spectroscopy (FTIR), UV-vis and thermogravimetric analysis (TGA), cyclic voltammetry, electrochemical impedance spectroscopy, linear sweep voltammetry, differential pulse voltammetry, and chronoamperometry were utilized in the electrochemical detection of nevirapine and glucose. The optimum pH for the electrocatalytic detection of nevirapine and glucose simultaneously were determined to be pH 11.0 The limits of detection and quantification were deduced to be 1.27×10^{-7} M for glucose and 1.282×10^{-7} M for nevirapine and limit of quantification were also deduced to be 3.882×10^{-7} M for glucose and 3.882×10^{-7} M for nevirapine respectively using differential pulse voltammetry. The rate constant of 1.655×10^1 M⁻¹s⁻¹ and 1.42×10^1 M⁻¹s⁻¹ for nevirapine and glucose respectively. surface area of the electrode and the surface coverage were determined to be 2.7×10^1 M⁻¹ s⁻¹, 0.238 cm² and 1.58×10^{-5} mol cm⁻² respectively. The adsorption equilibrium constant β was determined to be 3.3×10^4 M⁻¹ from the Langmuir adsorption kinetic model with a Gibbs free energy of 25.34 KJ mol⁻¹. GNRs/TiO₂-GCE showed excellent electrooxidation of nevirapine and glucose and oxidation over potential were lowered. The higher surface coverages were observed which indicating that modifiers were lying flat on the electrode surface. The GNRs/TiO₂-GCE gave catalytic rate constants The limits of detection observed for nevirapine and glucose were 9.66×10^{-7} and 7.2×10^{-7} M respectively. The adsorption equilibrium constants for nevirapine and glucose were found to be 1.05×10^5 M⁻¹ and 5.56×10^5 M⁻¹ respectively. Furthermore, the high Tafel slopes were observed which indicated that the adsorption of each analyte to the surface of the electrode. The Gibb's free energy for nevirapine and glucose were also found to be -28.63 kJ mol⁻¹ and -27.07kJ mol⁻¹ respectively. Interference studies were done and the electrode displayed the ability to detect both nevirapine and glucose. The electrode displayed good reproducibility with lower oxidation potential at 0.8 V and high sensitivity towards nevirapine and glucose. The developed sensor exhibited an excellent non-interference property and good reproducibility towards the detection of nevirapine and Glucose.

DECLARATION

I, APATH DANIEL R158049E, hereby declare that I am the sole author of this dissertation. I authorize Midlands State University to lead this dissertation to other institution or individuals for the purpose of scholarly research.

Signature.....

Date.....

APPROVAL

This dissertation entitled “Synthesis and application of graphene nanoribbon decorated with titanium dioxide towards the simultaneous detection of nevirapine and glucose” by APATH DANIEL meets the regulations governing the award of the degree of chemical technology of midlands state university, and is approved for its contribution to knowledge and literal presentation.

Supervisor.....

Date.....

LIST OF ABBREVIATIONS

GNR- Graphene nanoribbon.

TiO₂- Titanium dioxide.

GNR/TiO₂- Graphene nanoribbon/Titanium dioxide.

NEV- Nevirapine.

GLC- Glucose.

FTIR- Fourier Transform Infrared.

TGA- Thermogravimetric analysis.

NEG-Non-enzymatic glucose

GCE- Glassy carbon electrode

DPV- Differential pulse voltammetry.

LSV- Linear sweep voltammetry.

EIS- Electrochemical impedance spectroscopy

LOD- Limit of detection

LOQ- Limit of quantification

TABLE OF CONTENTS

DEDICATION	i
ACKNOWLEDGEMENTS	ii
ABSTRACT	iii
DECLARATION	iv
APPROVAL	v
LIST OF ABBREVIATIONS.....	vi
LIST OF FIGURES	x
LIST OF TABLES	xii
1.0 Introduction.....	1
1.1 Background.....	1
1.2 Aim of the study.....	5
1.3 Objectives	5
1.4 Problem Statement	7
1.5 Justification	8
2.0 Introduction.....	11
2.1 Antiretroviral drugs (ARVs).....	11
2.2 Glucose	13
2.3 Graphene chemistry	14
2.3.1 Graphene Nanoribbons	15
2.3.2 Graphene nanoribbons synthesis.....	16
2.3.3 Electrochemistry of graphene nanoribbons	17
2.5.0 Electrochemistry	19
2.5.1 Voltammetry	20
2.5.2 electrodes	21
2.5.3 Working Electrodes (WE).....	21
2.5.4 Reference Electrode	21
2.5.5 Counter electrode (CE)	22
2.5.6 Mass Transfer in Voltammetry	22
2.5.7 Diffusion	22
2.5.8 Convection	22

2.5.9 Migration.....	23
2.6.0 Cyclic voltammetry.....	23
2.6.1 Linear sweep voltammetry.....	24
2.6.2 Chronoamperometry	25
2.6.3 Electrochemical impedance spectroscopy	26
2.6.4 Bode Plots	26
2.6.5 Fourier Transform Infrared (FTIR).....	27
2.6.6 Summary	28
3.0 Introduction.....	30
3.1 Chemicals and reagents.....	30
3.2 Equipment.....	31
3.4.0 Experimental Section.....	31
3.4.1 Thermal Gravimetric Analyzer	32
3.4.2 Synthesis of graphene nanoribbon.....	32
3.4.3 Synthesis of GNR/TiO ₂ nanocomposite ex-situ hybridization	33
3.4.4 Physical Characterization of composites	33
3.5 Fourier Transfer Infrared Spectroscopy (FT-IR).....	33
3.5.1 Electrode modification.....	34
3.6 Cyclic voltammetry behavior of modifiers in 1 mM [Fe(CN) ₆] ^{-3/-4}	35
3.6.1 Electrochemical Impedance Spectroscopy	35
3.6.2 Standard preparation	36
3.7 Optimisation of parameters.....	36
3.7.1 Effect of pH.....	36
3.7.2 Comparative studies in pH 11.0 phosphate buffer solution (PBS)	37
3.7.3 Individual determination of nevirapine and glucose.....	38
3.7.4 Simultaneous detection of nevirapine and glucose.....	38
3.8 Kinetic studies.....	39
3.8.1 Catalytic rate constant.....	39
3.8.2 Simultaneous detection of nevirapine and glucose by using differential pulse voltammetry.	40
3.8.3 Detection limit for the simultaneous analysis of nevirapine and glucose by using DPV	41

3.9 Stability studies	42
3.10 Reproducibility studies	42
3.11 Applicability	43
3.12 Effect of interference	43
4.0 Introduction.....	44
4.1 Characterization of electrode modifiers.....	44
4.1.1 Fourier Transfer Infrared Spectroscopy (FTIR)	44
4.2.0 Electrochemical characterization	50
4.2.1 Cyclic voltammetry.....	50
4.2.2 Electrochemical impedance spectroscopy (EIS) characterization	52
4.2.3 Surface coverage	57
4.4 Catalytic oxidation of nevirapine and glucose.....	60
4.5 Kinetic analysis for nevirapine and glucose oxidation	63
4.6 Tafel slopes	64
4.8 Gibbs free energy determination.....	67
4.9 Catalytic Rate Constant.....	69
4.11 Limit of detection and quantification for simultaneous of nevirapine and glucose.....	75
4.13 Scan rate.....	78
4.14 Stability Studies	79
4.15 Reproducibility studies	80
4.16 Interference studies	81
4.17.0 Real sample analysis	83
4. 17.1 Determination of nevirapine in urine samples	83
4.17.2 Analysis of NVP in pharmaceutical tablets	85
4.19 Real sample detection for glucose.	89
Table 4.6: Determination of glucose in human urine.	91
CHAPTER FIVE	92
5.0 Introduction.....	92
5.1 Conclusion	92
5.2. Recommendations.....	93

LIST OF FIGURES

Fig 1.1 Chemical structure of glucose.....	2
Fig 1.2 Chemical structure of nevirapine.....	3
Figure 2.1 Different allotropes of graphene nanomaterials	15
Figure 2.2 Gradual unzipping of one wall of a carbon nanotube.....	17
Fig 2.7: A typical cyclic voltammogram for a reversible single electro transfer	24
Figure 4.1 IR spectra for: a) GNR, b) TiO ₂ and C) GNR/TiO ₂	45
Fig 4.3 Nyquist plots obtained for of bare (a) TiO ₂ NPs-GCE (b), GNR-GCE (c) and GNR/ TiO ₂ NPs/GCE (d) in equimolar solution of 1 mM [Fe(CN) ₆] ^{3-/4-} prepared in 1 M of KCl. Scan rate = 100mV/s	53
Fig 4.4: Cyclic voltammograms obtained at bare GCE (a), TiO ₂ NPs/GCE (b), GNR/GCE (c) and GNR/TiO ₂ NPs/GCE (d electrodes in 0.1M PBS (pH 11.0) at a scan rate of 0.1mV/s.....	58
Fig 4.5 Cyclic voltammograms (A) nevirapine and (B) glucose plot of current vs pH and for GNR/ TiO ₂ NPs/GCE (a) pH 2, (b) pH 3, (c) pH 4, (d) pH 5, (e) pH 6, (f) pH 7, (g) pH 8, (h) pH 9, (i) pH 10, (j) pH 11 and (k) pH 12 phosphate buffer solution containing 1 mM nevirapine and glucose at Scan rate = 100 mV/s.....	59
Fig 4.7: Voltammograms of bare (a) TiO ₂ NPs/GCE (b), GNR/GCE (c) and GNR/TiO ₂ NPs /GCE in 1 mM (A) nevirapine and (B) glucose 1 mM in a 0.1 M PBS (pH 11.0) at a scan rate of 0.1 mV/s.....	62
Fig 4.8 (A) nevirapine and (B) glucose: effect of scan rate on peak potentials and currents (50 mV/s to 400 mV/s), plot of I _{pa} vs \sqrt{v} on GNR/TiO ₂ NPs for nevirapine and glucose oxidation. [Nev/Glc] = 1 Mm. For an electrochemically irreversible electro-reduction process the value of	

Tafel slope (b) can be obtained from the variation of E_{pc} with v in voltammetric data through equation:.....	64
Fig 4.9: Plot of potential versus log scan rate in 1 mM nevirapine and glucose	65
Fig 4.10: Impedimetric response obtained at GNR/TiO ₂ in presence of various nevirapine (A) and glucose (B) concentrations i.e. from 0.2 μ M (a) 1 μ M (e) in 0.1M PBS pH 11.....	66
Fig 4.11 Linear sweep voltammograms.....	68
Fig 4.12 Chronoamperograms for different nevirapine (A) and glucose (B) concentrations in PBS pH 11 (a), 0.1 μ M (b), 0.2 μ M (c), 0.3 μ M (d), 0.4 μ M (e), 0.5 μ M (f), 0.6 μ M (g) and 0.7 μ M (h). Inset I_{pc} vs [Nev] and [Glc].....	70
Fig 4.16 Plot of slopes vs. $\sqrt{[\text{nevirapine}] \& [\text{glucose}]}$	71
Figure 4.17 DPV (A) nevirapine and (B) glucose for GNR/TiO ₂ /GCE in: a) 0.2 μ M, b) 0.4 μ M, c) 0.6 μ M, d) 0.8 μ M, e) 1 μ M, f) 1.2 μ M, g) 1.4 μ M. Inset: Plot of I_{pc} vs [Nev] and [Glc].....	73
Fig. 4.18 DPV voltammograms of: a) 0.2 μ M, b) 0.4 μ M, c) 0.6 μ M, d) 0.8 μ M, e) 1 μ M, f) 1.2 μ M, g) 1.4 μ M nevirapine in the presence of 0.2 μ M glucose (A) and DPV voltammograms of: a) 0.2 μ M, b) 0.4 μ M, c) 0.6 μ M, d) 0.8 μ M, e) 1 μ M, f) 1.2 μ M, g) 1.4 μ M nevirapine in the presence of 0.2 μ M glucose (B). Inserts: the calibration graphs of nevirapine and glucose.	76
Fig 4.19: Cyclic voltammograms of the detection of 0.1 mM nevirapine (A) and glucose (B) obtained after 20 continuous cycles scan rate = 100 mV/s. pH 11 PBS.....	80
Fig 4.20: Cyclic Voltammograms of the detection of 0.1 mM nevirapine (A) and glucose (B) obtained after 5 test runs scan rate = 100 mV/s in 0.1mM pH 11 PBS.	81

LIST OF TABLES

Table 3.2.0 Parameters in cyclic voltammetry.....	35
Table 3.2.1 Parameters for electrochemical impedance and bode plots	36
Table 3.2.2 Parameters for pH studies in 1 mM nevirapine and 1mM glucose.....	37
Table 3.2.3 Parameters used for comparative studies in pH studies in 1 mM nevirapine and 1 mM glucose.	38
Table 3.8 The Parameters used for the study of DPV.....	41
Table 3.9.0 The Parameters used for the study of DPV.....	42
Table 4.1 Electrochemical parameters for the Modified electrodes	52

CHAPTER ONE

1.0 Introduction

The present chapter serves to highlight the background of the research and the techniques used for the simultaneous sensing of nevirapine and glucose. The aim/s, objectives, problem statement and justification on the components such as GNR, TiO₂ and GNR/TiO₂ of the study are also presented.

1.1 Background

Diabetes, a global health problem affecting over 200 million people, can cause disorders of the kidney, heart, neural system and retina [1] and based on current projections, diabetes will be the 7th leading cause of death as of 2030 [1]. Development of glucose sensor is of great importance in a many fields including clinical diagnostics, biotechnology, environmental monitoring, pharmaceutical analysis and food industries [1,2]. Hence, the monitoring of blood glucose levels is essential to prevent diabetic complications such as diabetes from becoming more prevalent in modern society [1]. Conventional glucose sensors use glucose oxidase immobilized on a solid electrode, to catalyze the oxidation of glucose in the presence of oxygen to produce hydrogen peroxide and selectively monitor the glucose levels [2]. Most of the electrochemical detection of glucose is based on the enzymatic reaction [3]. However, the serious drawback is the instability of the enzyme activity, due to factors such as temperature, pH, toxic chemicals and oxygen, restricts the use of enzyme-based biosensor [4]. Besides, long-term monitoring of the blood glucose levels using an enzyme-based electrode is typically hampered by surface fouling by the absorption/passivation of the products. The surface fouling inevitably limits the selectivity and

sensitivity towards glucose oxidation over time [5]. As a result, development of non-enzymatic glucose (NEG) sensors is becoming essential [6].

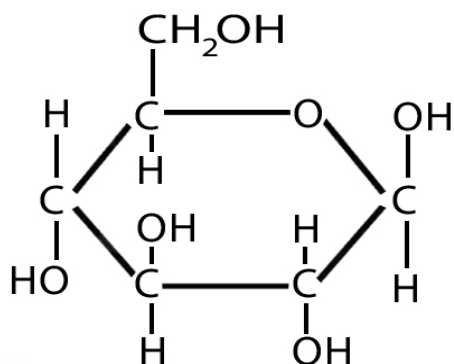


Fig 1.1: Chemical Structure of Glucose [7].

Antiretroviral drugs are used for the treatment of infections by retroviruses, primarily human immunodeficiency viruses (HIV) that can lead to acquired immunodeficiency syndrome (AIDS) [8]. Nevirapine is one of the three classes of drugs currently used to treat human immunodeficiency virus (HIV) infection which inhibits non-competitively the human immunodeficiency virus type-1 (HIV-1) reverse transcriptase (RT) [9]. The resulted NNRTIs bind either directly or reversibly to the catalytic site of the reverse transcriptase enzyme and interfere with viral RNA to DNA-directed polymerase activities [10]. It should be noticed that nevirapine does not inhibit HIV-2 reverse transcriptase [11].

Mechanism of action

It is proposed that the secondary ring nitrogen of nevirapine undergoes a single electron oxidation to yield a radical cation, which is further deprotonated to form a radical. Then, the free radical readily combines with another radical to form a dimerized product. This scheme is also in agreement with an earlier report [14].

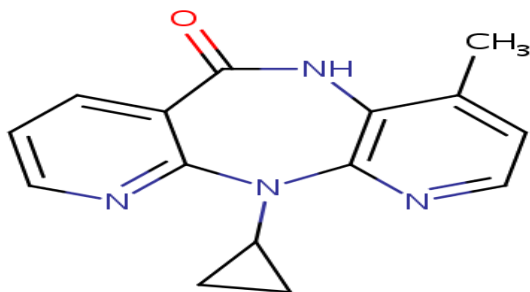


Fig 1.2: Chemical structure of nevirapine [11]

Most of the drugs are usually ingested after taking food. Most food staff contain high content of glucose so there is a need to regulate the amount of glucose during taking medical treatment in order to prevent diabetic complications [15]. Several techniques such as high-performance liquid chromatographic (HPLC) [16], matrix-assisted laser desorption/ionization time-of-flight mass spectrometry (MALDI-TOF/TOF) [17], micellar electro kinetic chromatographic (MEKC) [18],

liquid chromatography [19], capillary electrophoresis [20], high performance thin layer chromatography (HPTLC) [21], high-performance liquid chromatography–ultraviolet–visible spectroscopy (HPLC–UV) [22] have been published for the detection of nevirapine and glucose.

In spite of the great success of the above-mentioned methods, their high costs, time-consuming and complicated operations limit their applications in routine laboratories [22]. Recently,

electrochemical techniques appear as a simple, sensitive, inexpensive, accurate and fast alternative for the determination of pharmaceutical compounds compared with other methods.

Accompanied by the development of sensing technology, electrochemical sensors play an important role because of their simple, fast, low cost and high sensitive properties [22]. Due to low electron transfer kinetic and high over-potential along with oxidation of organic compounds

such as drugs at the bare solid electrodes, their modification has extended field research in

analytical chemistry.

Modification of the electrode surface has opened a wide window for the development of innovative electrodes for fundamental electrochemical investigations and electroanalytical applications. Electrode modification provides high selectivity, improved sensitivity and stability of the electrode response, which could not be achieved using bare electrodes. Electrochemical methods offer high selectivity and sensitivity, simplicity in sample preparation and low-cost instrumentation [23]. Nowadays, many modified electrodes with carbon materials are developed as electrochemical sensors for determination of nevirapine and glucose solutions [24]. Carbon nanomaterials especially graphene nanoribbon due to their unique physical and chemical properties are good candidates for electro analytical applications, particularly in the design of modified electrodes [15]. The selection of graphene nanoribbon as a functional nanomaterial for the detection of nevirapine is because of its good electronic conductivity [23], abundant amount of chemical oxygen groups [24] and simple preparation procedure. The active chemical oxygen groups, mainly composed of unsaturated carbonyl groups on the edge of graphene nanoribbon is good candidates for the selective and sensitive detection of nevirapine [25]. Graphene nanoribbons in comparison with carbon nanotubes, they have reactive edges which can increase the adsorption and electrocatalysis of certain molecules which are used as a promising electrode material [26, 27]. Titanium dioxide nanoparticles present high electro active superficial area and can promote the electro catalysis [28]. Titanium dioxide (TiO_2) film electrodes have been extensively used for electro analysis as alternatives to mercury electrodes since Titanium dioxide (TiO_2) is considered to be a safe material, ecofriendly, less toxic than mercury and non-carcinogenic element [5]. Titanium dioxide (TiO_2) nanoparticles have excellent chemical and physical properties, they have been used in the sensor preparation [28], solar cell [29] and photo catalyst applications [30]. These

nanoparticles have been incorporated with other compounds, such as graphite and carbon nanotubes, to make modified electrodes in the electrochemical analysis of some biological compounds [31] because they provide more active sites at the surface of the electrode. Titanium dioxide (TiO₂) nanoparticles can be used in wide potential windows and improve the stability of the electrode, therefore increase the repeatability of the electrode response [32]. Glassy carbon electrodes (GCE) are used as analytical tools in electro analysis, due to their advantages of broad operating potential window, low background current, easy possibility of surface modification, good mechanical and electrical properties and chemical inertness [33]. To the best our knowledge, Electrode modification provides high selectivity, improved sensitivity and stability of the electrode response, which could not be achieved using bare electrodes. Therefore, glassy carbon electrode modified with graphene nanoribbons decorated with titanium dioxide has not been reported so far. Therefore, it is very important to develop a simple, fast, sensitive and accurate method for the detection of nevirapine and glucose in food, pharmaceutical products and biological samples [25].

1.2 Aim of the study

Assess the efficiency of modified glassy carbon electrode on the electrochemical detection of nevirapine and glucose.

1.3 Objectives

- to synthesize graphene nanoribbon (GNR) and graphene nanoribbon decorated with titanium dioxide nanoparticles (GNR/TiO₂).
- to characterize the graphene nanoribbon (GNR), titanium dioxide (TiO₂) and graphene nanoribbon decorated with titanium dioxide nanoparticles (GNR/TiO₂) using (FTIR, UV-vis and TGA).

- to modify the bare glassy electrode separately with graphene nanoribbon (GNR), titanium dioxide (TiO₂) and graphene nanoribbon decorated with titanium dioxide nanoparticles (GNR/TiO₂) using the drop and dry method and characterization with cyclic voltammetry, electrochemical impedance spectroscopy and bode plot.
- to study the effect of pH, scan rate, effect of supporting electrolyte on peak currents and peak potentials on GNR/TiO₂/GCE in the electrochemical detection 1 μM of nevirapine and glucose.
- to perform comparative studies on modified electrodes ((i) Bare/GCE, (ii) GNR/GCE, (iii) TiO₂/GCE and (iv) GNR/TiO₂/GCE) on the analysis of μM nevirapine and glucose in optimized buffer solution.
- to study the effect of different supporting electrolytes on the simultaneous electrocatalytic detection of nevirapine and glucose.
- to determine the effective surface coverage of TiO₂/GCE, GNR/GCE and GNR/TiO₂ electrode by performing studies in buffer solution containing nevirapine and glucose.
- to determine the electrode, transfer kinetics, tafel slopes, Langmuir adsorption isotherm and catalytic rate constants by electrochemical impedance spectroscopy, cyclic voltammetry and chronoamperometry.
- to determine the limit of detection of nevirapine and glucose in buffer solution by using DPV.
- to perform simultaneous detection on the analysis of 1 μM nevirapine and glucose in optimized buffer solution by using cyclic voltammetry.

- to perform repeatability, reproducibility and stability studies of the developed electrode towards oxidation of nevirapine and glucose in buffer solution.
- to study the effect of interferences and applicability in the presence of nevirapine and glucose on the modified glassy carbon electrode.

1.4 Problem Statement

The rapid increase in death associated with HIV is increasing enormously resulting in the development of new antiretroviral drugs [33]. These drugs need to be monitored in order to prevent excess consumption which might result in affecting the healthiness of the body. Diabetes has now become a prevalent disease due to the consumption of food products containing high glucose content. So consumption of high sugar content foods can cause disorders of the kidney, heart, neural system and retina [4]. Hence, the monitoring of blood glucose levels during drug ingestion is essential to prevent diabetic complications such as diabetes from becoming more prevalent in modern society [2]. Glucose content must be monitored in food during consumption of drugs. Several analytical methods have been reported for determination of nevirapine including reversed phase high-performance liquid chromatography (RP-HPLC) [21], high performance liquid chromatography (HPLC) [16], high performance thin-layer liquid chromatography (HPTLC) [15], micellar electrokinetic chromatography (MEKC) [18], liquid chromatography [19, 20], MALDI/ionization time-of-flight mass spectrometry [17], capillary electrophoresis [20]. These methods, however are very complex, requiring extensive sample preparation and skilled operators, are expensive and are not designed to give rapid analysis and real time measurements. In this regard electrochemical methods appear as a cost effective, simple and fast alternative to the above, mostly expensive, methods.

Electrochemical determinations of nevirapine were almost based on adsorptive stripping voltammetry on thin-film mercury electrode [22]. However the utilization of the mercury would contaminate the environment because of their environmental toxicity, Therefore, it was highly advisable to establish nontoxic and selective electrochemical methods for the determination of nevirapine [27]. Besides, long-term monitoring of the blood glucose levels using an enzyme-based electrode was typically hampered by surface fouling by the absorption/passivation of the products [3]. The surface fouling inevitably limits the selectivity and sensitivity towards glucose oxidation over time. As a result, development of non-enzymatic glucose (NEG) sensors is becoming essential.

1.5 Justification

Several analytical methods have been reported for determination of nevirapine and glucose but no reports has been documented on the electrochemical detection of nevirapine and glucose simultaneously. These was important, especially in African countries where the majority of antiretroviral and diabetic treated adults' rates in these population are high [26]. This challenge has motivated the integration of chemical sensors and natural resources in designing monitoring techniques. Hence, the aim of the present work was to develop a simple, sensitive and accurate method for the detection of nevirapine and glucose since it was more sensitive compared to reported methods [17, 35]. These was carried out for detection of nevirapine on modified electrodes at buffer solution containing (pH11) [22] and non-enzymatic sensors have been applied towards the detection of glucose at alkaline conditions (pH 11) [9]. Hence according to these information nevirapine and glucose can be detected in the same matrix at the same pH as both nevirapine and glucose which produce two distinct peaks at different potentials. Additionally, detection can be performed through analyst's oxidation: allowing for application of a greater range

of chemical systems. Further, electrochemical methods can be performed to monitor changes in current (amperometric), voltage (voltammetric), or impedance (electrochemical impedance) [33]. To overcome these problems, there was an urgent need for rapid, simple, sensitive and cost effective method techniques for the simultaneous detection of nevirapine and glucose. Electrochemical techniques are sensitive techniques that are able to detect minute concentrations [17]. Electrochemistry involves the surface modification of glassy carbon electrode with sensitive materials in order to increase the sensitivity of the sensor towards the detection of analytes in sample matrix [20]. Hence these research based on the simultaneous electrochemical detection of nevirapine and glucose by using glassy carbon electrode modified with graphene nanoribbon decorated with titanium dioxide nanoparticles. Graphene nanoribbon (GNR), a strip of graphene with a high length-to-width ratio, was a potential material owing to their high flexibility, large surface area, outstanding electrical conductivity with extended electrochemical stability and high optical transmittance [22]. The graphene nanoribbon incorporates functional groups, such as carboxylic which are easily blended with other functional materials to improve their dispensability and process ability. In the preparation of the nanocomposites, the functional groups on the graphene nanoribbon surfaces are also helpful for nucleation and formation of metal oxide nanoparticles [35]. The integration of graphene nanoribbon (GNR) and TiO_2 nanoparticles may increase the electrochemically active surface area and electronic transmission speed, resulting in current magnification and sensitivity improvement. Large surface area was an essential characteristics of an electrode material, particularly in sensing devices and energy production and storage [36]. The high surface area of graphene nanoribbon can give rise to fast electron transfer and high densities of attached molecules. These in turn can facilitate high sensitivity and device miniaturization. However, to the best of our knowledge, graphene nanoribbon decorated with TiO_2

has not been studied as sensing material and its application as an electro catalyst for electrochemical sensing of nevirapine and glucose has not been explored. Hence decoration of (GNR) with (TiO₂) nanoparticles may improve electrochemical properties of the hybrid material due to the synergistic effects of both (GNR) and (TiO₂) hence facilitating the electron transfer properties of the composite towards the simultaneous detection of nevirapine and glucose.

CHAPTER TWO

LITERATURE REVIEW

2.0 Introduction

The present chapter gives an outline of graphene nanoribbons, titanium nanoparticles and the theory of electrochemistry techniques used in these study.

2.1 Antiretroviral drugs (ARVs)

The HIV reverse transcriptase is an important antiviral target for the chemotherapy of AIDS because of its key role in virus replication [36]. The most significant advancement in the medical management of HIV-1 infection has been the treatment of patients with antiviral drugs i.e., medicines that stop or slow virus actions [37], by suppressing HIV-1 replication to undetectable levels [38]. The conventional approach to the control of viral diseases is to develop effective vaccines, but this is not always feasible. Because of their mode of replication, viruses present a larger therapeutic challenge than bacteria [39]. Because of the genetic flexibility of viruses, new strains constantly emerge, the most well-known example being human immunodeficiency virus (HIV), the causative agent of AIDS [40].

2.1.1 Classification of Antiviral Drugs

Antiviral drugs are classified into two main groups namely antiretroviral (ARVs) drugs and general antiviral drugs (Non-antiretroviral drugs) [41]. Currently, one-half of all antiviral agents are antiretroviral. Presently, four classes of antiretroviral drugs are available viz., (i) nucleoside/tide reverse transcriptase (NRTI) inhibitors, (ii) non-nucleoside (NNRTI) inhibitors, (iii) protease (PI) inhibitors and (iv) fusion inhibitors [42]. Nevirapine (NVP), (11-cyclopropyl-4-methyl-5, 11-

dihydro-6H- dipyrido [3,2-b:2',3'-e][1,4]diazepin-6-one) is a NNRTI with activity against human immunodeficiency virus type 1 (HIV-1) [43].

2.1.2 Nevirapine

Nevirapine was discovered by [10] pharmaceuticals group of companies. It has a chemical formula of (C₁₅H₁₄N₄O) and molar mass of 266.298 g/mol. The common side effects include rash, nausea, feeling tired, headache, and liver problems [8]. Currently, nevirapine (NVP) is one of the most prescribed antiretroviral drugs in the developing world, both as a single drug to prevent mother-to-child HIV transmission and as a component of currently recommended combined antiretroviral therapy (CART) [44]. The high efficacy levels of the drug, favorable lipid profile, and suitability for use during pregnancy have since granted nevirapine-based regimens a significant role in HIV-1 treatment strategies [45]. Nevirapine is recommended for treating HIV infections in combination with other reverse transcriptase inhibitors such as stavudine and lamivudine [43-46]. The resulted NNRTIs bind either directly or reversibly to the catalytic site of the reverse transcriptase enzyme and interfere with viral RNA to DNA-directed polymerase activities [47]. It should be noticed that nevirapine does not inhibit HIV-2 reverse transcriptase [48].

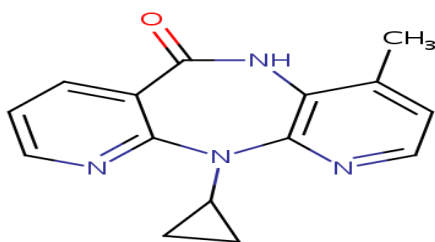


Fig 2.1: Structure of Nevirapine [49].

2.1.3 Detection methods for Nevirapine

Electrochemical methods have proven to be sensitive and reliable for the determination of numerous electroactive compounds [50]. Under some circumstances, electrochemical methods can offer optimal solutions for drug analysis [50]. Simplicity, low cost and relatively short analysis times make electrochemical techniques more useful for routine analytical applications thus provides best alternative approach in this case [51]. Lately applications of modified electrodes for the determinations of drug molecules has attracted more attention because the modifiers could greatly enhance the responds and selectivity for analysts [52].

2.2 Glucose

Diabetes is a rapidly growing problem; the number of people with diabetes increased from 153 million in 1980, to 347 million in 2008 [53]. In 2004, an estimated 3.4 million people died as a result of the consequences of high blood sugar. This number is estimated to double by 2030 [54]. Diabetes may lead to serious complications such as lower limb amputations, blindness, as well as cardiovascular and kidney disease. Electrochemical biosensing has been reported [4] that describes potentiometric measurement coupled with enzyme glucose oxidase to determine glucose in blood plasma. The successful of enzyme-coupled electrochemical sensors is due to the excellent selectivity that enzymes have for analysis of biomolecules of interest, as well as the simplicity and sensitivity of the electrochemical measurement [1]. Electrochemical sensors are attractive due to their low-cost, relatively fast time-response, their operational simplicity, and the robust nature of electrochemical measurements [22]. In electrochemical biosensor, an electrode serves as the signal transducer, where the measureable response is either an electrical current due to a redox reaction (with an amperometric sensor), or to change in electrode potential (with a potentiometric sensor).

2.3 Graphene chemistry

Graphene has been given nicknames such as “super carbon”¹ or “the material of the 21st century”, all for its intrinsic high electrical and thermal conductivity, excellent mechanical strength and flexibility, large surface area, and exceptional catalytic properties [55]. It consists of a single atomic layer of sp^2 hybridized carbon atoms that result in a hexagonal lattice. Around each carbon atom, three strong σ bonds are established with the other three surrounding carbon atoms. Graphene can have different morphologies exhibiting different dimensionalities, which some of them discovered so far and some other possibilities still to be found [56]. For instance, graphite is a 3-D allotrope, graphene nan sheets are 2-D, single/multi-walled carbon nanotubes (SWCNTs, MWCNTs) and graphene nanoribbons (GNRs) are 1-D, and graphene quantum dots (GQDs) are 0-D allotropes (Fig 2.3) [57]. Graphite is an infinite 3-D crystal made of stacked layers of graphene that interact weakly through van der Waals forces. Graphite crystals can be found naturally, and can also be artificially synthesized by thermolytic processes; such as the production of highly oriented pyrolytic graphite. Graphene nanosheets are infinite 2-D layer of sp^2 hybridized carbon atoms that could essentially be considered as the building blocks of 3-D graphite, rolled to form 1-D SWCNTs or MWCNTs, and cut into narrow elongated stripes or minute fragments to produce nanoribbons and quantum dots, respectively [4].

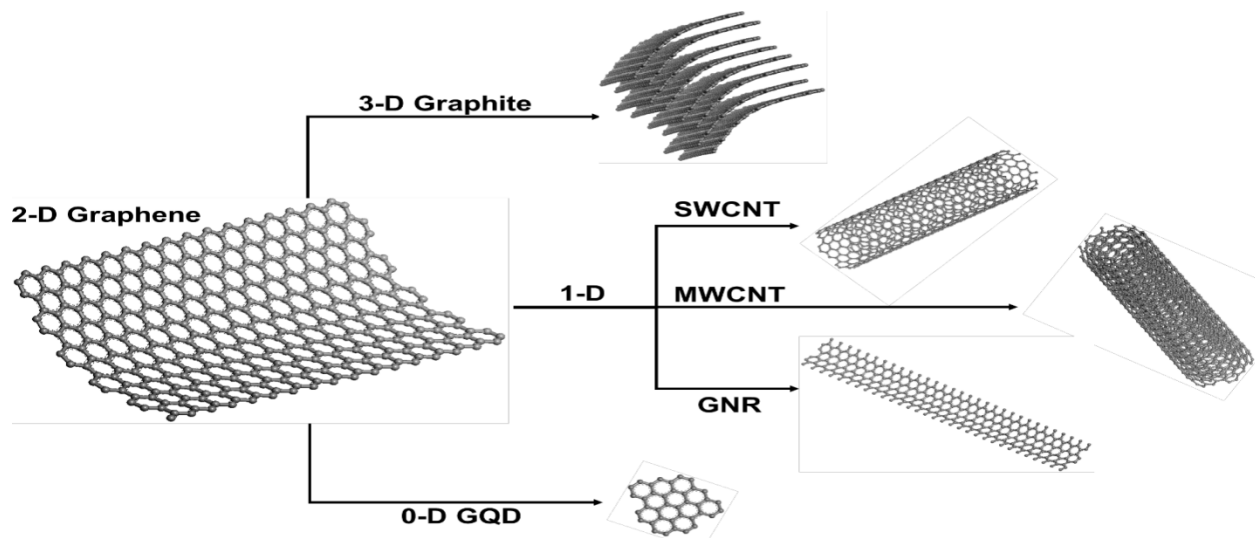


Figure 2.2: Different allotropes of graphene nanomaterials [4].

Graphene, two-dimensional allotrope of carbon and one layer of graphite, has been a target of theoretical studies for more than 60 years [14-18]. However, the feasibility of free-standing graphene was doubted until the unexpected preparation of stable single- to few- layer graphene [58]. This method is called hummers methods which is currently most method used for preparation of graphite oxide [59].

2.3.1 Graphene Nanoribbons

Graphene nanoribbons thin, elongated strips of graphene that possess abundant edges, graphene nanoribbon (GNRs), change from semiconductors to semimetals as their width is increased; hence they represent a particularly versatile variety of graphene [60]. Owing to the high available surface area, high mechanical strength and electrical conductivity of (GNRs), and the scalability of the synthesis, they have been investigated for the fabrication of composites [61] and for use in batteries,7 supercapacitors8 and fuel cells [61].

2.3.2 Graphene nanoribbons synthesis

GNRs can be made using bottom-up approaches, including examples of surface-mediated planarizations of polyphenylene precursors to give GNRs with incredible structural precision [62]. Another attractive route to (GNRs) would be to prepare them using conjugated polymers, such as polythiophenes or poly(para-phenylene)s, beginning with small molecule monomers and carrying out a bulk solution-phase synthesis. Indeed, some examples of this approach towards GNRs have been reported previously, but the resulting nanoribbons are relatively short (short (<50 nm), and the generally low solubility of the products has limited both their characterization and ultimate usefulness [61]. The drawback of these methods, however, is that only limited quantities of surface-bound products are produced. On the other hand, there are top-down techniques to produce GNRs including the lithographic patterning of larger graphene sheets or the unzipping of carbon nanotubes [63]. Prior to the reports of unzipping of MWCNTs, typically synthesized in minute yields and with limited width control. Synthesized by unzipping of MWCNTs through chemical oxidation, nanoparticles, electron beam etchings, sodium/potassium intercalation [64].

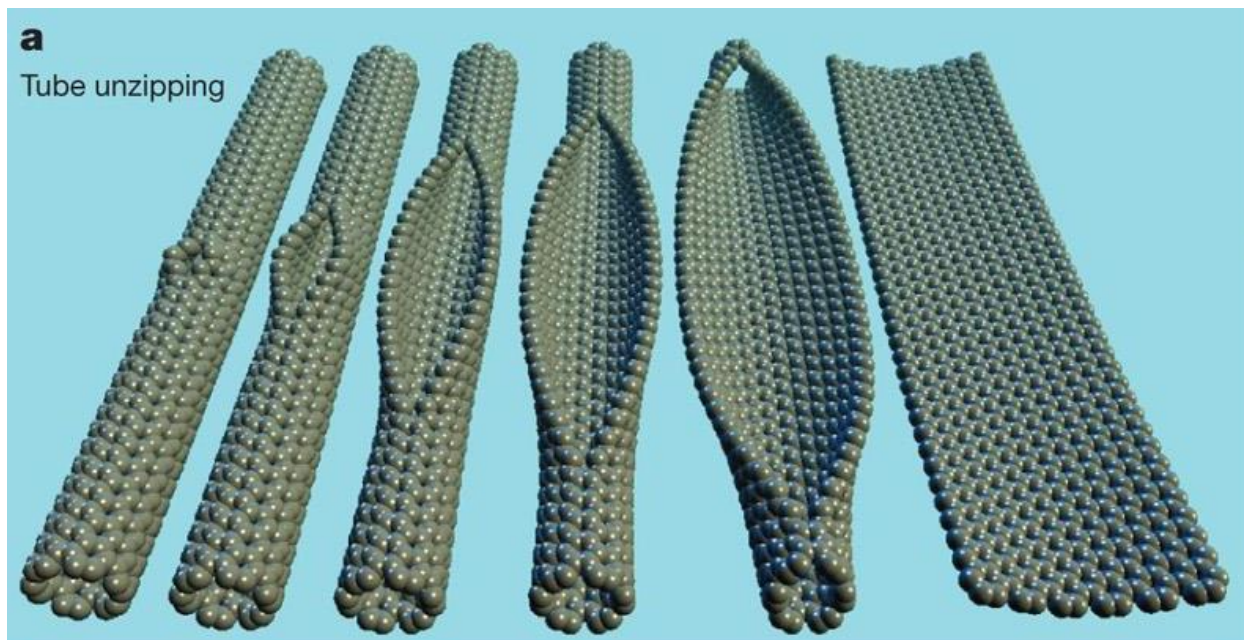


Figure 2.3: Gradual unzipping of one wall of a carbon nanotube to form a nanoribbon [64].

Tour and co-workers synthesized GNRs by lengthwise cutting of MWCNTs by a simple, efficient, and scalable oxidation method. The MWCNTs were suspended in a mixture of concentrated sulfuric acid and a second acid, and treated with potassium permanganate to intercalate the nanotube structure, and ultimately break the C—C bonds. Terrones and coworkers also exploited transition metal nanoparticles as chemical scissors to cut MWCNTs [9]. In the cutting procedure, the nanoparticles serve as catalysts to break H—H and C—C bonds, and as solvents for etched carbon atoms. In addition, applied the technique of current-induced electrical breakdown of MWNTs to produce GNRs. The key is to avoid the typical catastrophic wall blow-out, but instead promote controlled thermally induced unwrapping of the outer walls of the nanotube. Another route to more highly conductive GNRs was proposed by splitting pristine MWCNTs using potassium vapor.

2.3.3 Electrochemistry of graphene nanoribbons

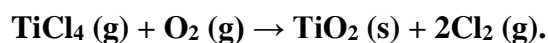
Graphene nanoribbons are electrochemically inert materials similar to other carbon-based materials used in electrochemistry, i.e. glassy carbon, graphite, and diamond. They possess distinct electrochemical properties because of their unique electronic structure. The carbon atoms of graphene nanoribbons at the sidewall and the end of the tubes are not same and their behavior can be compared with the basal plane and edge plane of highly oriented pyrolytic graphite (HOPG), respectively [62]. Studied the redox reaction of ferricyanide at the C₆₀ and graphene nanoribbons modified electrodes and compared these results with basal and edge planes pyrolytic graphite electrodes. They observed similar electron transfer rate constants for graphene nanoribbons -

modified and the edge plane (HOPG) electrodes. They reported that the graphene nanoribbons acted as an efficient electron transfer pyrometer [63]. Considering these electronic properties, carbon nanotubes are known for their capacity of boosting electron transfer reactions and enhancing sensitivity in electro analysis [17]. The mix of graphene nanoribbons with different nanomaterials has been accounted to be very helpful for creating electrochemical sensors [16]. Graphene nanoribbons have similar properties to multi-walled nanotubes, yet the outer walls on multi-walled nanotubes can protect the inner carbon nanotubes from chemical interactions with external materials. Electrochemical characterization involving conjugates of graphene nanoribbons and nanoparticles is expanding rapidly in electro-analytical researches because the conjugates have more appreciable electro-catalysis effect compared to the nanotube or nanoparticles alone [65].

2.4 Nano titanium dioxide

Titanium dioxide (TiO_2) is a widely occurring transition metal-oxide semiconductor used in science and technology. Due to its opacity, it has been used over the years as a white pigment in paints [67] and paper [68]. However, nowadays nano sized titania is broadly used as a raw material in electronics and structural ceramics. Since metal oxides possess unique advantages such as high sensitivity, good selectivity and large surface-to-volume ratio, so far increasing number of researchers have reported the production of novel CNT–metal oxide nanocomposites for biosensors applications [16], [17]. To enhance the performance features of the chemical sensor various nanomaterials matrices have been used. Titanium dioxide is well known for its interesting features and has been a promising material with good biocompatibility, high surface activity, and rapid electron communication features [18]. These salient features of titanium dioxide are highly advantageous for chemical sensor applications, Apart from these interesting aspects of TiO_2 , great

interest has been shown toward the synthesis of GNR/TiO₂ composites with interesting morphologies using versatile strategies including hydrothermal [19], thermal decomposition, drop casting and electrodeposition [20]. Among the various approaches, drop casting is cost-effective, simple, and eco-friendly. It is also found in the literature that titanium dioxide occurs in eleven different polymorphs with distinct structure [21]. The reaction involved can be represented as



2.5.0 Electrochemistry

Electrochemistry is the study of chemical processes that can cause movement of the electrons and the production of electricity which cause redox reaction. A redox reaction involves both reduction and oxidation reactions at the same time [69,70]. The process also involves the relationship between electricity and chemistry. It also involves the measurement of electrical variables such as potential or charge and currents and their relationship to chemical parameters. This technique is also used for the determination and the detection of quite a various range of substances. And is also applied in the detection and quantification of electroactive species. This research focuses its attention synthesis and application of graphene nanoribbon decorated with (TiO₂) towards the simultaneous detection of nevirapine and glucose in a three electrodes system by a combination of a computer and a potentiostat [71]. This branch of chemistry studies chemical reactions that involves the transfer of electrons between the reactant molecules and electrodes in a solution producing electric power [72]. A chemical reaction is brought about by application of excess voltage from an external power and the resultant current flow is measured to obtain characteristics of the analysts of interest.

2.5.1 Voltammetry

In voltammetry a time dependent potential is applied to an electrochemical cell, and the current flowing through the cell is measured as a function of time. The current is also corresponding to the quantity of material transported by diffusion and reacting at the electrode surface is usually measured. The current is also proportional to the concentration of electroactive component present in the testing solution [73]. Voltammetric methods enable the sensitive and selective measurement of compounds based on their specific electrochemical behavior at the working electrode surface [56]. It makes use of a three electrode system potentiostat that measures current as a function potential. The cell is made up of three electrodes immersed in a solution containing the analysts and also an excess of a non-reactive electrolyte called a supporting analyst. One of the three electrodes is the working electrode, whose potential is varied linearly with time. Its dimensions are kept small to enhance its tendency to become polarized. The second electrode is a reference electrode whose potential remains constant throughout. The third electrode is a counter electrode, which is often a coil of platinum wire that simply conducts electricity from the signal source through the solution to the working electrode [60]. Electrochemical methods are very useful if the selectivity achieved eliminates the need for separation procedures, which simplifies procedures, enables short analysis times and lower cost of analysis by using a relatively cheaper instrument and less consumables [63]. electrochemical methods are very useful if the selectivity achieved eliminates the need for separation procedures, which simplifies procedures, enables short analysis times and lower cost of analysis by using a relatively cheaper instrument and less consumables [71].

2.5.2 electrodes

The principle of potentiostat normally depends on its connection to the electrochemical cell. It controls the potential of the counter electrode (CE) against the working electrode (WE) so that the potential difference between the reference electrode (RE) which is distinct and agrees with the values specified between the user. The potential difference between the reference electrode and working electrode and the current flowing between the current and working electrode are constantly monitored [74].

2.5.3 Working Electrodes (WE)

The working electrode is the electrode where the potential is controlled and where the current is measured. In many physical chemistry, the working electrode is an “inert” material such as glassy carbon electrode, gold, platinum, and semiconductor or a metal coated with a film of mercury [75]. In these case, the working electrode serves as a surface on which the electro chemical reaction takes place. The working electrode can be bare electrode or coated.

2.5.4 Reference Electrode

The reason of the reference electrode is to provide a stable, reproducible voltage to which the working electrode of an electrochemical cell [70]. A reference electrode should have a constant electrochemical potential as long as no current flows through it. The reference electrode is a calomel electrode (SCE) and the silver/silver chloride (Ag/AgCl) electrodes [76]. The potential (E) of an electrode is determine by the Nernst equation, which relates to standard potential (E^0) and the activities of the redox components. The Nernst equation for the Ag/AgCl electrode is

$$E = E^0 + (RT/nf) \cdot \ln. 1/{}^3\text{Cl}.$$

2.5.5 Counter electrode (CE)

The counter electrode is normally made of an inert material of platinum (Pt) or metallic foil, gold may be used counter electrode does not usually take part in the electrochemical reaction but the total surface act as source of electron so that current can flow between the working electrode and counter electrode which make it not to be isolated from the reaction. The surface area of counter electrode should be higher than that of working electrode so that it will limit the kinetics of the process under investigation [78]. The role of counter electrode is to supply the current need by working electrode.

2.5.6 Mass Transfer in Voltammetry

Electron transfer in voltammetry can be influenced by the mass transfer for ions to move towards or away from the electrode. The movement of electron in an electrochemical cell is controlled by mass transport processes and mechanisms involved in the mass transport. There are three types of mass transfer processes to or from an electrode surface [64].

2.5.7 Diffusion

It is the movement of a chemical species from a region of high concentration to a region of low concentration under the influence of a concentration gradient.

2.5.8 Convection

Convection occurs when a mechanical means is used to carry reactants toward the electrode and to remove products from the electrode. The most common means of convection is to stir the solution using a stir bar. Other methods include rotating the electrode and incorporating the electrode into a flow cell.

2.5.9 Migration

Migration occurs when charged particles in solution are attracted or repelled from an electrode that has a positive or negative surface charge. Unlike diffusion and convection, migration only affects the mass transport of charged particles. There are versatile techniques that can be used in voltammetry and these include cyclic voltammetry, electrochemical impedance spectroscopy, chronoamperometry, linear scan, square wave voltammetry and differential pulse voltammetry.

2.6.0 Cyclic voltammetry

Cyclic voltammetry (CV) has become an important and widely used electro analytical technique in many areas of chemistry. It is often used to study a variety of redox processes, to determine the stability of reaction products, the presence of intermediates in redox reactions, [65] and electron transfer kinetics, [67] and the reversibility of a reaction. CV can also be used to determine the electron stoichiometry of a system, the diffusion coefficient of an analyte, and the formal reduction potential of an analyte, which can be used as an identification tool. In addition, because concentration is proportional to current in a reversible, Nernstian system, the concentration of an unknown solution can be determined by generating a calibration curve of current vs. concentration. Cyclic voltammetry is a technique devoted to the theoretical study of the behavior of redox couples. Cyclic voltammetry performs a triangular shaped scanning at the working electrode. In this way a redox couple in solution is exposed first to an oxidation and afterwards to a reduction (or vice versa) [68]. The plot of a cyclic voltammetry consists of a closed curve: reversible redox couples show both as cathodic and anodic peak, while irreversible redox systems show only one peak. The following relations can be useful to establish the standard potential of a reversible redox couple and the number of electrons involved in the discharge process:

$$E^O = \frac{E_{pa} - E_{pc}}{2} \quad (2.1)$$

$$E_{pc} - E_{pa} = \frac{57\text{mV}}{n} \quad (2.2)$$

And where E_{pa} = anodic peak potential, in mV and E_{pc} = cathodic peak potential, which gives an indication of the rate at which the electrodes are being transferred between the redox species and electrode.

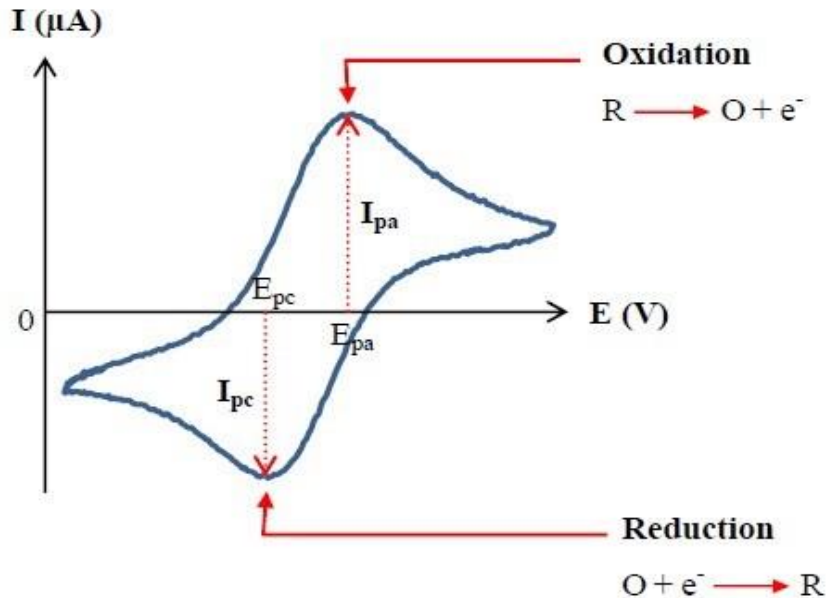


Figure 2.4: A typical cyclic voltammogram for a reversible single electro transfer [79].

2.6.1 Linear sweep voltammetry

Linear sweep voltammetry is a voltammetric method where the current at a working electrode is measured while the potential between the working electrode and a reference electrode is swept linearly in time. Oxidation or reduction of species is registered as a peak or trough in the current

signal at the potential at which the species begins to be oxidized or reduced. Linear sweep voltammetry can identify unknown species and determine the concentration of solutions. $E_{1/2}$ can be used to identify the unknown species while the height of the limiting current can determine the concentration. The sensitivity of current changes vs. voltage can be increased by increasing the scan rate. Higher potentials per second result in more oxidation/reduction of a species at the surface of the working electrode [69].

2.6.2 Chronoamperometry

The basis of all controlled potential techniques is the measurement of the current response to the applied potential of which chronoamperometry is one of them [80]. Chronoamperometry is an electrochemical technique whereby the potential of the working electrode is stepped and the resulting current from faradaic processes occurring at the electrode (caused by the potential step) is monitored as a function of time [81]. The ratio of the peak oxidation current versus the peak reduction current is used to obtain limited information about the identity of the electrolyzed species. However, as with all pulsed techniques, chronoamperometry generates high charging currents, which decay exponentially with time as any RC circuit. Since the current is integrated over relatively longer time intervals, chronoamperometry gives a better signal to noise ratio in comparison to other amperometric technique [82]. This technique is also used to obtain the initial information about nucleation and growth mechanism in a studied system. Additionally, the amount of charge for deposition (dissolution) can be determined. Also, this method can be applied for the determination of a nucleation rate constant and an adsorption isotherm. With the chronoamperometry, the current is measured versus time as a response to a (sequence of) potential

pulse. The recorded current can be analyzed and its nature can be identified from the variations with time [67].

2.6.3 Electrochemical impedance spectroscopy

EIS is a perturbative characterization of the dynamics of an electrochemical process. A tool for unraveling complex non-linear processes [46]. Electrochemical impedance is the response of an electrochemical system (cell) to an applied potential. The frequency dependence of this impedance can reveal underlying chemical processes. It is regarded as a derivative of linear sweep voltammetry or staircase voltammetry, with a series of regular voltage pulses overlaid on the potential linear sweep or stair steps. The current is measured instantaneously before each potential change, and the current difference is plotted as a function of potential [74]. The nyquist plots obtained in electrochemical impedance spectroscopy comprise of a straight line and a semi-circle. The diameter of the semicircle corresponds to the charge transfer resistance and diffusion controlled process respectively. The straight line portion represents the Warburg impedance which takes into account the frequency dependence on diffusion transportation to the electrode surface [75].

2.6.4 Bode Plots

The nature of bode plot which confirms the structural differences between the bare electrode and modified electrode. The figure shows a well-defined symmetrical peak for the bare electrode at particular angel and corresponding frequency representing the relaxation process at the electrode to different phase angles and frequencies on modifiers electrode. The relaxation process confirm that the reaction normally take place at the modifiers electrode surface than the bare electrode [83]

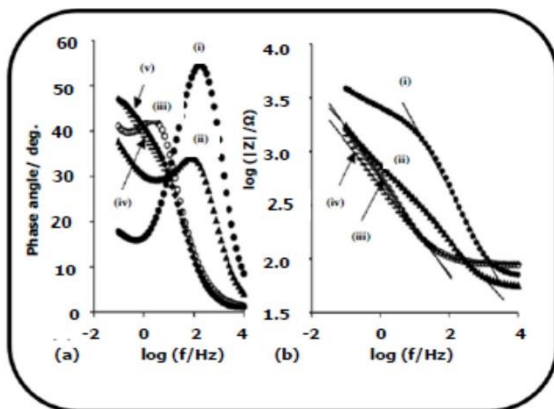


Fig 2.5: Bode Plots

The figure typically represents bode plots of phase angle vs logarithm and logarithm of complex impedance vs logarithm of frequency for the following electrodes (i) bare/GCE, (ii) GNRs/GCE, (iii) TiO₂/GCE, and (iv) GNRs/TiO₂/GCE in 0.1M KCl containing 1mM [Fe(CN)₆]^{3-/4-} solution [84].

2.6.5 Fourier Transform Infrared (FTIR)

This is a technique that probes molecular structure. It gives information on the functional groups for examples -OH, -C=O, -C=C-, -NH₂, -CONH₂, aromatics. The bonds between atoms in the molecule stretch and bend (vibrate), absorbing infrared energy and creating the infrared spectrum. The infrared radiation occurs between the visible and microwave radiation. When a molecule absorbs a certain wavelength of IR radiation it vibrates faster and functional groups influence bond stiffness and consequently alter the vibration frequency. One of the great advantages of IR is that any sample in any state, such as liquids, powders, films, gases and fibres can be studied [84]. The primary source of infrared radiation is thermal radiation (heat). It is the radiation produced by the motion of atoms and molecules in an object. The higher the temperature, the more the atoms and

molecules move and the more infrared radiation they produce. Any object radiates in the infrared. Infrared spectroscopy is a vital technique in organic chemistry where it is used to identify the presence of certain functional groups in a molecule. It is also used for confirmation of identity of a pure compound or to detect the presence of specific impurities where one can use the unique collection of absorption bands. It is based on the vibrations of atoms of a molecule [85]. The frequency of vibration of bonds depends on the masses of the atoms in the bond and the bond stiffness. This is expressed in Hooke's law

$$v = \frac{1}{2\pi} \left(\frac{k}{m_1 m_2 / (m_1 + m_2)} \right)^{1/2}$$

Where v - Frequency

k -is the force constant of the bond

$m_1 m_2 / (m_1 + m_2)$ -is the reduced mass of the system and m_1 & m_2 are the masses of the two atoms.

IR peaks appear at energies which correspond to the frequencies of vibrations of different parts of the molecule being analyzed. The results give information about the type of functional groups present in that molecule.

2.6.6 Summary

Various types of techniques have been utilized for determination of nevirapine and glucose; however electrochemical sensing is becoming wide spread due to its advantages such as simplicity, fastness, high sensitivity and can obtain perfect results with minimum supervision. IR peaks appear

at energies which correspond to the frequencies of vibrations of different parts of the molecule being analyzed. Chemical and physical combination of these nanomaterials can produce very efficient electrochemical sensors. Based on this known attractive properties the research will be pursued following a series of sequential steps which are to follow in the next chapter.

CHAPTER THREE

EXPERIMENTAL

3.0 Introduction

In the present chapter, chemicals, equipment, synthetic routes and characterization techniques used in these study are reported. The synthesis of graphene nanoribbon and graphene nanoribbons decorated with titanium dioxide was done and evaluated for the simultaneous detection of nevirapine and glucose. Thermal analysis data were obtained using a TGA 5000 Thermogravimetric Analyzer. The synthesis of graphene nanoribbon and graphene nanoribbon decorated with TiO₂ was done and evaluated for the simultaneous detection nevirapine and glucose. Electrochemical characterization of nevirapine and glucose was evaluated using cyclic voltammetry, electrochemical impedance spectroscopy (EIS), linear sweep, chronoamperometry and differential pulse voltammetry (DPV).

3.1 Chemicals and reagents

All the chemicals used were of analytical grade, multiwall carbon nanotubes (MWCNTs) (purity of 95%, diameter~20–40 nm and length~5-15 μm), Potassium ferricyanide and Potassium Ferro cyanide $[\text{Fe}(\text{CN})_6]^{-3/4}$ were obtained from Sigma Aldrich (South Africa), di-potassium hydrogen phosphate (K_2HPO_2), potassium dihydrogen phosphate (KH_2PO_4), acetic acid, sodium hydroxide (NaOH), glucose (GLC), 5% nitric acid, nevirapine (NVP), dimethylformamide (DMF), ethanol ($\text{C}_2\text{H}_5\text{OH}$), were obtained from Associated chemical enterprises (South Africa), potassium chloride (KCl) and hydrochloric acid (HCl), Sodium Acetate ($\text{C}_2\text{H}_3\text{NaO}_2$) were obtained from Skylabs (Johannesburg, South Africa), ethanol 99% ($\text{C}_2\text{H}_5\text{OH}$), potassium bromide (KBr), concentrated sulfuric acid (H_2SO_4 , 98%), sodium nitrate (NaNO_3), sodium chloride (NaCl),

potassium permanganate (KMnO_4), hydrogen peroxide (30% H_2O_2) were purchased from associated chemical enterprises (ACE) ascorbic acid (AA), uric acid (UA) and GA. All the solutions were prepared using distilled water from Midlands state University laboratory. All glassware was first cleaned in a bath of freshly prepared aqua regia solution and then thoroughly rinsed with distilled water.

3.2 Equipment

Fourier transform infrared spectroscopy (FTIR, Nicolet 6700 model) was used in IR characterization which equipped with OMNIC software. Sonicator model KQ-250B was used for agitation of samples. Electrochemical analysis was performed using Auto lab potentiostat PGSTAT 302N equipped with NOVA version 1.10 software and encompassed with a three electrochemical cell comprising of a glassy carbon electrode (GCE), platinum wire counter and Ag/AgCl reference electrode. All the experiments in the study were carried out at room temperature (25 °C) and pressure conditions (101.3 KPa) and the nitrogen purge gas in a 66.4 kg gas cylinder was supplied by BOC gases (Gweru, Zimbabwe). A digital analytical balance (model JJ224BC) was used for weighing. Dry oven (model MH302F), was used for dry sample. The pH of the solutions was measured and adjusted by a thermoscientific Orion Star A211 pH meter.

3.4.0 Experimental Section

3.4.1 Fourier Transform Infrared Spectroscopy

All the synthesized compounds TiO_2 , GNR and TiO_2/GNR nanocomposites were characterized using FT-IR. About 0.0100 g of samples were weighed and mixed with 1 g of KBr in a pestle and mortar to form a pellet and this was characterized within the range (400- 4000 cm^{-1}).

3.4.1 Thermal Gravimetric Analyzer

All the synthesized samples were analyzed using TGA whereby about 2.0 mg of the samples were weighed and then analyzed over the temperature range 25- 700 °C.

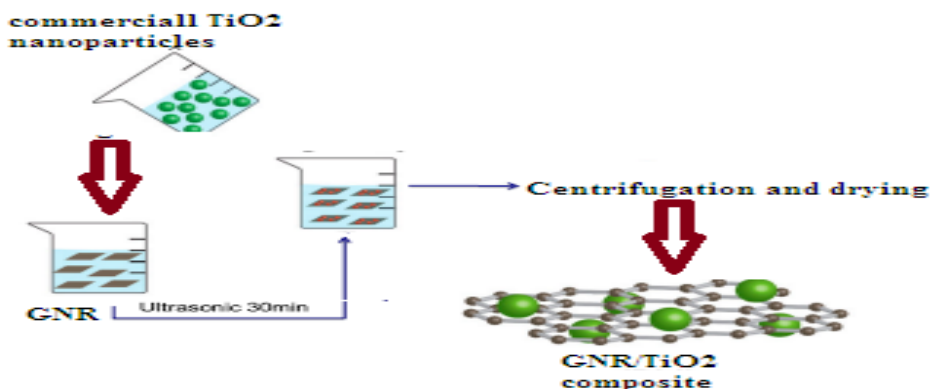
3.4.2 Synthesis of graphene nanoribbon

An Oxidation-Reduction method was tried in preparing GNRs with MWCNTs as the raw material. MWCNTs were oxidized according to the modified method as Kosynkin et al. tried [12, 19]. Graphene nanoribbons (GNRs) were prepared according to the procedure described before [86]. Briefly, 100 mg of multi walled carbon nanotubes (MWCNT) was dissolved in 3.4 mL of sulfuric acid (H₂SO₄, 98%) and the resulting suspension was homogenized via ultra-sonication for 1 h. The suspension solution was then placed in an ice bath with further vigorous stirring and 75 mg of sodium nitrate (NaNO₃) was added. Next, 450 mg of potassium permanganate (KMnO₄) was added into the suspension. The rate of addition was carefully controlled to keep the reaction temperature below 20 °C. After a reaction was completed (2.5-5 h), 20 mL of 5% sulfuric acid solution was transferred and was allowed to cool. After removal of the ice bath, 2 mL H₂O₂ (30%) and 6 mL deionized water were added to the mixture to prevent precipitation of insoluble MnO₂. After 30 min, the resulting suspension was centrifuged and carefully washed with 5% nitric acid three times and deionized water five times, this washing process was repeated until the pH of the solution became neutral. Finally, the solid sample was collected after washing with ethanol, deionized water, and then dried in an oven at 90 °C for 12 h under vacuum. Samples of the GNRs material were prepared as black powders in appearance. The prepared GNRs contained high amounts of oxygen-containing functional groups. There are many advantages of this approach, for instance, plenty of raw materials, simple process, low test costs etc.

3.4.3 Synthesis of GNR/TiO₂ nanocomposite ex-situ hybridization

The TiO₂/GNR nanocomposites was prepared by procedure as follows: 100 mL suspension of ethanol in TiO₂ nanoparticles (70 mg) was mixed with GNR (30 mg) followed by ultra-sonication for 15 min and then transferred in a rotary evaporator under vacuum for 45 min. After the rotation, the ethanol was evaporated out and dried [87].

EX-SITU HYBRIDIZATION METHOD



Scheme 3.1: Synthesis of GNR decorated with TiO₂ nanoparticles.

3.4.4 Physical Characterization of composites

3.5 Fourier Transfer Infrared Spectroscopy (FT-IR)

100 mg of samples such as GNR, TiO₂ and GNR/TiO₂ were weighted using analytical balance and mixed in a mortar and pestle with (1g; 8mmol) of KBr. The small amount sample compressed to form a transparent pellet using chrome bolt and nut. The sample was then placed into the FTIR Spectrophotometer and analyzed in the range 400 cm⁻¹ to 4000 cm⁻¹. The procedure was repeated for all synthesized graphitic materials.

3.5.1 Electrode modification

The glassy carbon electrode (GCE) was polished on Buehler Felt pad using Alumina (<10 μm) and then was ultrasonically cleaned in ethanol for about 10 min. The electrode was further cleaned in water for about 10 min. The electrode was finally rinsed with distilled water and then air dried. The cleaned glassy carbon electrode was modified using drop and dry method. Modifiers used were GNR/GCE, TiO_2 and GNR/ TiO_2 (table 3.1). GNR/ TiO_2 were placed on top of carbon based materials. An aliquot (0.5 μL) of each modifier was placed on the polished GCE, dried in an oven at 70 $^\circ\text{C}$ before use [9]. The electrodes are designated as GNR/GCE, TiO_2/GCE , GNR/ TiO_2/GCE . The cleaned bare/GCE, GNR/GCE, TiO_2/GCE and GNR/ TiO_2/GCE were dipped in solution and then dried using nitrogen gas.

Table 3.1: working electrodes used in this research.

Electrode modifier	Method of modification	Electrode designation
Bare glass carbon electrode	-	B/GCE
Graphene nanoribbon	Drop and dry	GNRs/GCE
Titanium dioxide	Drop and dry	TiO_2/GCE
Graphene nanoribbon decorated with titanium dioxide	Drop and dry	GNRs/ TiO_2/GCE

3.6 Cyclic voltammetry behavior of modifiers in 1 mM $[\text{Fe}(\text{CN})_6]^{3-/4-}$

Cyclic voltammetry was used for the investigation of electron transfer kinetics for the bare/GCE, GNRs/GCE, TiO_2/GCE , and $\text{TiO}_2/\text{GNRs}/\text{GCE}$. The study was carried out in 1 mM $[\text{Fe}(\text{CN})_6]^{3-/4-}$ solution at a scan rate of 100 mV/s from -0.4 to 0.6 V. A volume of about 50 mL of 1 mM $\text{Fe}(\text{CN})_6^{3-}/\text{Fe}(\text{CN})_6^{4-}$ in 1 M KCl was used [88].

Table 3.2: Parameters in cyclic voltammetry.

Start potential (V)	-0.600
Upper vertex potential (V)	0.400
Lower vertex potential (V)	-0.600
Stop potential (V)	-0.600
Step potential (V)	0.00244
Scan rate mVs^{-1}	100

3.6.1 Electrochemical Impedance Spectroscopy

Nyquist plots were performed using electrochemical impedance spectroscopy in 1 mM $[\text{Fe}(\text{CN})_6]^{3-/4-}$ solutions for bare/GCE, GNRs/GCE, TiO_2/GCE , and GNRs/ TiO_2/GCE at a potential (V) 0.2000 for all electrodes in order to investigate the electron transfer resistance of the electrodes in correspondence to results obtained in cyclic voltammetry. The bode plots and electrochemical impedance spectroscopy occurs at the same time during the analysis but in different windows [88].

Table 3.3: Parameters for electrochemical impedance and bode plots

Potential (V)	0.400
Set cell	On

3.6.2 Standard preparation

Nevirapine tablets were bought from a local pharmacy in Gweru town Zimbabwe. Ten tablets of nevirapine formulation containing 200 mg were ground to fine powder using pestle and mortar. A mass of (1069.3171 mg) was accurately weighed and transferred to a 500 mL volumetric flask then dissolved with ethanol. The resulting solution was then gravity filtrated to remove excess and then it was used as a stock solution for preceding experiments. On the other hand, the glucose solution was prepared by dissolve a mass of (1.8025 g) was also dissolved in 100 mL of distilled water.

3.7 Optimisation of parameters

3.7.1 Effect of pH

The effect of pH was investigated in the range from pH 2.0 to pH 12.0. Adjusting of the buffer solution was carried out with dilute concentration of 0.1 M NaOH and 0.1 M HCl. The studies were carried out by preparing different pH phosphate buffer solution containing 1 mM of nevirapine/glucose. The studies were carried out in cyclic voltammetry by using GNR/TiO₂/GCE electrode.

Parameters for pH studies in 1 mM nevirapine and 1 mM glucose are show in table 3.4

Parameter	Nevirapine	Glucose
Start potential (V)	0.0	0.0
Upper vertex potential (V)	1.00	1.200
Lower vertex potential (V)	0.00	0.0
Stop potential (V)	0.0	0.0
Scan rate mVs^{-1}	0.100	0.100

3.7.2 Comparative studies in pH 11.0 phosphate buffer solution (PBS)

Comparative studies were performed in the optimized pH buffer solution containing 1 mM nevirapine and 1 mM of glucose. The studies were carried out by using modified electrodes such as Bare/GCE, GNR/GCE, TiO_2 /GCE and GNR/ TiO_2 /GCE in order to confirm increase in anodic peak currents on the oxidation of each analyst. Scan rate studies of each analyst were carried out in order to determine reaction kinetics. The purpose for this study was to determine whether the detection of each analyst was diffusion controlled or not. It was observed on plotting graphs of anodic peak current against square root of scan rate.

Parameters used for comparative studies in pH studies in 1 mM nevirapine and 1 mM glucose are show in table 3.5

Parameter	Nevirapine	Glucose
Set potential	0.0	0.0
Set potential	1.00	1.200
Set potential	0.00	0.0
Duration	0.0	0.0
Interval time	0.500	0.400

3.7.3 Individual determination of nevirapine and glucose.

The individual cyclic voltammetric response of 0.1 mM nevirapine and 0.1 mM of glucose were carried out in a pH 11.0 phosphate buffer solution at various scan rate of 100 mVs⁻¹, 125 mVs⁻¹, 150 mVs⁻¹, 175 mVs⁻¹, 200 mVs⁻¹, 225 mVs⁻¹, 250 mVs⁻¹, 275 mVs⁻¹ and 300 mVs⁻¹. The potential used for nevirapine was set from 0.0 to 0.6 mVs⁻¹ and for the glucose was also set to be from 0.3 to 1.4 mVs⁻¹.

3.7.4 Simultaneous detection of nevirapine and glucose.

The cyclic voltammetric response for simultaneous (0.1 mM) nevirapine and glucose (0.1 mM) were carried out in a pH 11.0 phosphate buffer at various scan rate of 100 mVs⁻¹, 125 mVs⁻¹, 150 mVs⁻¹, 175 mVs⁻¹, 200 mVs⁻¹, 225 mVs⁻¹, 250 mVs⁻¹, 275 mVs⁻¹ and 300 mVs⁻¹. For the simultaneous detection for effective surface coverage the potential was set from 0.2 to 1.6 mVs⁻¹.

3.8 Kinetic studies

3.8.1 Catalytic rate constant

The catalytic rate constant was determined using chronoamperometry. The studies were performed by preparing working standard solutions 10 μM , 20 μM , 30 μM , 40 μM , 50 μM and 60 μM from 1 mM stock solution of each analyt. The prepared working standard solutions were filled in the electrochemical cell respectively and the behavior was observed on GNR/TiO₂/GCE. Catalytic rate constant was obtained by plotting graph of slope against square root of analyt concentration. The gradient of the slope is equivalent to πk which gives the catalytic rate constant.

Table 3.7.1 shows the parameters used for chronoamperometry for the catalytic rate constant of nevirapine and glucose. Scan rate studies were performed in order to determine the tefel slopes of the modified electrodes bare/GCE, GNR/GCE, TiO₂/GCE and GNR/TiO₂/GCE [50].

$$E_p = \frac{2.3RT}{2(1-\alpha)n_\alpha F} \log v + K \quad (3.3)$$

The value of b is $2.303RT/(1-\alpha)n_\alpha F$ and E_p , α , n_α and v are the cathodic peak potential electron transfer coefficient, number of electrons in the rate determining step and scan rate respectively.

Parameters for chronoamperometry catalytic rate constant are show in table 3.6.

parameter	Nevirapine	Glucose
Set potential	0.000	0.000
Set potential	0.400	0.400
Set potential	0.400	0.400
Duration	5	5
Interval time	0.01	0.01

3.8.2 Simultaneous detection of nevirapine and glucose by using differential pulse voltammetry.

Simultaneous detection on the analyst of 1 mM nevirapine and 1 mM glucose were performed in the optimized pH 11.0 buffer solution containing equimolar solution of nevirapine and glucose. The study was carried out by preparing working standard solution of 0.2 μM , 0.4 μM , 0.6 μM , 0.8 μM , 1.0 μM , 1.2 μM and 1.4 μM from 1 mM stock solution of nevirapine and glucose in pH11.0 phosphate buffer solution. The study was carried out in a solution containing equimolar of nevirapine and glucose and varying concentration of both analysts. The studies were carried out using modified electrode GNR/TiO₂/GCE.

Parameters for DPV are show in table 3.7.

Parameter	Nevirapine	Glucose
Initial potential (V)	0.400	0.400
end potential (V)	1.200	1.200
Step potential (V)	0.00500	0.00500
Modulation amplitude (V)	0.0500	0.0500
Interval time	0.50000	0.50000
Scan rate mVs ⁻¹	0.0100	0.0100

3.8.3 Detection limit for the simultaneous analysis of nevirapine and glucose by using DPV

Detection limit of 1 mM nevirapine and glucose were performed in the optimized pH 11.0 buffer solution containing equimolar solution of nevirapine and glucose and varying concentration of one analyte while keeping the other constant. The limit of detection was carried out using differential pulse voltammetry (DPV). The working standards were prepared in 100 mL volumetric flask and diluted to the mark with pH11.0 phosphate buffer solution. The prepared 100 mL solution of working standards were placed in the electrochemical cell respectively and the behavior was observed on modified electrode GNR/TiO₂/GCE.

Parameters for DPV are show in table 3.8.

Parameter	Nevirapine	Glucose
Initial potential (V)	0.400	0.400
end potential (V)	1.200	1.200
Step potential (V)	0.00500	0.00500
Modulation amplitude (V)	0.0500	0.0500
Interval time	0.50000	0.50000
Scan rate mVs^{-1}	0.0100	0.0100

3.9 Stability studies

Stability studies were performed using the GNR/TiO₂/GCE for each analyst by performing 20 cycles by using cyclic voltammetry at 0.1 mVs^{-1} scan rate at a potential 0.2 to 0.9 V.

3.10 Reproducibility studies

Reproducibility studies of the (GNR/TiO₂/GCE) modified electrode were performed using cyclic voltammetry technique. Replicate analysis, thrice, was performed on 1 mM of each analyst PBS (pH 11.0) at a scan rate of 0.1 mVs^{-1} and potential from 1.00 V to 1.200 V.

Parameters for cyclic voltammetry are show in table 3.9.

Parameter	Nevirapine	Glucose
Start potential (V)	0.0	0.0
Upper vertex potential (V)	1.00	1.200
Lower vertex potential (V)	0.00	0.0
Stop potential (V)	0.0	0.0
Scan rate mVs^{-1}	0.100	0.100

3.11 Applicability

The study was carried out by employing the DPV technique. The developed sensor was used to detect each analyst in milk and human urine sample in nevirapine and human urine in glucose at different amount using addition method. The milk and urine were spiked with aliquots amount of each analyst.

3.12 Effect of interference

Differential pulse voltammetry was used to investigate the interference for each analyst. Equimolar of nevirapine and glucose were prepared in the same matrix with phosphate buffer solution (pH 11.0). The mixture was analyzed from 0 to 1.3 for nevirapine and 0 to 1.2 V for glucose potential and amplitude of 0.05 V.

CHAPTER FOUR

RESULTS AND DISCUSSION

4.0 Introduction

This chapter illustrates and presents experimental findings and their discussion. Fourier-transform infrared spectroscopy (FT-IR) and thermogravimetric analysis (TGA) analysis were performed on graphene nanoribbon (GNRs), titanium dioxide (TiO₂) and graphene nanoribbon decorated with titanium dioxide (GNRs/TiO₂) were explained. In addition, the results obtained from electrochemical characterization of electrode modifiers using Cyclic voltammetry (CV), Electrochemical impedance spectroscopy (EIS) with bare/GCE, GNRs/GCE, TiO₂ and GNRs/TiO₂/GCE electrodes in 1 mM [Fe(CN)₆]^{-3/-4}. The electrochemical studies on the detection of nevirapine and glucose by utilization of linear sweep voltammograms (LSV), chronoamperometry, and differential pulse voltammetry (DPV) are also discussed.

4.1 Characterization of electrode modifiers

4.1.1 Fourier Transfer Infrared Spectroscopy (FTIR)

Fourier transform infrared spectroscopy (FT-IR) is an analytical technique in which infrared light is used to measure the absorption and emission of liquid, solid or gas, to characterize their properties. The information about the chemical bonds and molecular structure of the material is provided by creating an absorbance spectra of the sample as a function of wavenumber during the FTIR analysis.

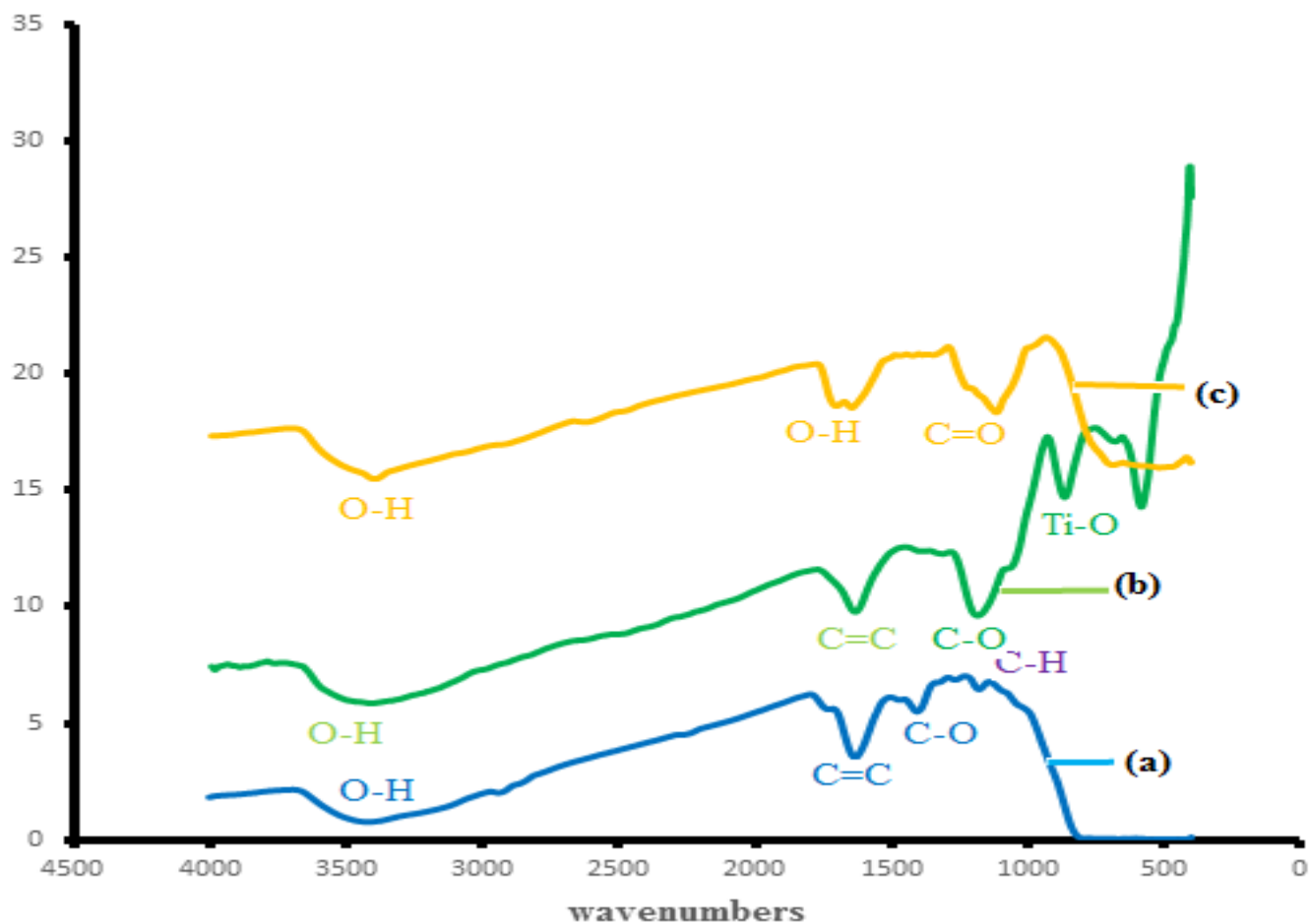


Figure 4.1 IR spectra for: a) GNR and b) TiO₂ c) GNR/TiO₂

FTIR spectra of GNR, TiO₂ and GNR/TiO₂ nanocomposites.

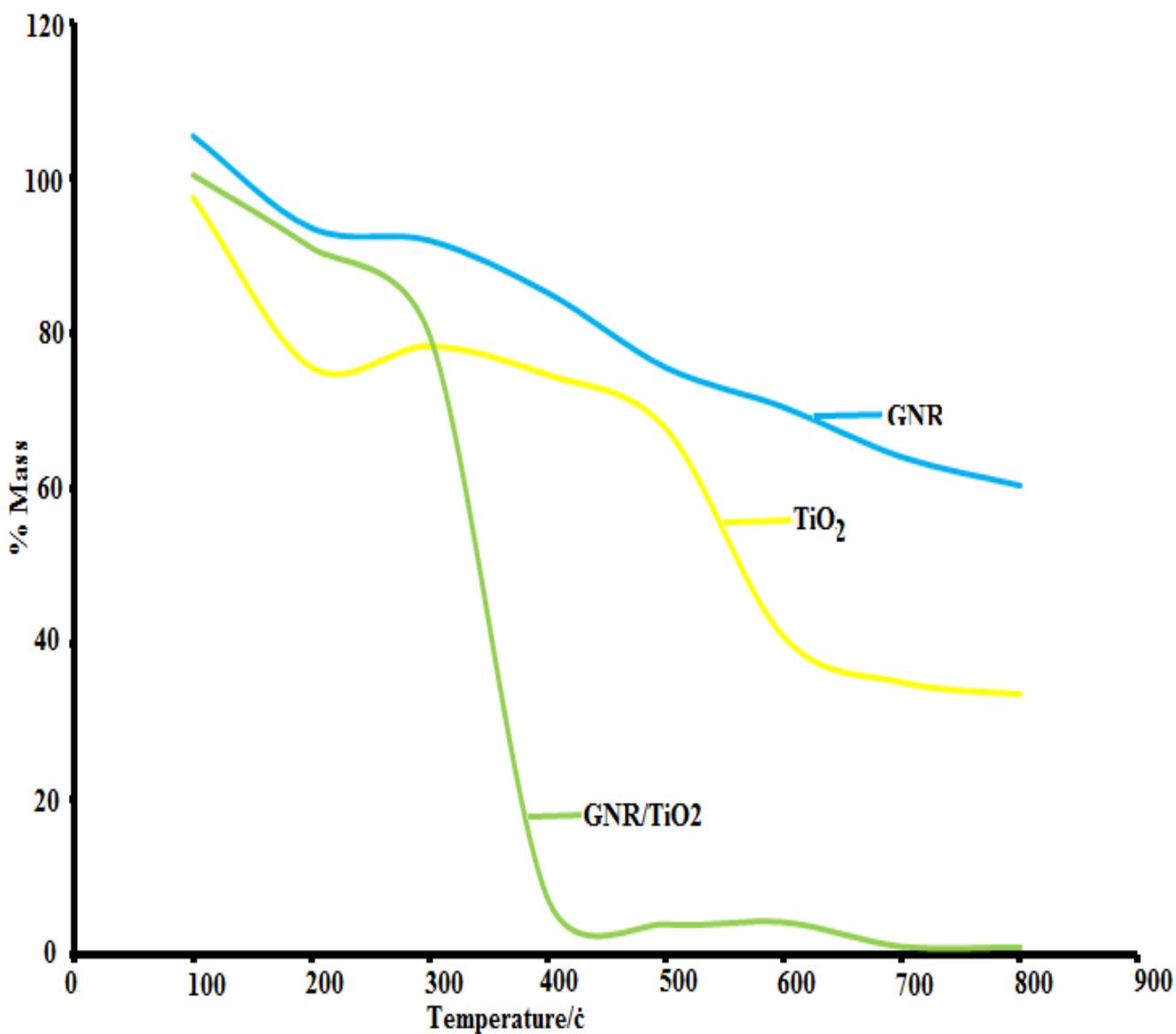
The FTIR spectrum of (GNR Figure 4.1 a) showed a broad and intense peak at around 3282 cm⁻¹, a strong COOH of carboxylic acid at 1654 cm⁻¹ which attributed to the stretching vibrations of carboxyl and additional peaks were observed at 1419 cm⁻¹ and 1041 cm⁻¹ which corresponded to C-O-H bending and alkoxy (C-OH) groups attached around the edges of a GNRs which indicating the hydride structure of graphene nanoribbon [89].

The FT-IR spectrum of TiO₂ NPs (Fig 4.1 b) showed the presence of functional group for TiO₂ peaks at 3413, 1169, 1631, 860 and 583 cm⁻¹ represent the OH functional groups, carbonyl group (C=O), stretching C=C aromatic ring and C-OH stretching vibrations the broad band around 1420 cm⁻¹ could be generally attributed to the bending vibration of H-OH groups for TiO₂, respectively.

The FT-IR spectrum of GNR/TiO₂ (Fig 4.1 C) showed the presence of Ti-O intrinsic stretching vibrations at 579 cm⁻¹ indicating that the nanoparticles had successfully decorated the graphene nanoribbon. The peak intensity of C=O in GNR/TiO₂ decrease due to the incorporation of nanoparticles indicating the was an interaction of carboxyl group ion with the TiO₂ nanoparticles. The intensity of the absorption peak at 1656 in GNR decreased as compared from the spectra of GNR indicating that there nanoparticles were successfully embedded within the GNR [90].

4.1.2 Thermogravimetric Analysis

The thermal stability of the synthesized materials was determined using a thermogravimetric analyzer. (TGA) is an evaluation technique that measures different substance masses as their temperature is changed or at a constant temperature over a given time. It is used to analyze decomposition and evaporation rates, oxidation, material purity and many other properties.



From the thermograms in (Fig 4.2), it can be observed that GNRs suffered gradual loss of mass at temperature below 150°C. The initial mass loss was observed for GNR (around 97°C-125°C) which can be attributed to the removal of absorbed water. The major weight loss occurred below 250°C which corresponded to the decomposition of oxygen-containing functional groups on the surface of GNR layers [91]. On the other hand, the weight loss around 200°C indicated the decomposition of GNR into carbon soot. The broad exothermic peak continued until around 800°C,

which corresponded to the anatase-rutile transformation finishing temperature, since it was an exothermic process which was confirmed by thermochemical data [81]. Finally, we selected 600°C as the optimum calcination temperature, high enough to achieve crystallization, and optimum to reduce the thermal growth of the crystallites and maintain nanoscale features in the calcined powder [92].

The successful decoration of TiO₂ nanoparticles on GNR was also reflected in the thermogravimetric analysis (TGA) curves. 350°C was mainly due to the release of the absorbed water and coordinated water [93]. While the mass loss ratio of GNRs/TiO₂ composite between 350 and 450°C was mainly resulted from the oxidization of GNRs. At temperatures above 700°C, the curve is rather stable, indicating GNRs have been completely disappeared. The amount of GNRs in the composite is determined to be about 28.3%. It is stressing that the special structure of GNRs can significantly provide increased accessible area [93].

4.1.3 Ultraviolet Visible Spectroscopy

UV-Vis refers to absorption spectroscopy or reflectance spectroscopy in the ultraviolet-visible spectral region. The operation mechanism of UV-Vis is based on the interaction between light and matter. The absorption or reflectance in the visible range will have an effect in the perceived colour of the chemicals involved. Absorption spectroscopy measures transitions from the ground state to the excited state [94]. Diluted graphene nanoribbons aqueous solution was used for UV-vis characterization. The measurement was performed with a thermo scientific (GENESYS 10S) UV-Vis spectrophotometer. The characteristic features in the UV-vis spectrum of graphene nanoribbon (Fig. 4.2) are the sharp peak at 245 nm which can be attributed to the $\pi \rightarrow \pi^*$ transitions of C=C bonds, the broad and less obvious peak at 294-350 nm which can be attributed to $n \rightarrow \pi^*$ transitions

of C-O bonds on the terminal ends of the graphene nanoribbon which were introduced into the MWCNT via the use of potassium permanganate oxidizing agent [95-96]. This observation was in line with the IR characterization which reviewed absorption bands of C=C and C-O at about 1654 cm^{-1} and 1419 cm^{-1} respectively.

The optical properties of TiO_2 nanoparticles Was also studies using UV-vis spectroscopy and a strong absorption peak at around 3413 cm^{-1} which represent the OH functional group and it can be attributed to the $\pi \rightarrow \pi^*$ transitions of OH bonds on the formation of TiO_2 nanoparticles [91].

UV-vis absorption spectroscopy measurements for GNR/ TiO_2 nanocomposites are shown in (fig b) which indicate the degree of reduction in the increase of GNR as the reaction temperature increased. The GNR/ TiO_2 sample had a broad peak centered at 227 nm which is approximately 300 nm. The peak at 227 nm was assigned to the pi to anti-pi ($\pi \rightarrow \pi^*$) transition of the aromatic carbon = oxygen (C=O) bonds [97].

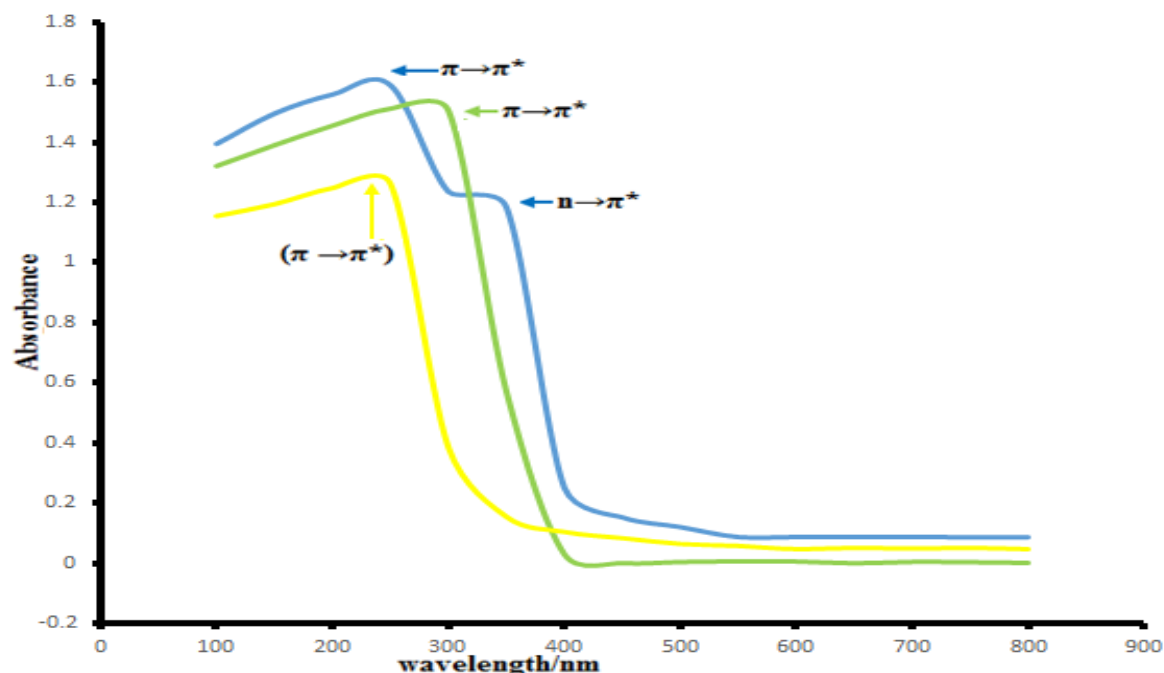
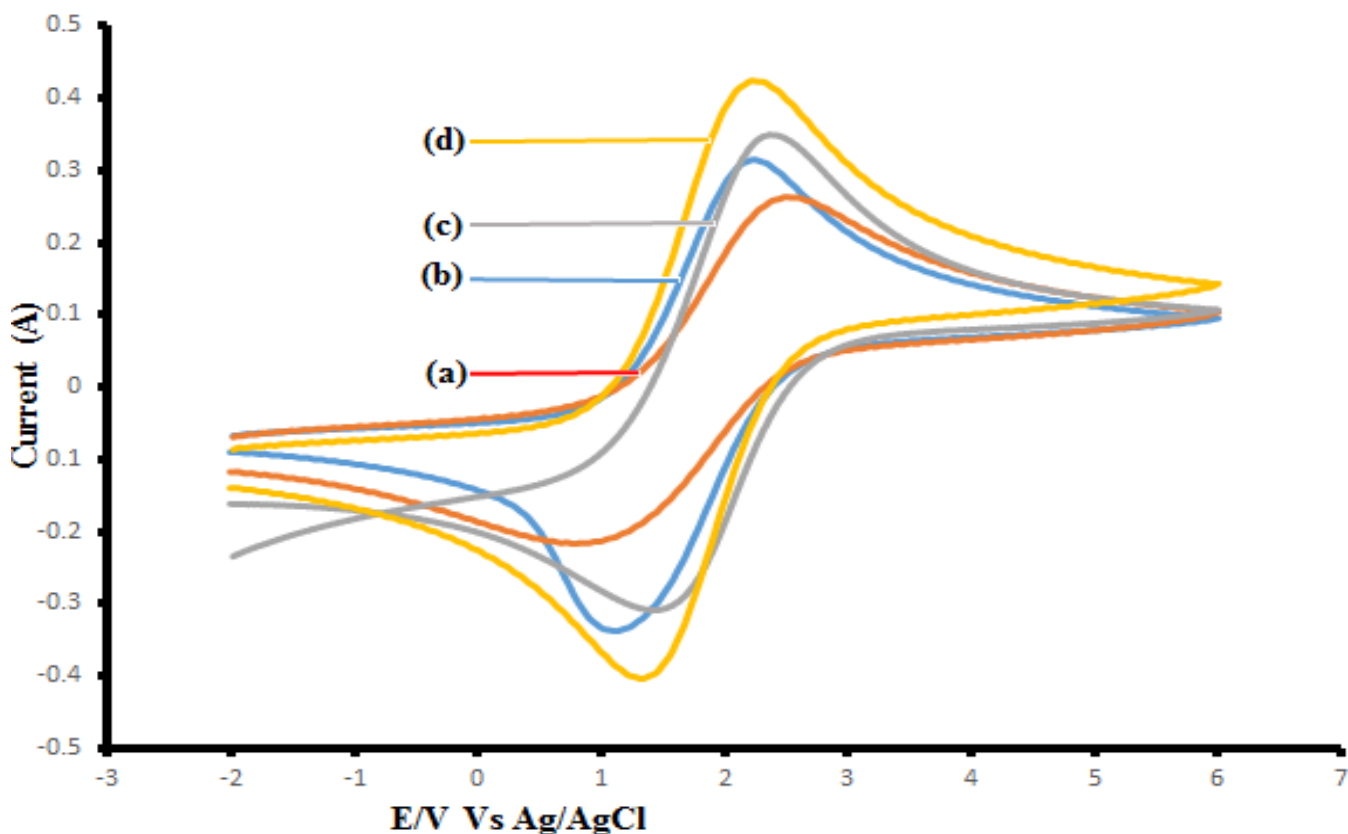


Fig. 4.2: UV-Vis spectra of (a) GNR, (b) TiO₂ and (c) GNR/TiO₂.

4.2.0 Electrochemical characterization

4.2.1 Cyclic voltammetry

Cyclic voltammetry is a highly useful technique to examine the heterogeneous electron transfer (HET) rate and the characteristics of the interaction between different molecules and the electrode surface [58]. Electrochemical behaviour of modified electrodes in redox couple acquired by the use of cyclic voltammetry in 1 μM $[\text{Fe}(\text{CN})_6]^{3-/4-}$ solution with 0.1 M KCl as the supporting electrolyte at a scan rate of 0.1 mVs^{-1} is shown in Fig 4.3.



(Fig 4.3) Voltammograms of bare/GCE (a) TiO₂/GCE (b), GNR/GCE (c) and GNR/TiO₂/GCE (d) in equimolar solution of 1 μM $[\text{Fe}(\text{CN})_6]^{3-/4-}$ prepared in 1 M of KCl. Scan rate = 100 mVs^{-1}

Electrochemical behaviour of redox probe in 1 M KCl was investigated at bare/GCE, TiO₂/GCE, GNR/GCE and GNR/TiO₂/GCE CVs are shown in Fig 4.3. A well-defined pair of redox peaks attributable to one electron transfer of [Fe(CN)₆]^{3-/4-} were seen in all cases. The peak currents were influenced by the functional groups of GNRs such as COOH and OH [98], which could absorb the [Fe(CN)₆]^{3-/4-}. Comparatively the peak-to-peak separation, ΔE_p for [Fe(CN)₆]^{3-/4-} redox couple was observed to be 0.08 mV at bare/GCE, 0.13 mV TiO₂/GCE, 0.056 mV GNR/GCE and 0.051 mV GNR/TiO₂/GCE (Table 4.1). The order in terms of electron transfer efficiency is therefore GNR/TiO₂/GCE (0.051 mV) > GNR/GCE (0.056 mV) > Bare/GCE (0.08 mV) > TiO₂/GCE (0.13 mV). Comparatively higher peak currents and smaller ΔE_p values in cyclic voltammetry recorded for 1 μM [Fe(CN)₆]^{3-/4-} redox probe in 1 μM KCl over GNR/TiO₂/GCE suggest the facilitation of electron transfer for [Fe(CN)₆]^{3-/4-} redox couple due to the enhancement in the reversibility of the electron transfer and a larger surface area on the modified electrode [90]. The electron transfer kinetics of the modifiers on the surface of glassy carbon electrode were also confirmed by the increase in anodic peak current. The smaller E_{pc} (0.051 mV) value for GNR/TiO₂/GCE was indication of decorated of titanium dioxide nanoparticles on the surface of graphene nanoribbon compared to the E_{pc} (0.13 mV and 0.056 mV) values for TiO₂/GCE and GNR/GCE, hence improving electron transfer properties of graphene nanoribbon [69]. The surface roughness factor of the modified electrodes were determined using [Fe(CN)₆]^{3-/4-} redox system and applying the Randles–Sevcik Equation for reversible system [99].

$$I_p = (2.69 \times 10^5) n^{3/2} D^{1/2} C A_{\text{eff}} v^{1/2} \quad (4.1)$$

whereas I_p the peak current, n is equal to the number of electrons transferred at the surface of the electrode, D is the diffusion coefficient of the analyt in solution 7.6 x 10⁻⁶ cm²/s⁻¹ and C is the

solution concentration in ($\text{mol}/\text{cm}^{-3}$), A_{eff} is the effective surface area and v is the scan rate (mV/s^{-1}). The values given in (table 4.1) were determined for all the probes and the results showed that there was increased roughness for GNR/ TiO_2 /GCE electrode compared to TiO_2 /GCE. The real electrode areas were calculated using the formula: roughness factor \times theoretical surface area (0.072 cm^2). The real electrode area for GNR/ TiO_2 /GCE was larger than the bare electrode 0.071 cm^2 . Therefore, the GNR/ TiO_2 /GCE was expected to perform better than all electrodes based on the effective electrode area.

Table 4.1 Electrochemical parameters for the modified electrode

Electrode	ΔE_p for $\text{FeCN}_6^{3-}/4-$	Surface roughness factor	Effective electrode area	Surface coverage (cm^{-2})	R_{ct} ($\text{k}\Omega$)	K_{app}
Bare/GCE	0.08	-	-	-	7.91	1.25×10^{-2}
TiO_2 /GCE	0.13	1.738	0.1204	3.14×10^{-9}	20.53	5.63×10^{-3}
GNR/GCE	0.056	1.761	0.1221	5.35×10^{-9}	4.92	2.27×10^{-2}
GNR/ TiO_2	0.051	1.833	0.1272	6.07×10^{-9}	1.53	2.98×10^{-2}

4.2.2 Electrochemical impedance spectroscopy (EIS) characterization

Electrochemical impedance spectroscopy is a highly effective technique to investigate the electron-transfer properties of the modified electrodes [98]. It is also a potent tool for the proper determination of both kinetic and mass-transport parameters as well as the charge transfer coefficient [96]. (Fig 4.4) shows the EIS response for bare/GCE, TiO_2 /GCE, GNR/GCE, and GNR/ TiO_2 /GCE. The Nyquist plot shows a representation of charge transfer (RCT) and the

diffusion controlled processes which are represented by the diameter of semi-circles and a straight line portion extending from the semi-circle. The semicircle diameter in the impedance spectra represent the electron transfer resistance (RCT) [100] and the straight lines represent diffusion controlled processes. The diameter of the semicircle is usually equal to the electron transfer resistance (Ret), which normally reflects the conductivity and the electron transfer process [101].

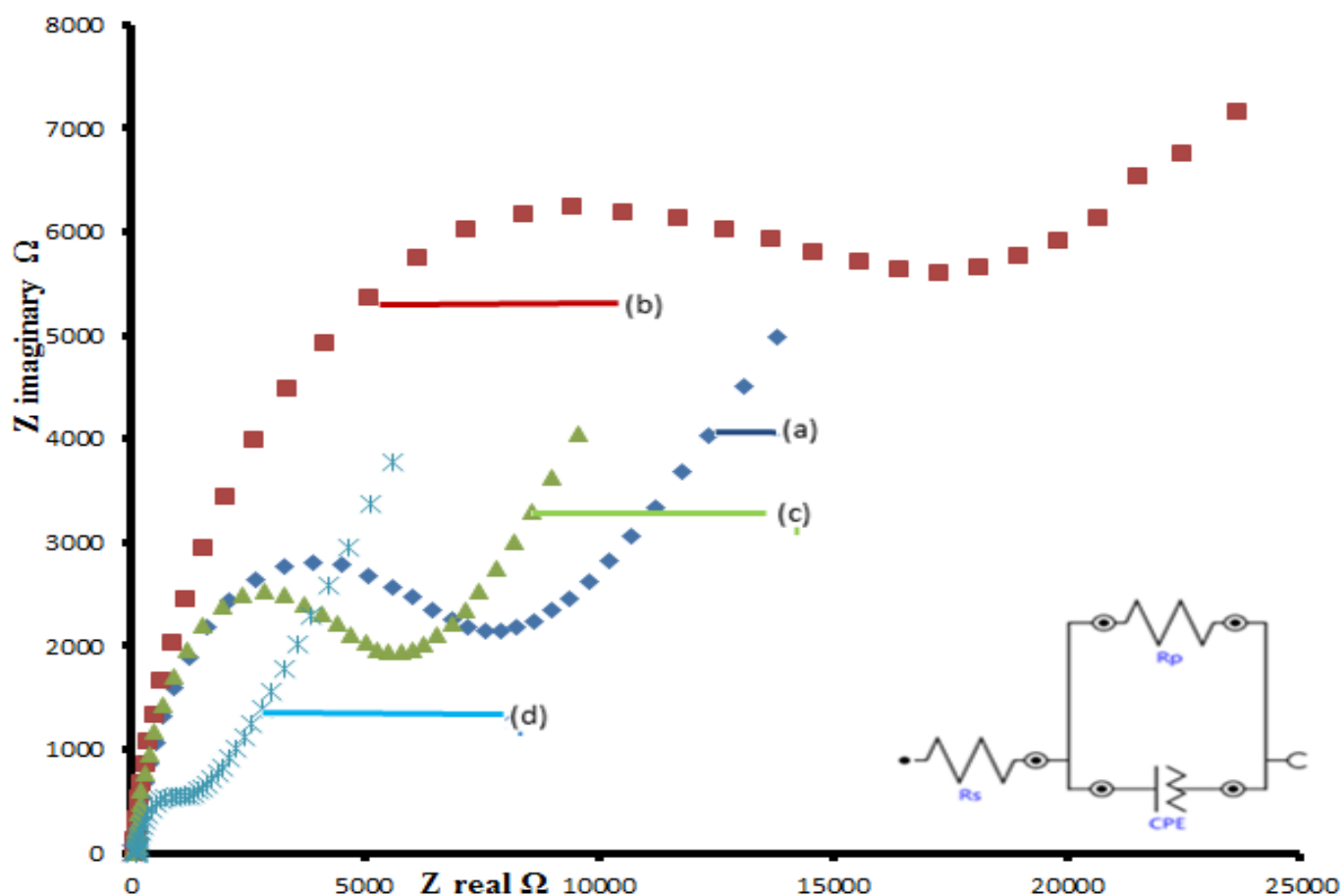


(Fig 4.3. b) Nyquist plots obtained for of bare/GCE (a) TiO₂/GCE (b), GNR/GCE (c) and GNR/TiO₂/GCE (d) in equimolar solution of 1 μM [Fe(CN)₆]^{3-/4-} prepared in 0.1 M of KCl. Inset is the Randles circuit model used in fitting the data. Inset in (fig 4.3) shows the Randle equivalent circuit for electrode process.

This equivalent circuit is made up of R_s which represents the resistance of the electrolyte in series connection with parallel elements of Cdl (double layer capacitance), the charge transfers resistance (RCT) and the Warburg impedance (Z_w) in the Faradaic branch of the circuit and this is connected in parallel with Cdl. The two parallel branches are then connected together to the R_s [76]. As shown in (Fig 4.3), the lowest RCT value was recorded for GNR/TiO₂/GCE which showed that it was a good electron conductor as it experienced the lowest charge transfer resistance [101]. It can be seen that the electron transfer resistance of B/GCE (7.91 k Ω) decreased rapidly on GNR/GCE (4.92), indicating that GNR has been modified on the surface of electrode and improved the conductivity and electron transfer process [102]. As shown in Fig.4.3, at a bare GCE, the redox process of the probe showed an electron-transfer resistance of about 7.92 k Ω while the TiO₂ modified electrode showed a higher resistance (20.53 K Ω). The increase of RCT was due to insulating bioconjugates interaction which block the electron-transfer process of the redox probe of [Fe(CN)₆]^{3-/4-} to the electrode surface [98]. Therefore, the results of electrochemical impedance spectroscopy (EIS) assays were in correspondence with those of the above CV measurements [103]. Moreover, the decoration of TiO₂ NPs nanoparticles on graphene nanoribbon resulted in a significantly increased surface area and enhanced the electrical conductivity of the electrode accounting for the decrease of (RCT) of GNR/TiO₂/GCE electrode. The Rct reduced from 4.92 k Ω to 1.53 k Ω as titanium dioxide nanoparticles were embedded on GNR hence their synergistic effect resulted in the decrease of (RCT) value indicating the incorporation of a catalytic material within the composite [104]. Electrochemical impedance spectroscopy (EIS) results are in agreement with cyclic voltammetry (CV) measurements demonstrating the successful fabrication of the sensor. The n values; whereas n was an exponent related to depression angle were important to mention as they give information about the behavior of bare and modified electrodes surfaces.

If the electrode behaves like pure resistor ($n=0$), Warburg diffusion ($n=0.5$) and pure capacitor ($n=1$). The n values ranges from 0.85 to 0.94 and these values are all close to unity ($=1$) indicating that the electrode behaves like a capacitor [105]. The RCT can be used to calculate the heterogeneous electron transfer rate constant K_{app} across the electrode interface under study. The RCT is inversely proportional to K_{app} constant, in according to the Equation [106]:

$$K_{app} = \frac{RT}{n^2 F^2 R_{ct} AC} \dots\dots\dots (4.4).$$

where C is the concentration ($[\text{Fe}(\text{CN})_6]^{3-/4-} 1.0 \times 10^{-3} \text{ mol cm}^{-3}$), with R and F having their usual meanings the decrease in k_{app} value from GNR/TiO₂/GCE ($2.98 \times 10^{-2} \text{ cm s}^{-1}$) > GNR/GCE ($2.27 \times 10^{-2} \text{ cm s}^{-1}$) > TiO₂/GCE ($5.63 \times 10^{-3} \text{ cm s}^{-1}$) > Bare/GCE ($1.25 \times 10^{-2} \text{ cm s}^{-1}$) > indicating that electron transfer process between the redox and the underlying bare surface are much easier at TiO₂/GCE compared to other electrodes. The higher k value obtained for the $[\text{Fe}(\text{CN})_6]^{3-/4-}$ redox at GNR/TiO₂/GCE in comparison to other electrode systems indicates that the presence of TiO₂ nanoparticles on the structure of GNR facilitates the electron transfer reaction to higher extent as compared to other individual electrodes [107]. Information about the frequency of the electrode cannot be established from Nyquist plot data, and so this information can be extracted from the "Bode Plot" as it gives frequency information. Bode plot is the representation of phase shift (θ) plot against the logarithmic value of frequency.

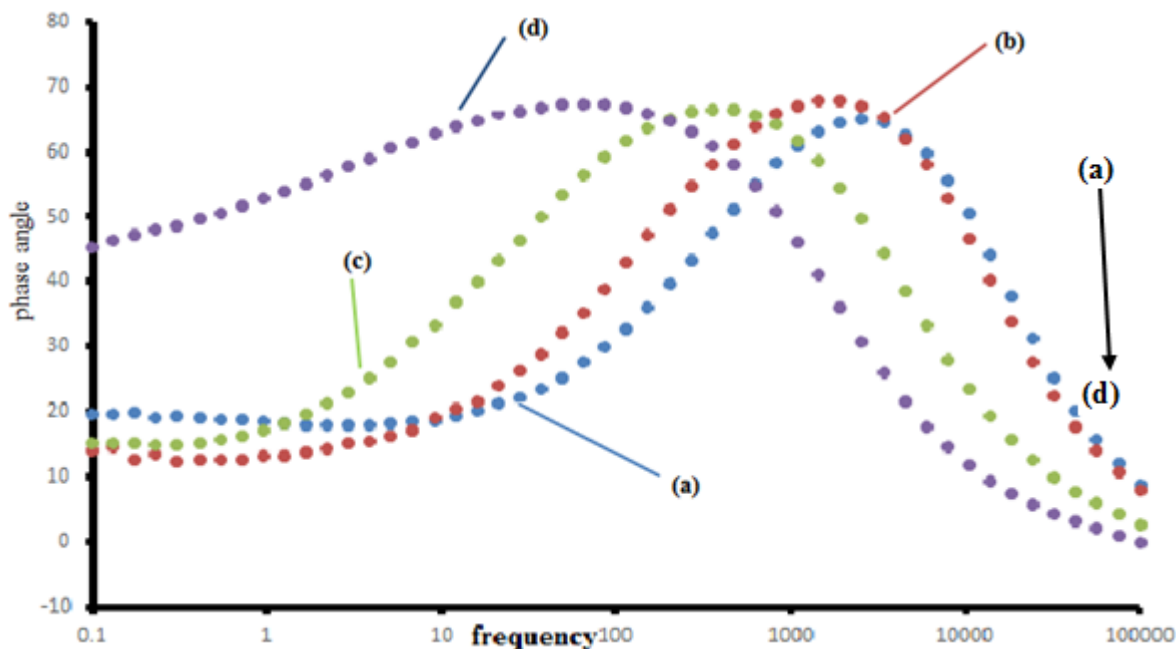


Fig 4.4: Bode plots obtained for (a) B/GCE (b) TiO₂/GCE (c) GNR/GCE (d) GNR/TiO₂/GCE in 1mM [Fe(CN)₆]^{3-/4-} solution in 0.1 M of KCl. Inset is the Randles circuit model used in fitting the data.

This plot confirms the structural differences of the modified glass carbon electrode. (Figure 4.5) shows bode (phase angle versus log f) plots obtained for (a) TiO₂/GCE (b) Bare/GCE (c) GNRs/GCE (d) GNR/TiO₂/GCE. Nyquist plots cannot reveal frequency related information, however these information was then obtained from the bode plots. The nature of bode plots confirmed structural differences of the modified electrodes. A maximum phase angle value was recorded for the bare/GCE with a quantity of 72 o at 3393 Hz which corresponds to the relaxation process of the GCE/electrolyte interface [108]. After modification electrode modification with graphitic material (GNR, TiO₂), the phase angle decreased dramatically, and the peaks shifted to lower frequencies for the relaxation process of the GCE/electrolyte interface were observed. This observation, confirms that the redox reaction of [Fe(CN)₆]^{3-/4-} was taking place at the surface of

the modified electrode rather than on the Bare/GCE surface [108]. However, it was observed that the nanocomposite electrode had a phase angle lower than that of GNRs, as per expectation but these lower phase angle was observed at a higher frequency. However, these GNR/TiO₂/GCE showed peaks well defined than the other electrodes. This confirms the presence of both the TiO₂ nanoparticles and GNRs nanostructure. The peak at a lower frequency corresponds to GNR/TiO₂/GCE incorporated in the hybrid nanostructure [108].

4.2.3 Surface coverage

Fig 4.4 shows the cyclic voltammograms of different electrodes obtained at a scan rate of 0.1 Vs⁻¹ in 0.1 M PBS (pH 11.0) for bare electrode (curve a), TiO₂ (curve b), GNR (curve c) and GNR/TiO₂ NPs (curve d). The surface coverage of bare electrode (curve a), TiO₂ (curve b), GNR (curve c) and GNR/TiO₂ (curve d) on GCE was determined using the Eq.4.3 [84].

$$I_{Pa} = \frac{n^2 F^2 v A_{eff} \Gamma}{4RT} \dots\dots\dots (4.3)$$

Where I_{pa} is the cathodic peak current, n is the number of transferred electrons, F is the Faraday constant which is equal to 9.6487 C/mol, v is the scan rate, Γ is the surface coverage in molcm⁻², A_{eff} is the surface area of the modified electrode, R is the gas constant (8.314 KJ/mol) and T is the temperature in Kelvin. The surface coverage of all electrodes in media follow the order GNR/TiO₂ > GNR > TiO₂. The higher surface of GNR/TiO₂ indicates the electrode surface area which offers more electro catalytic surface different orientation compared to the rest of electrode modifiers. The lower surface coverage of TiO₂ indicates different orientation on the electrode surface compared to the rest of electrode modifiers.

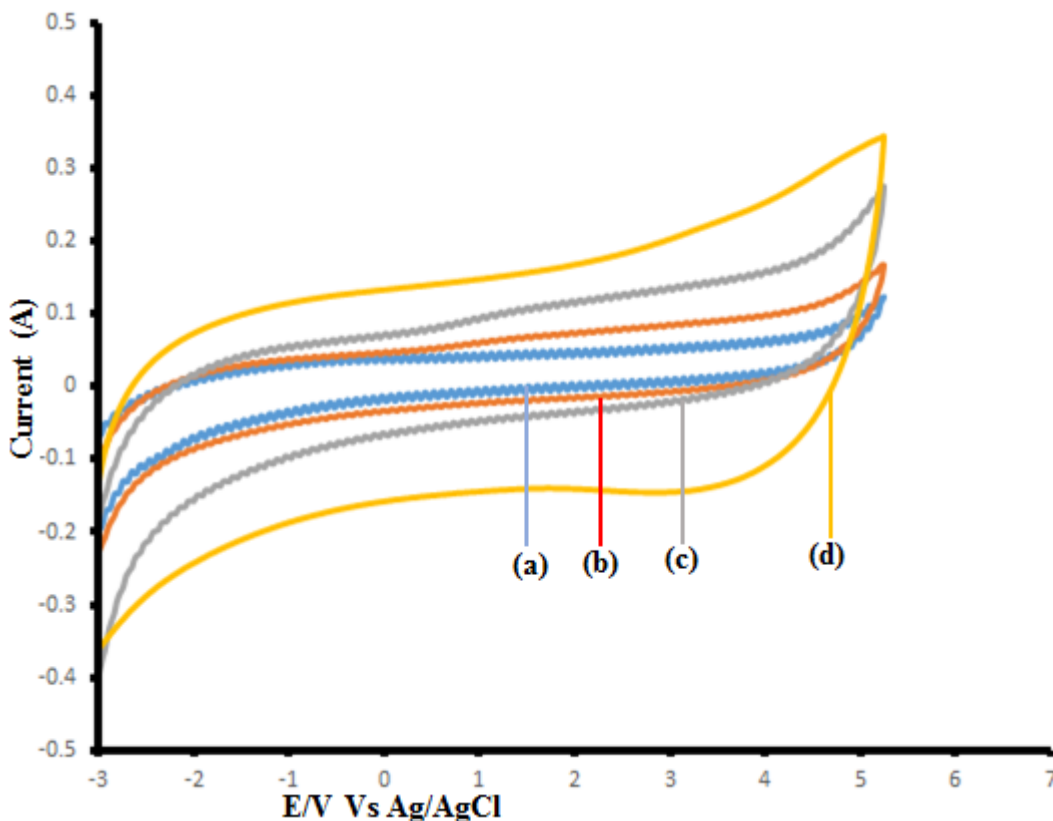


Fig 4.4: Cyclic voltammograms obtained at bare/GCE (a), TiO₂/GCE (b), GNR/GCE (c) and GNR/TiO₂/GCE (d) electrodes in 0.1 M PBS (pH 11.0) at a scan rate of 0.1 mVs⁻¹.

4.3. Effect of pH

The influence of pH on the electrochemical response of GNR/TiO₂/GCE towards nevirapine and glucose were investigated. As the pH of supporting electrolyte changes, the peak current and potential of nevirapine and glucose oxidation was also changed (Fig 4.5 a). The oxidation peaks current increases as the pH increases from 2 to 12 and reached maximum at pH 11 [105]. Afterwards, the current follows a decreasing trend and hence the electrode performed poorly at pH 12. Thus, the oxidation of nevirapine and glucose was more favorable at pH 11 and hence we have

chosen pH 11 as optimum pH for all the electrochemical studies performed in this work (Fig 4.5

b).

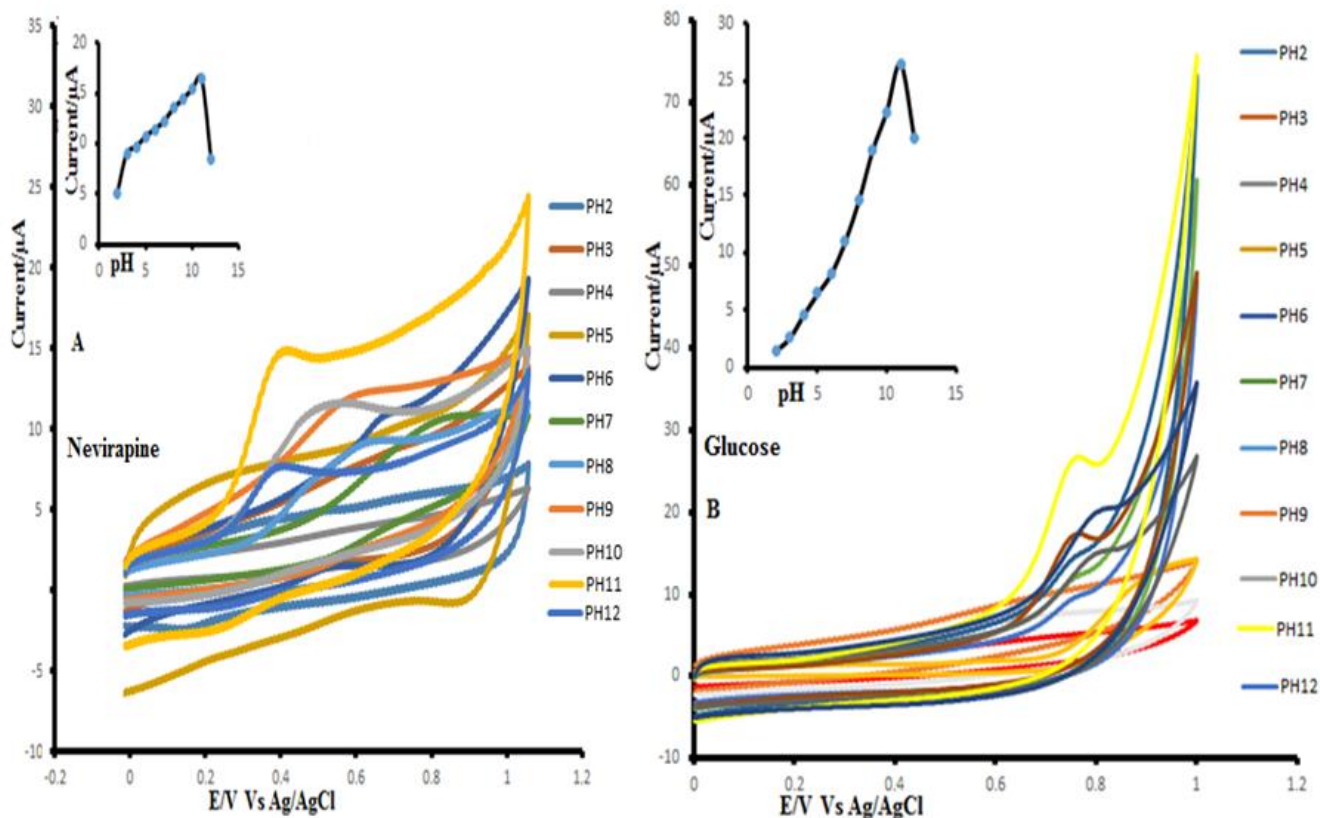
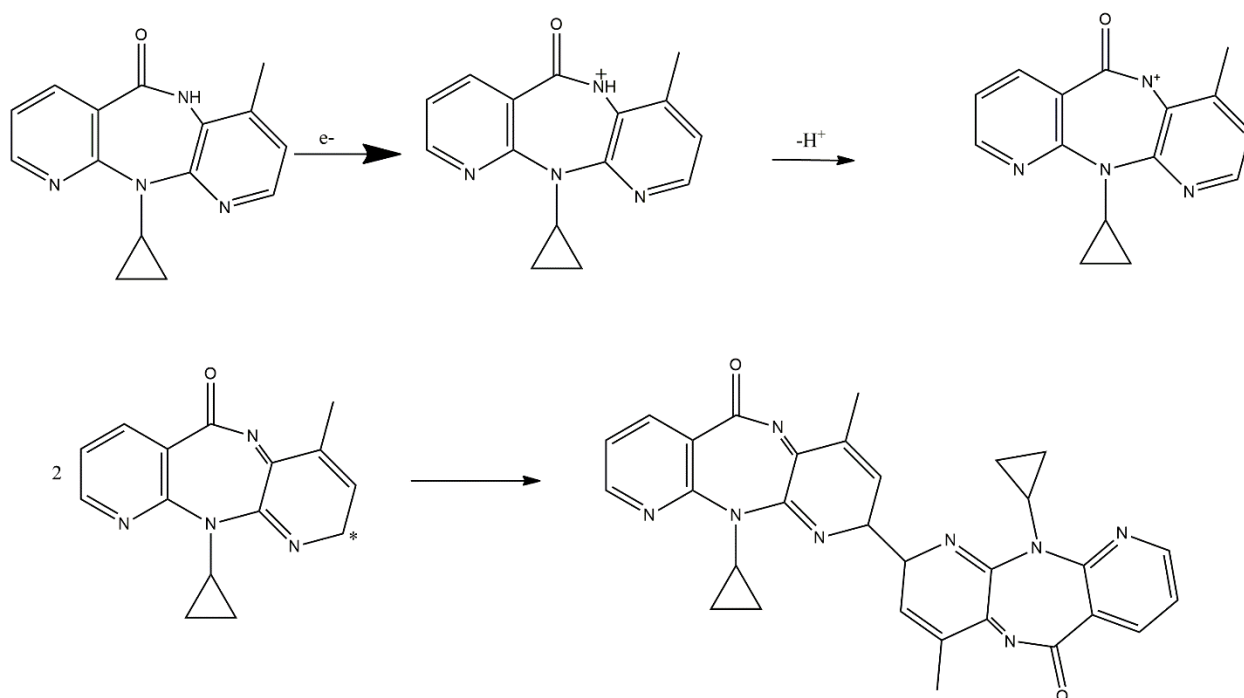


Fig 4.5 Cyclic Voltammograms nevirapine (A) and (B) glucose plot of Current vs pH and for GNR/TiO₂/GCE (a) pH 2, (b) pH 3, (c) pH 4, (d) pH 5, (e) pH 6, (f) pH 7, (g) pH 8, (h) pH 9, (i) pH 10, (j) pH 11 and (k) pH 12 phosphate buffer solution containing 1 mM nevirapine and glucose Inset: plot of I_{pa} vs pH Scan rate = 100 mV/s⁻¹.

Hence, we propose the electrooxidation of nevirapine involves the transfer of one electron.

Based on the above results, a probable mechanism for electrooxidation of nevirapine was proposed

(Scheme 1). It was proposed that the secondary ring nitrogen of nevirapine undergoes a single electron oxidation to yield a radical cation, which is further deprotonated to form a radical. Then, the free radical readily combines with another radical to form a dimerized product. This scheme was also in agreement with an earlier report [109].



Scheme 1. Probable reaction mechanism for electrooxidation of nevirapine.

4.4 Catalytic oxidation of nevirapine and glucose.

Cyclic voltammograms was utilized to study the electrochemical properties of the prepared modified electrodes and the peak potential and peak current were determined. As shown in Fig 4.6 oxidation peak current increased according to the following sequence of electrode modification on the electrode Bare/GCE < TiO₂/GCE < GNR/GCE < GNR/TiO₂. The bare/GCE showed limited current and high reduction potentials towards the detection of nevirapine and glucose implying insensitive electrochemical activity for the oxidation of both nevirapine and glucose. On the

contrary, a typical response current of GNR/TiO₂/GCE appeared responding to both nevirapine and glucose oxidation, which implying that the GNR/TiO₂/GCE exhibited excellent electro catalytic activity for nevirapine and glucose. The oxidation peak currents (I_{pa}) of GNR/TiO₂/GCE was attributed to the synergistic effect of TiO₂/GCE and GNR/GCE resulting in facilitating a remarkable high electron transfer indicating a more notable sensitivity toward the detection of both glucose and nevirapine. The significant catalytic property of GNR/TiO₂/GCE may be attributed to numerous active sites provided by GNR/GCE and the high electron transfer properties of TiO₂/GCE [110].

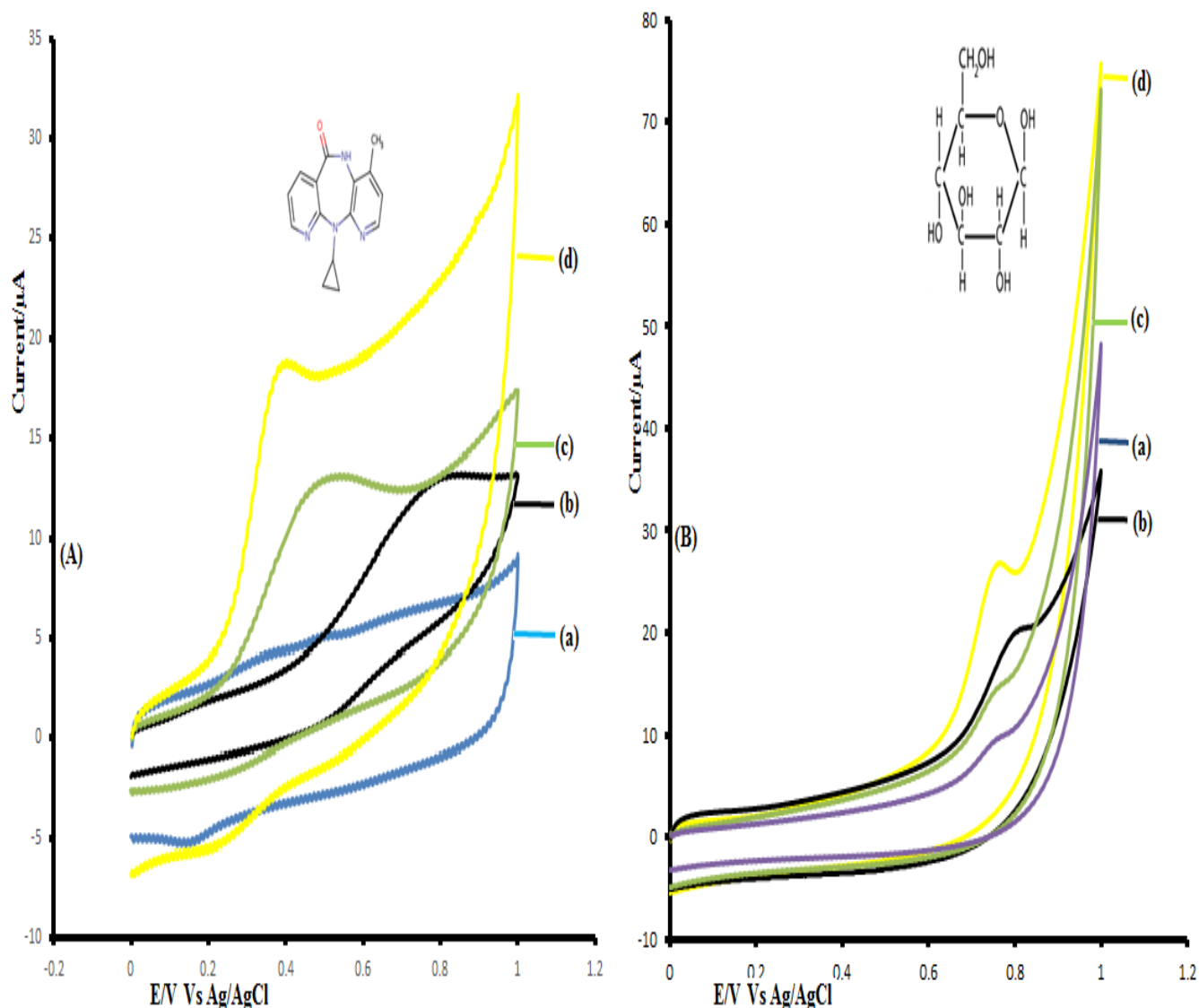


Fig 4.6 Voltammograms of bare/GCE (a) TiO₂/GCE (b), GNR/GCE (c) and GNR/TiO₂/GCE in 1mM (A) nevirapine and (B) glucose 1 mM in a 0.1 M PBS (pH 11.0) at a scan rate of 0.1 mV/s⁻¹. The entrapment or decoration of TiO₂ nanoparticles on the surface of graphene nanoribbon resulted in increased sensitivity towards the detection of both nevirapine and glucose and this composite forms three dimensional surface arrays on the electrode surface. These composites have very large surface area and are highly porous, therefore easily accessed by the analyte resulting in the easy oxidation of nevirapine and glucose on GNR/TiO₂/GCE [102]. The fast electron transfer

of TiO₂ can be attributed to the large surface area and high electronic communication capability of GNR composite [105].

4.5 Kinetic analysis for nevirapine and glucose oxidation

The influence of the scan rate on the electrochemical oxidation of nevirapine (A) and glucose (B) Fig 4.7 at GNR/TiO₂/GCE were investigated using cyclic voltammetry. The results showed that on increasing the scan rates, the oxidation potential of nevirapine and glucose shifts to more positive values confirming the kinetic limitation of the electrochemical reaction [106]. Moreover, a plot of peak current (*I*_{pc}) versus the square root of the scan rate (\sqrt{v}) Fig 4.7 insert for GNR/TiO₂/GCE the range of 50-400 mV/s⁻¹ was found to be linear following the linear regression equation $I_{pc} (\mu A) = 3 \times 10^{-6} (mV/s^{-1}) - 2 \times 10^{-6} (R^2 = 0.9914)$ and $I_{pc} (\mu A) = 3 \times 10^{-6} (mV/s^{-1}) + 5 \times 10^{-6} (R^2 = 0.9926)$ revealing that the electro-catalytic oxidation of nevirapine and glucose respectively followed diffusion controlled electron transfer process [106].

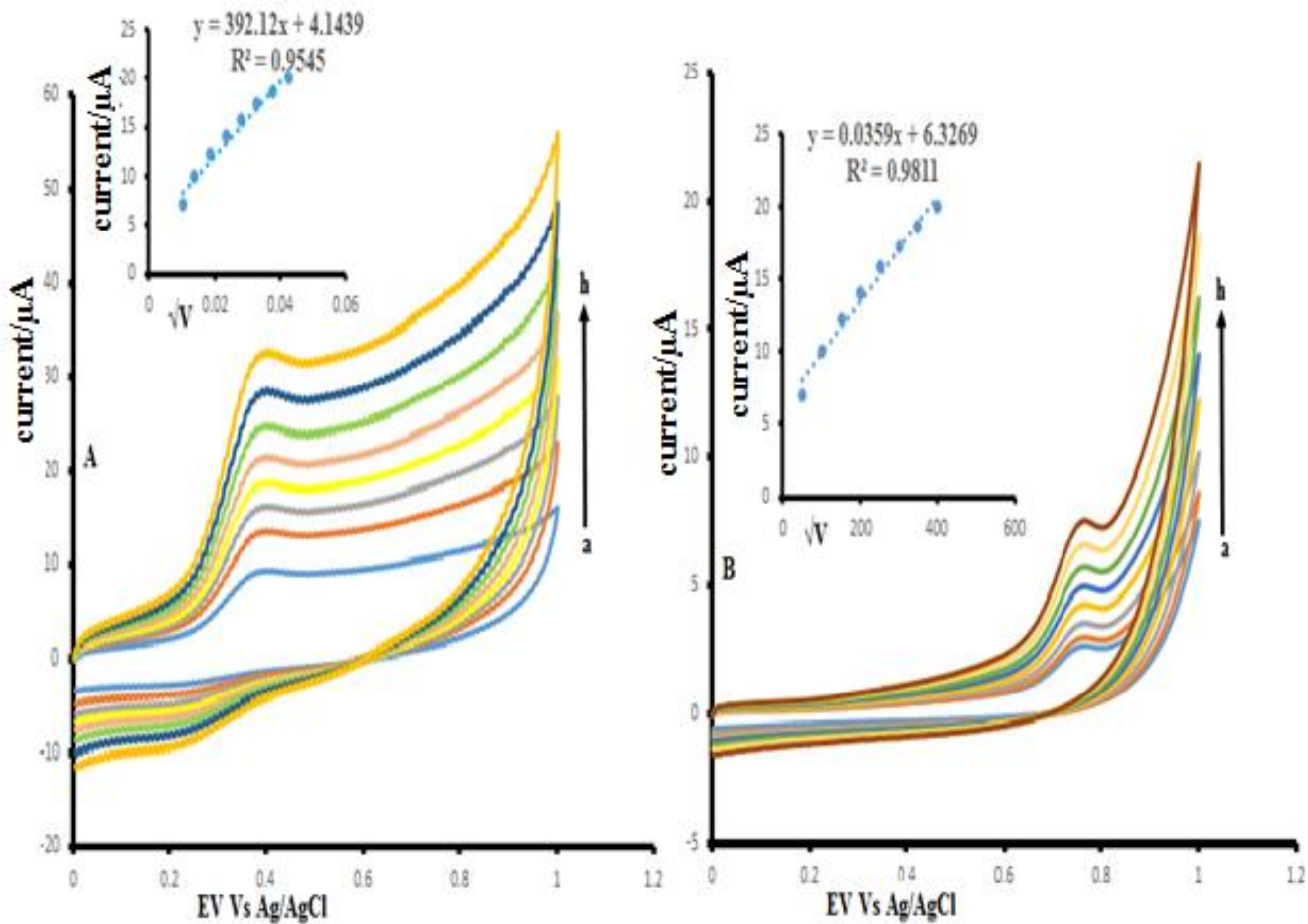


Fig 4.7 (A) nevirapine and (B) glucose: Effect of scan rate on peak potentials and currents a) 50 mV/s⁻¹ b) 100 mV/s⁻¹, c) 150 mV/s⁻¹, d) 200 mV/s⁻¹, e) 250 mV/s⁻¹, f) 300 mV/s⁻¹, g) 350 mV/s⁻¹, h) 400 mV/s⁻¹ on GNR/TiO₂/GCE for nevirapine and glucose oxidation. [NVP/GLC] = 1 mM. Inset: plot of I_{pa} vs √v.

4.6 Tafel slopes

For an electrochemically irreversible electro-reduction process the value of tafel slope (b) can be obtained from the variation of E_{pc} with v in voltammetry data through equation:

$$E_{pc} = \frac{b(\log v)}{2} + \text{constant} \dots\dots\dots (4.4)$$

where b is the Tafel slope.

The value of b is $2.303RT/(1-\alpha) n\alpha F$ and E_{pc} , α , $n\alpha$ and v are the oxidation peak potential, electron transfer coefficient, number of electrons in the rate determining step and scan rate respectively. The value of Tafel slope gives an idea about the number electrons transferred in the rate determining step. From the Tafel plot, value of b for nevirapine and glucose oxidation were found to be 140 mV/decade and 226 mV/decade at GNR/TiO₂/GCE respectively value is above the usual range of 0.03-0.120 V indicating a strong binding interaction of the analyte and the catalyst [108].

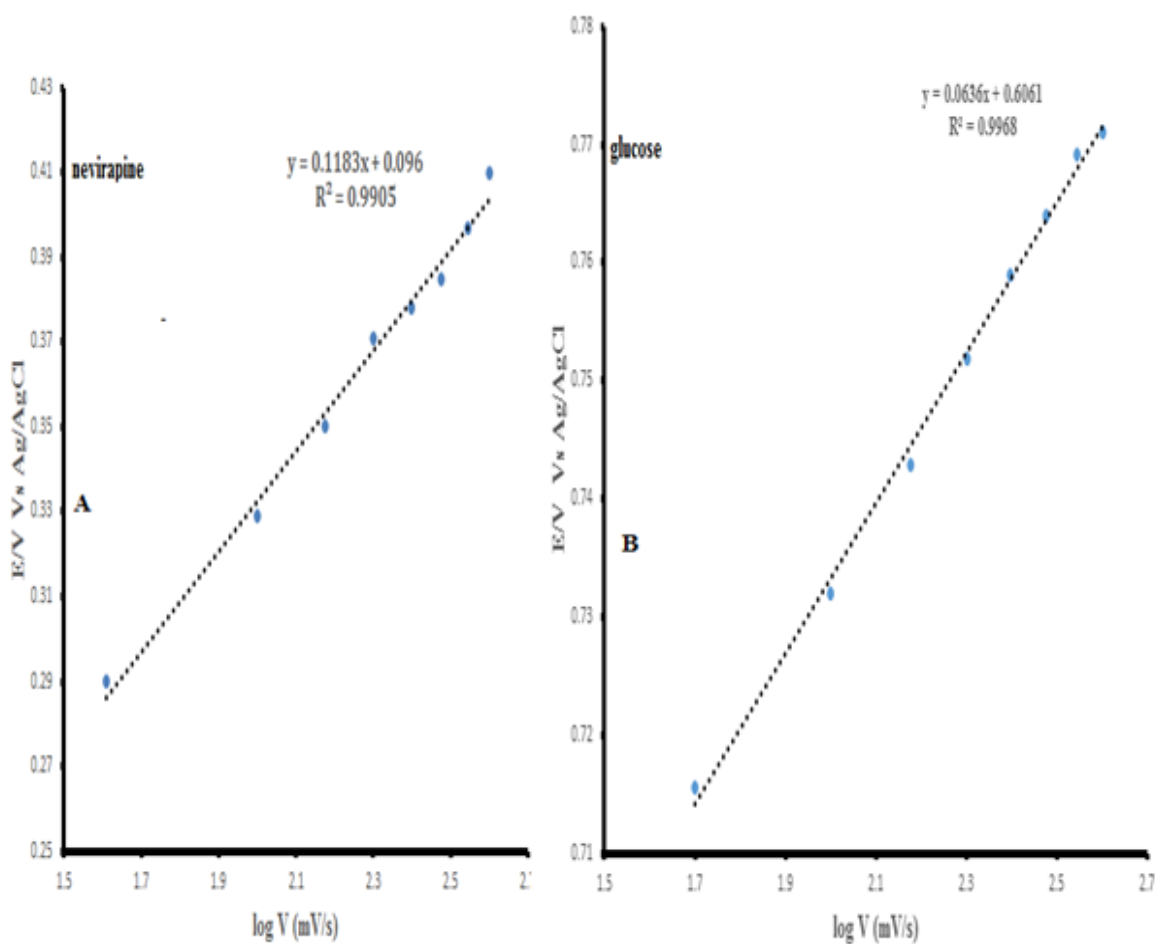


Fig 4.7 (A) nevirapine and (B) glucose: Plot of potential versus log scan rate in of 0.1 mV/s⁻¹.

4.7 Electrochemical Impedimetric spectroscopy

Electrochemical impedance spectroscopy (EIS) is measured by applying an AC potential to an electrochemical cell and then measuring the current through the cell. This response of an electrochemical system (cell) to an applied potential is called electrochemical impedance.

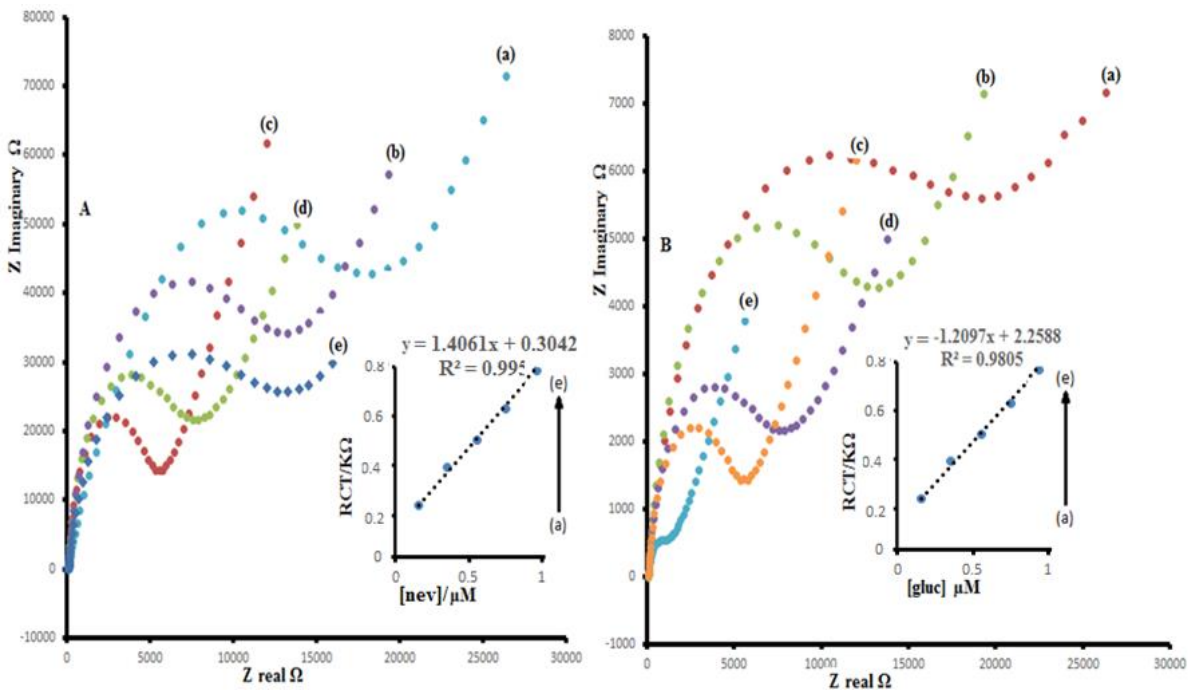


Fig 4.8: Impedimetric response obtained at GNR/TiO₂ in presence of various nevirapine (A) and glucose (B) concentrations i.e. from 0.2 μM (a) – 1 μM (e) in 0.1 M PBS (pH 11).

The result obtained was presented in Nyquist plot (Fig 4.8), which includes a semi-circular portion corresponding to the electron-transfer-limited process and a linear part resulting from the diffusion process. The representative circuit for the Nyquist plots is shown in Fig 4.8: insert, whereas RS, CPE, RCT and W represent solution resistance, a constant phase element, the charge transfer resistance and the Warburg impedance respectively. Further to understand the effect of nevirapine (A) and glucose (B) on the charge transfer resistance (RCT) of the synthesized material the

electrochemical impedance analysis was carried out by obtaining the real and imaginary parts of the impedance values from Nyquist plot and shown as Fig 4.8 (A) and (B). The RCT values were taken as the diameter of the curve and found that with increasing nevirapine and glucose concentration, the resistance increases and hence the conductivity decreases. It can also be observed that both the charge transfer resistance and especially the interface resistance decreased when concentration of nevirapine and glucose increased and there was accelerated electron transfer. The depressed arc radius of the nyquist plot corresponds to the electron transfer limited process. There was a linear behaviour (fig 4.8 A and B) with a good correlation coefficient and R^2 value was found to be 0.9832 for nevirapine and 0.9805 for glucose. The technique was also used to determine limit of detection of nevirapine and glucose and it was found to be 2.27×10^{-7} and 3.05×10^{-7} . Therefore, impedimetric techniques was very effective techniques since it shows higher sensitivity for the detection of both nevirapine and glucose. In the present study, the reason for the augmentation in semicircle diameter with increase in glucose and nevirapine concentrations could be attributed to competition of glucose and nevirapine ions adsorbed at modified electrode surface which inhibits the charge transfer for the redox probe in solution. The good impedimetric glucose and nevirapine detection results achieved at the GNR/TiO₂ film in these study could be attributed to the excellent compatibility of graphene nanoribbons and titanium oxide nanoparticles the good affinity of the composite film towards.

4.8 Gibbs free energy determination

Linear sweep voltammetry (LSV) was done to show adsorption behavior of GNR/TiO₂/GCE. Fig 4.9 shows LSV plots obtained after keeping the electrode in a stirred solution for 10 minutes (to allow for adsorption).

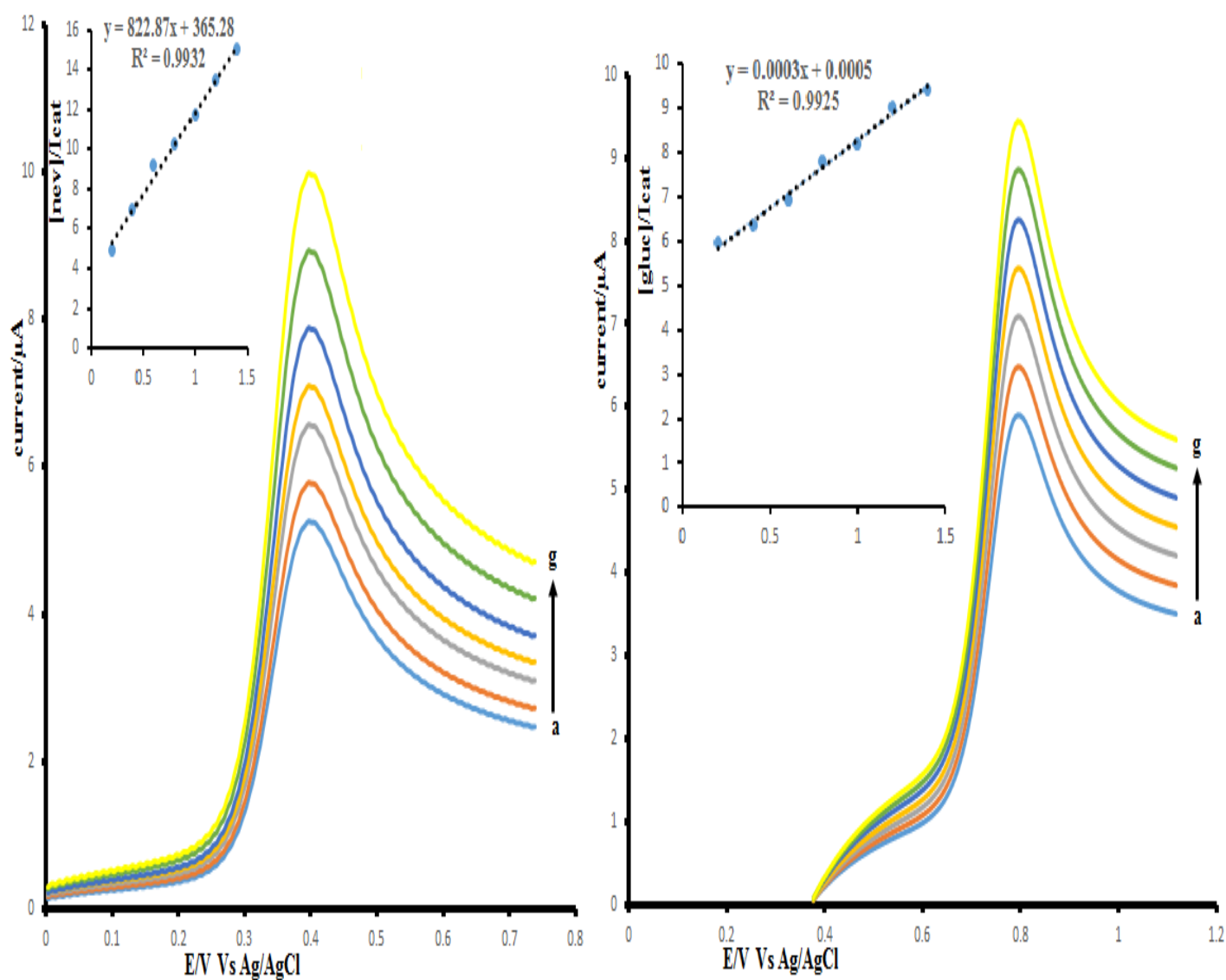


Fig 4.9 Linear sweep voltammograms (a) 0.1 μM , (b) 0.2 μM , (c) 0.3 μM (d) 0.4 μM , 0.5 μM , 0.6 μM and (e) 0.7 μM of (A) nevirapine and (B) glucose concentrations in pH 11 PBS. Inset plot of [nevirapine/glucose]/ I_{pc} vs [nevirapine/glucose].

Applying the Langmuir adsorption theory (Eq. 4.5) [107] a plot of the ratio of nevirapine/glucose concentration to catalytic current against concentration of nevirapine/glucose gave a linear plot which is indicative of adsorption further consolidating the observed high tafel slopes. where β is the adsorption equilibrium constant, I_{max} is the maximum current and I_{cat} is the catalytic current.

From the slope and the intercept of Fig 4.9, the adsorption equilibrium constant (β) for nevirapine and glucose were established to be $3.3 \times 10^3 \text{ M}^{-1}$ and $4.05 \times 10^3 \text{ M}^{-1}$ respectively. Using equation 4.5 which relates Gibbs free energy change due to adsorption (ΔG°) equilibrium constant (β), ΔG° was found to be -25.8 k J and -25.8 k J for nevirapine and glucose.

$$\Delta G^\circ = RT \ln \beta \dots\dots\dots (4.5)$$

4.9 Catalytic Rate Constant

Chronoamperometry was used to determine the catalytic rate constant (k) [69]. Fig. 4.11 shows the chronoamperograms that were obtained at concentrations of nevirapine and glucose which ranged from $0.1 \text{ }\mu\text{M}$ to $0.8 \text{ }\mu\text{M}$ in $0.1 \text{ }\mu\text{M}$ PBS (pH 11.0). The electro-catalytic oxidation of glucose and nevirapine by GNR/TiO₂/GCE was also studied by chronoamperometry. The chronoamperograms response for nevirapine and glucose in the concentration range from $0.1 - 0.8 \text{ mM}$ at the potential step of -300 mV are shown in Fig 4.10 inset shows that current was linearly proportional with increase in concentration with a linear regression equation $I_{pc} (\mu\text{A}) = 1.1492 [\text{nev}] - 5 \times 10^{-5}$ ($R^2 = 0.9911$) and linear regression equation $I_{pc} (\mu\text{A}) = 1.1697 [\text{glc}] - 2 \times 10^{-5}$ ($R^2 = 0.9959$). The insert shows a linear relationship between concentration and the current and slopes of that plot represent the sensitivity of electrode towards the analyte [74].

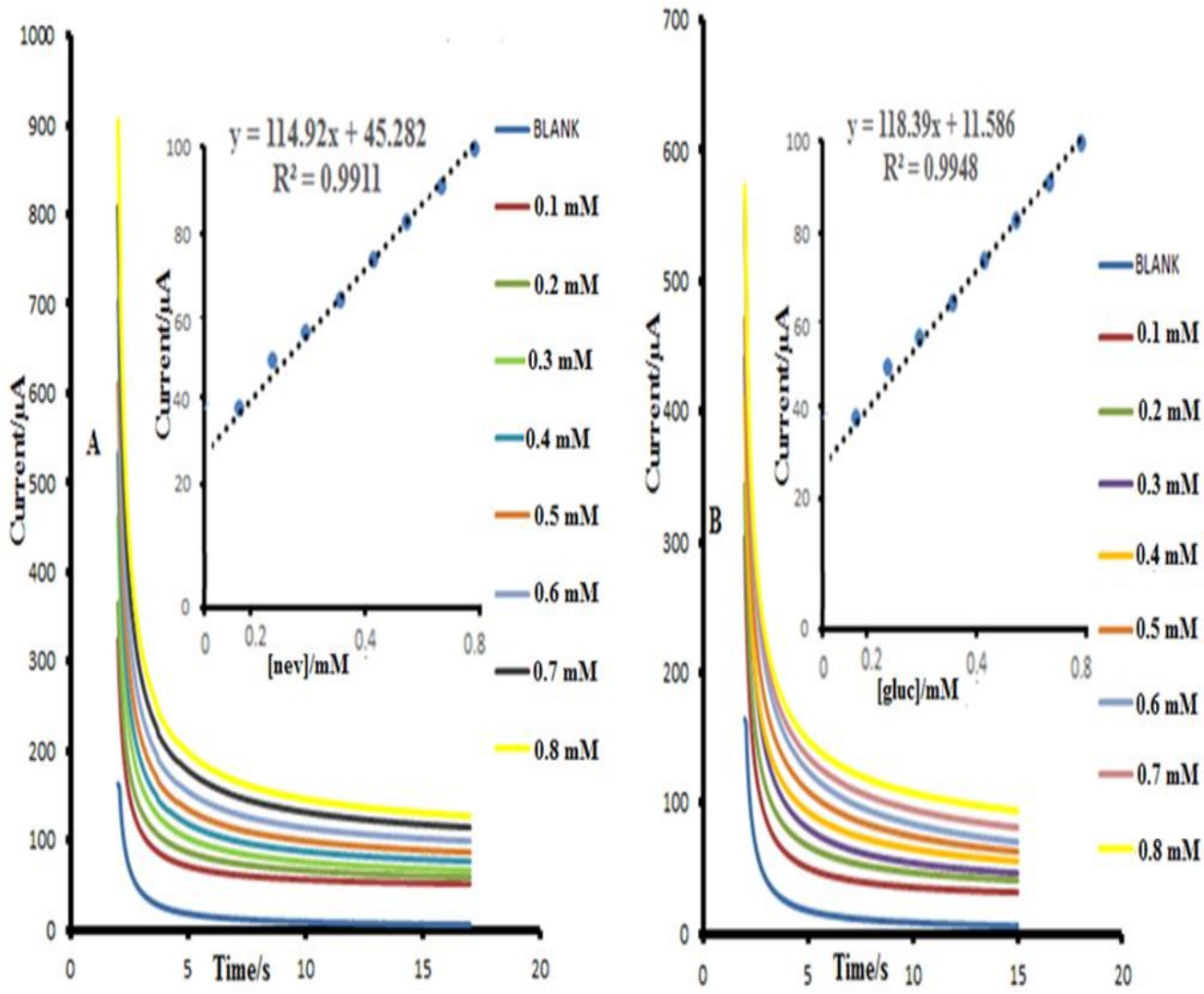


Fig 4.10 chronoamperograms for different nevirapine (A) and glucose (B) concentrations in PBS pH 11 (a), 0.1 μ M (b), 0.2 μ M (c), 0.3 μ M (d), 0.4 μ M (e), 0.5 μ M (f), 0.6 μ M (g) and 0.7 μ M (h). Inset I_{pc} vs [nev] and [glc].

Fig 4.10 a: Plots of I_{cat}/I_{buf} Vs time (s) for nevirapine and glucose. The rate constant for the detection of nevirapine and glucose were calculated using the equation [111].

$$\frac{I_{cat}}{I_{buf}} = \pi^{\frac{1}{2}}(kC_0t)^{\frac{1}{2}} \dots \dots \dots (4.6)$$

where I_{cat} and I_{buf} were currents in the presence and in the absence of nevirapine and glucose, k is the catalytic constant ($M^{-1}s^{-1}$) for nevirapine and glucose oxidation and t is the time in seconds. Fig 4.10 showed the linear relationships for the I_{cat} and I_{buf} vs $t^{1/2}$ plots for different nevirapine and glucose concentrations obtained from the chronoamperogram. Fig 4.10 showed the linear relationship for the slope vs. $\sqrt{[nev]}$ and $[gluc]$. The slope of fig 4.11 is equal to πk and these gives a k value of $2.45 \times 10^1 M^{-1}s^{-1}$ for nevirapine and $2.45 \times 10^1 M^{-1}s^{-1}$ for glucose respectively [112]. The value of k obtained were comparable with those obtained in literature [9] and the value obtained was larger for k and therefore, the larger k value, the faster the rate of oxidation at the modified electrode [113].

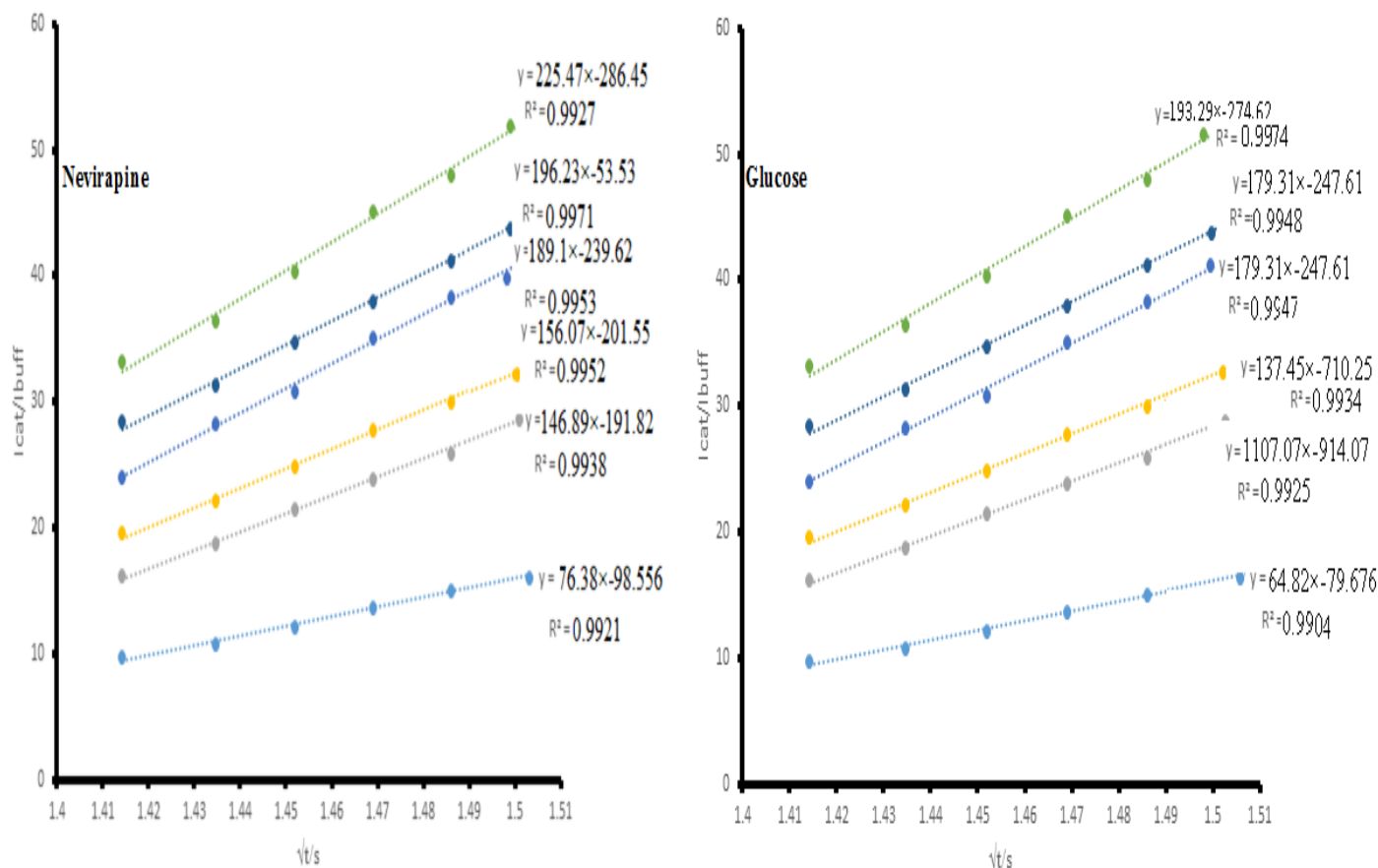


Fig 4.10.b Plot of slopes vs. $\sqrt{[nevirapine]}$ and $[glucose]$

4.10 Limit of detection and quantification of nevirapine and glucose.

The limits of detection (LOD) and quantitation (LOQ) were calculated using the relation kS_b/m [61], where $k = 3$ for LOD and 10 for LOQ, S_b representing the standard deviation of the peaks current of the blank ($n = 6$) and m representing the slope of the first calibration curve for nevirapine. Both LOD and LOQ values were found to be 53.2 nM and 177.5 nM respectively. These values indicated the sensitivity of the proposed method. Differential pulse voltammetry (DPV) was used to determine the linear ranges and the detection limit of glucose or nevirapine at GNR/TiO₂/GCE [114]. The use of (DPV) was based on the fact that it has a much higher current sensitivity than cyclic voltammetry. Fig 4.11 shows the voltammograms obtained for GNR/TiO₂ electrode in different concentrations (0.2 - 1.4 μ M) of nevirapine (A) and glucose (B) in a 0.1 M phosphate buffer solution (pH 11). The inset shown in Fig 4.11 demonstrates the linear relationships of electro catalytic current versus nevirapine (A) and glucose (B) concentration in the linear range 0.2 to 1.4 μ M. The lower detection limit C_m was found to be 1.282×10^{-7} M for nevirapine and 1.27×10^{-7} M for glucose using the equation $C_m = \frac{3s_{bl}}{m}$ where s_{bl} is the standard deviation of blank solution, m is the slope calibration plot. More over the limit of quantification was calculated to be 3.882×10^{-7} M for nevirapine and 3.882×10^{-7} M for glucose by limit of quantitation $= \frac{10s}{m}$ [115].

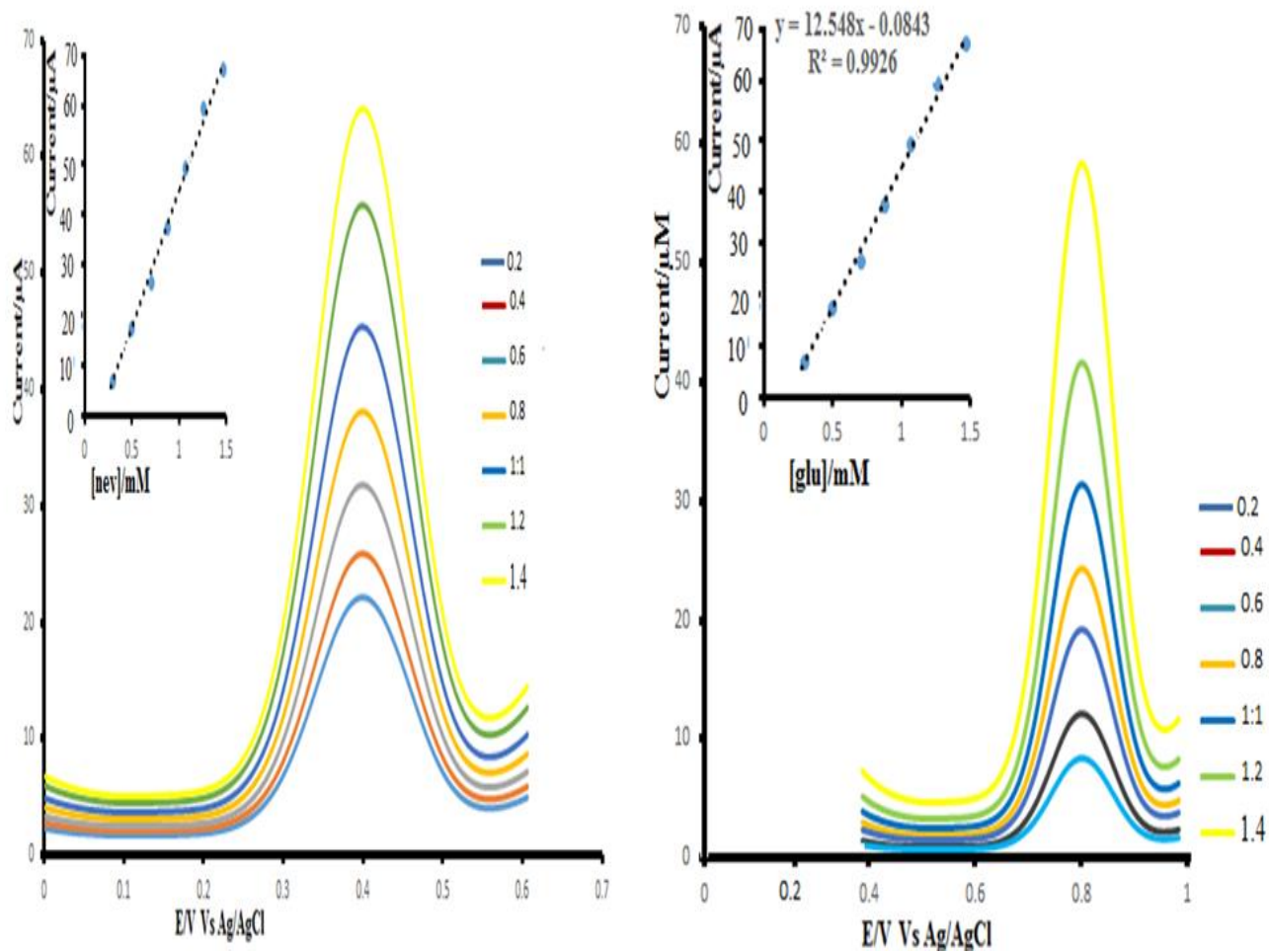


Fig 4.11 DPV (A) nevirapine and glucose (B) for GNR/TiO₂/GCE in: a) 0.2 μM, b) 0.4 μM, c) 0.6 μM, d) 0.8 μM, e) 1 μM, f) 1.2 μM, g) 1.4 μM. Inset: Plot of I_{pc} vs [nev] and [glc] [104].

Table 4.2: Detection limits of nevirapine and glucose

Analyst	Modifier	Linear working range(M)	Limit of Detection	Reference
Nevirapine	Ura/CPE	0.1-70.0 μM	1.026 μM	[25]
	Gold electrode	-	1.1- 6 μM	[14]
	GCE	5.0-350 μM	1.026 μM	[13]
	CuO/CNP/GCE	0.1-100 μM	66 Mm	[16]
	AuNPs/p((MB)/MWCNTs/GE	0.1-50 μM	55.6 μM	[14]
	GNR/TiO ₂ /GCE	50-400 μM	$1.282 \times 10^{-7} \mu\text{M}$	This work
Glucose	Pt _{0.7} Co _{0.3} /C	0.1-142	30	[49]
	Pd,pt ₃ /graphene	1-23	5	[50]
	PtCo-CD-1L/GCE	Up to 20	100	[51]
	Nanoparticles/MWNTs	1-15	25	[55]
	NiCo ₂ S ₄ /GCE	0.0005-0.1	2	[56]
	GNR/TiO ₂ /GCE	0.2-1.4	$1.27 \times 10^{-7} \text{M}$	This work

4.11 Limit of detection and quantification for simultaneous of nevirapine and glucose.

The simultaneous detection of nevirapine and glucose at GNR/TiO₂/GCE functionalized electrode was detected by differential pulse voltammetry (DPV). Figure 4.12 a shows DPV voltammograms responses of different concentrations of nevirapine in 0.1 M PBS buffer (pH 11) with a constant of 0.2 μM glucose. The consequences show that the peak current was proportional to the concentration of nevirapine while the peak current of glucose almost keeps constant, indicating that the oxidation of nevirapine and glucose at GNR/TiO₂/GCE takes place independently. As shown in the Fig. 4.12 inset the peak current linearly increased with the increase in glucose concentration ranging from 0.2 to 1.4 μM with a correlation coefficient (R²) of 0.9961. The linear regression equation was expressed as $I (\mu A) = 341.49 C (\mu M) + 0.0002$, and the limit of detection (LOD) of the method at a signal to noise ratio of 3 was found to be 7.094×10^{-8} M. Sensor responses for different concentrations of nevirapine at a fixed concentration of 0.2 μM glucose are presented in Fig. 4.12 b. The linear regression equation was expressed as $I (\mu A) = 113.08 C (\mu M) + 8 \times 10^{-5}$, and the limit of detection (LOD) of the method at a signal to noise ratio of 3 was found to be 1.064×10^{-7} M [129]. sensor response for different concentrations of glucose at a fixed concentration of 0.2 μM while the concentration of nevirapine at (0.2 to 0.8 μM) in this relationship [116]. Differential pulse voltammograms was used for the study of both nevirapine and glucose in the same solution were also recorded and it was found that when concentrations of both compounds increase simultaneously, both compounds exhibits oxidation peaks separately without interfering each other [121]. However, there was no paper been published for the simultaneous detection of nevirapine and glucose by electrochemical methods. In this report, a voltammetric sensor for the simultaneous detection of nevirapine and glucose was developed at a GCE modified with GNR/TiO₂/GCE composite. This aforesaid sensor exhibited a wide linearity of 0.2-0.8 μM for

nevirapine and glucose and It was also found that the limit of detection of nevirapine was found to be 7.094×10^{-8} M and 1.064×10^{-8} M for glucose [117]. It was also found that oxidation peaks observed for nevirapine and glucose in same solution do not interfere with each other using GNR/TiO₂ [127]. Thus, it can be concluded that the proposed sensor can be successfully applied for the simultaneous determination of nevirapine and glucose [128].

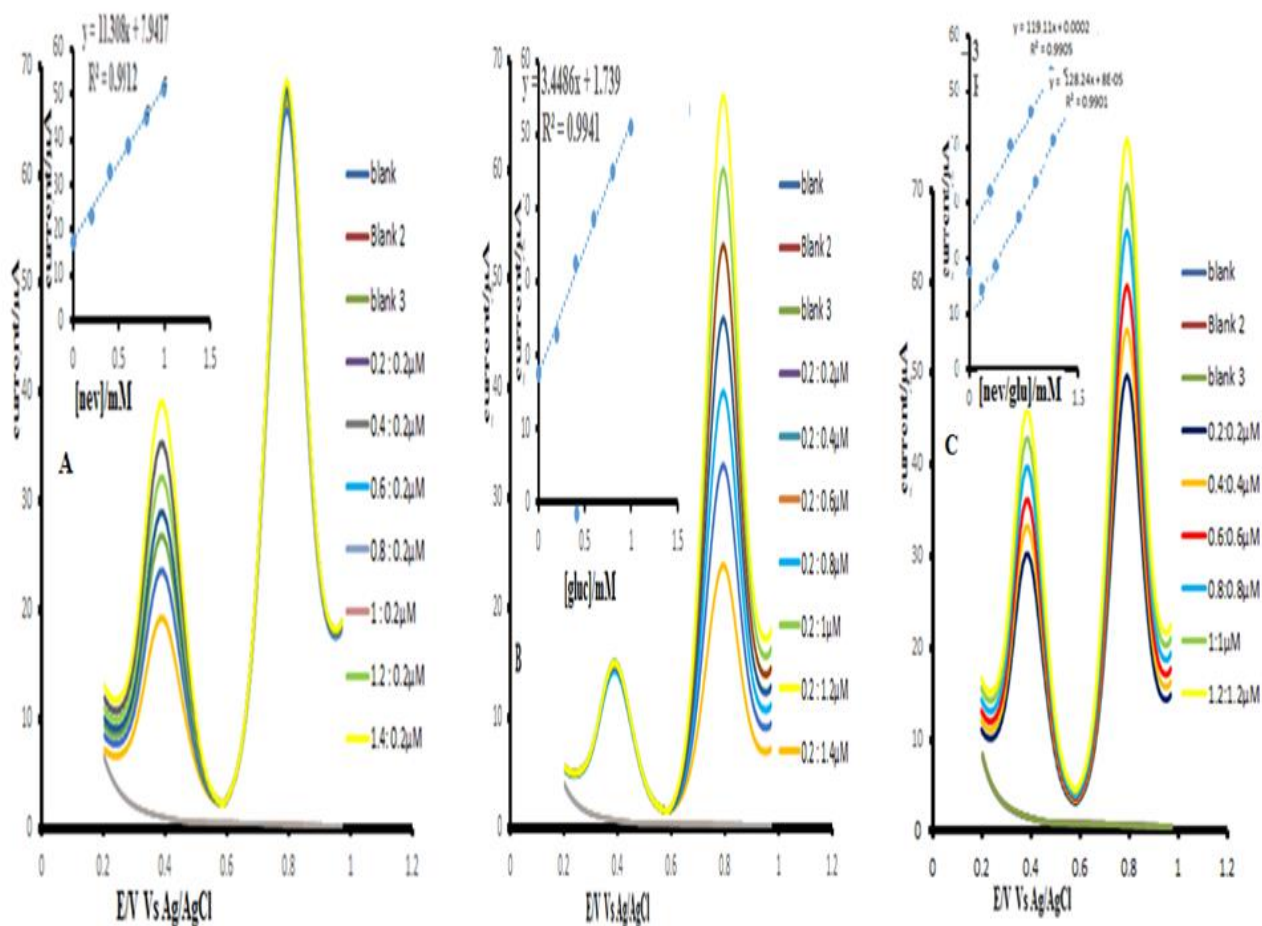


Fig. 4.12 DPV voltammograms of: a) 0.2 μ M, b) 0.4 μ M, c) 0.6 μ M, d) 0.8 μ M, e) 1 μ M, f) 1.2 μ M, g) 1.4 μ M nevirapine in the presence of 0.2 μ M glucose (A) and DPV voltammograms of: a) 0.2 μ M, b) 0.4 μ M, c) 0.6 μ M, d) 0.8 μ M, e) 1 μ M, f) 1.2 μ M, g) 1.4 μ M glucose in the presence of 0.2 μ M nevirapine (B). Insets: the calibration graphs of nevirapine and glucose (c).

4.12 simultaneous detection of nevirapine and glucose.

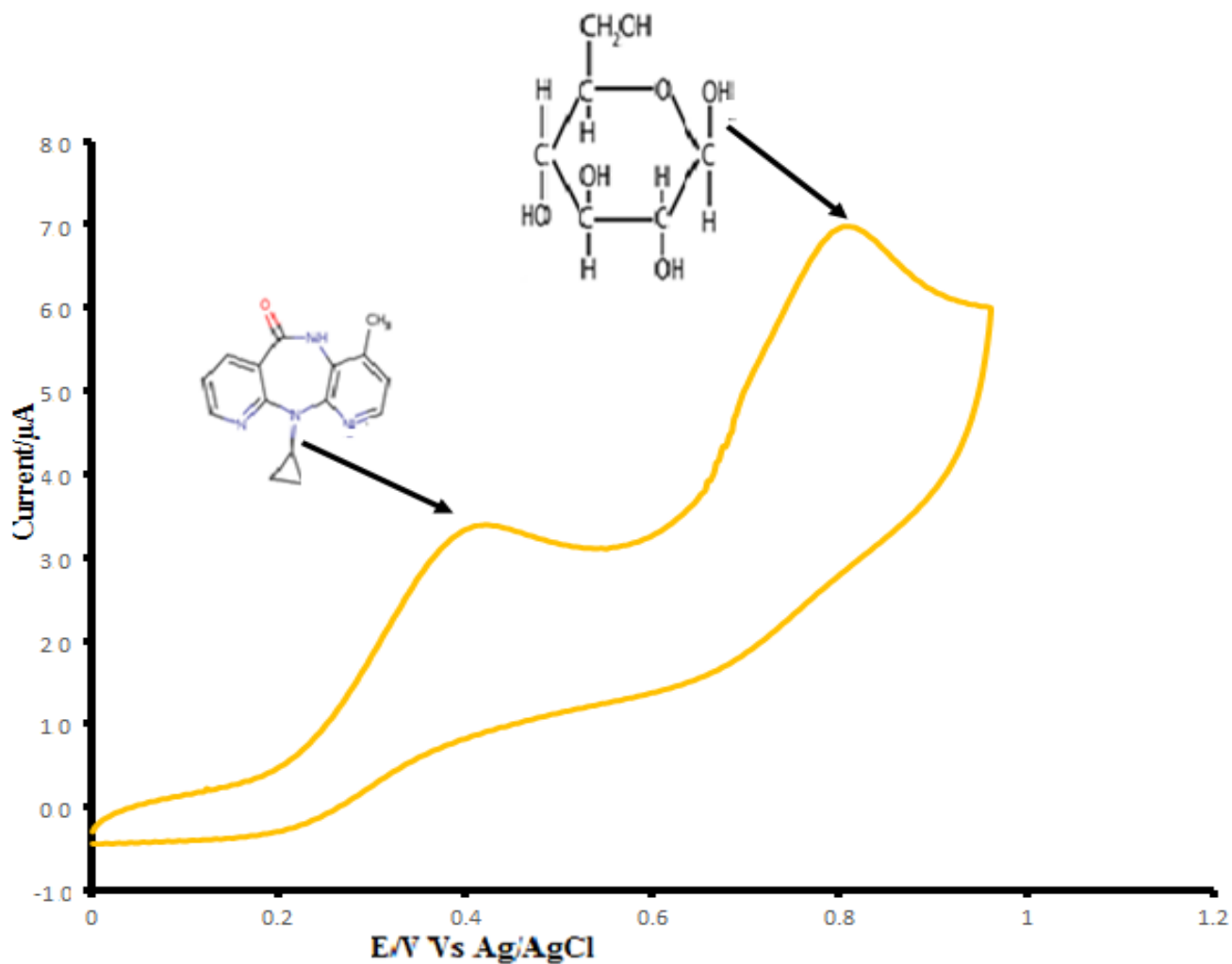


Fig 4.13: simultaneous determination of 0.1 mM nevirapine and glucose in 0.1 M PBS buffer (pH 11). The simultaneous determination of nevirapine and glucose was first conducted in 0.1 M PBS buffer (pH 11). The concentrations of nevirapine and glucose were 0.1 mM.

4.13 Scan rate

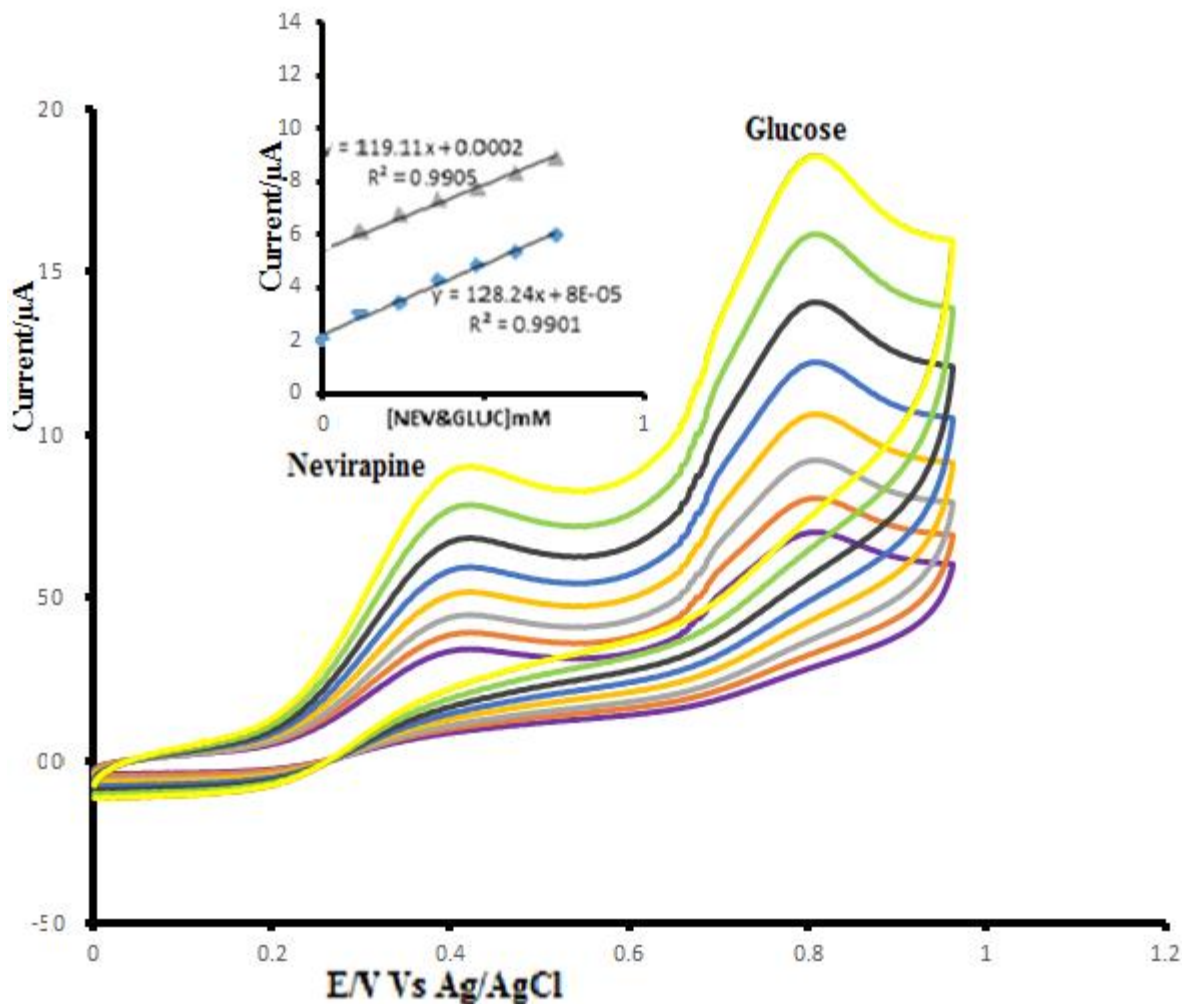


Fig 4.14 cyclic voltammetry (CV) was performed for simultaneous detection of 0.1 mM nevirapine and glucose in 0.1 M PBS buffer (pH 11) at GNR/TiO₂/GCE. Inset: plot of the relationship of ipa and $\sqrt{\text{scan rate}}$. The relationship between the peak current intensity and scan rate increase obviously when scan rate increase [118]. As can be seen in fig. 4.15, the value of the oxidation peak potential of nevirapine shifted to more positive potential with increase in (pH 11.0). The effective surface coverage of the modified electrode (GNR/TiO₂/GCE) for the simultaneous determination of nevirapine and glucose was found to be 0.18109 cm² and 0.1615 cm² [130]. Scan

rate studies were done from 50 to 400 mV/s⁻¹. The value of R² for nevirapine was 0.9905 and R² for glucose was 0.9901 [119].

4.14 Stability Studies

The stability of GNR/TiO₂ under working conditions was investigated using cyclic voltammetry by continuous scanning the electrode for 20 cycles in the presence of 1 mM of nevirapine (A) and glucose (B) Fig 4.15 indicates the response stability of GNR/TiO₂/GCE in 1 mM of nevirapine (A) and glucose (B) solution at a scan rate of 0.1 mV/s⁻¹ and a potential range of 0 to 1.0. As shown the anodic peak current of nevirapine (A) oxidation remained almost constant during the experiment indicating that there was minimum signal loss of about 1% for the sensor as it remained stable after continuous cycles in nevirapine solution. But for glucose there was a high signal loss which was attributed to strong interaction between electrode and the glucose molecule after the first scan the current stabilized.

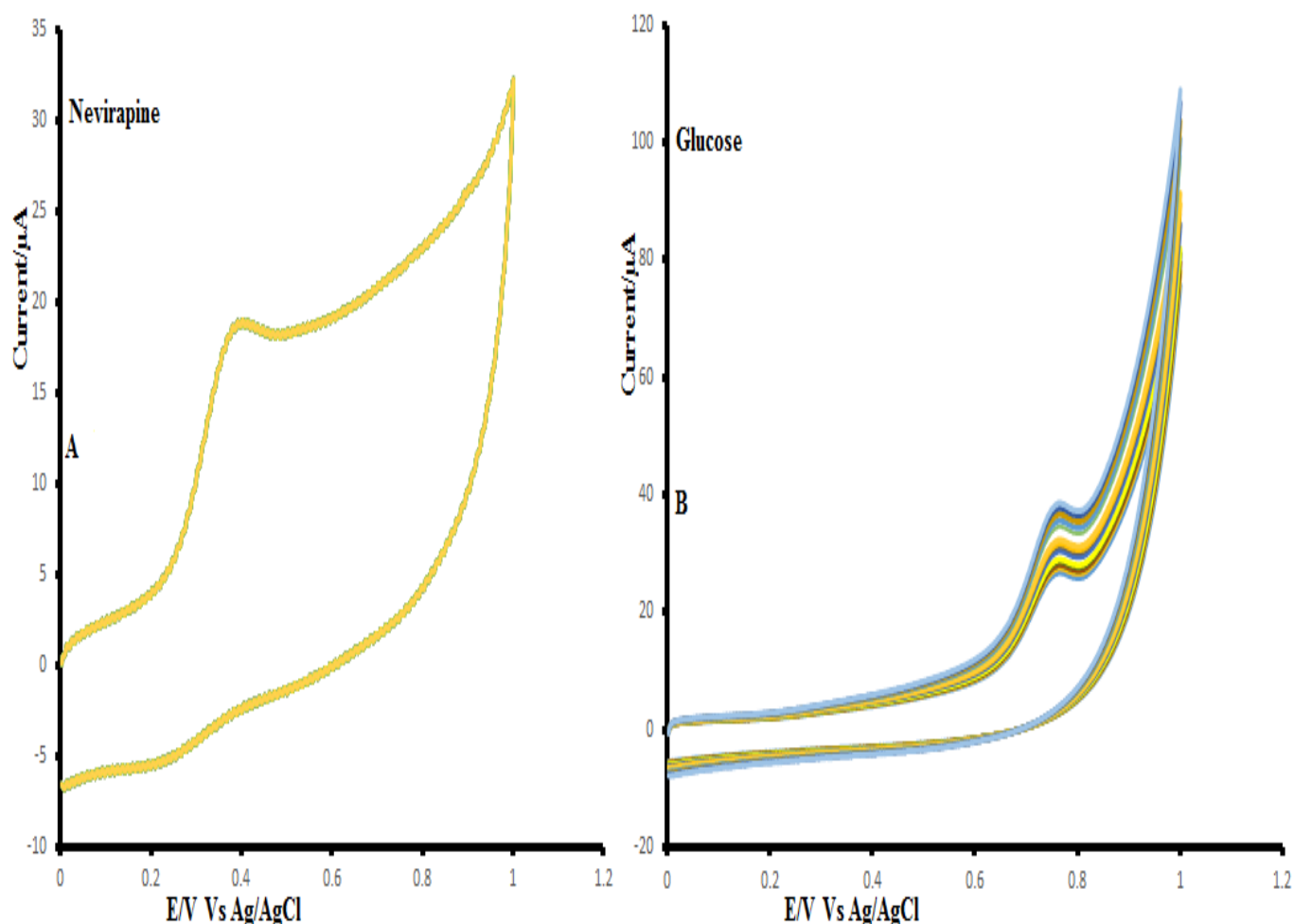


Fig 4.15: Cyclic voltammograms of the detection of 0.1 mM nevirapine (A) and glucose (B) obtained after 20 continuous cycles scan rate = 100 mV/s^{-1} PBS pH 11.

4.15 Reproducibility studies

To evaluate the reproducibility of GNR/TiO₂, the cyclic voltammetry was carried out in 0.1 mM nevirapine (A) and glucose (B) in PBS pH 11 at scanning potential range of 0 to 0.05V. After each run, the electrode was washed with ethanol to remove any substrate on the electrode surface and the procedure was repeated four times [89]. These study was done to evaluate the performance of the electrode by investigating current response from the study it was found that the electrode

showed only 3% decrease in current for both nevirapine and glucose response suggesting that the electrode is highly stable and reproducible.

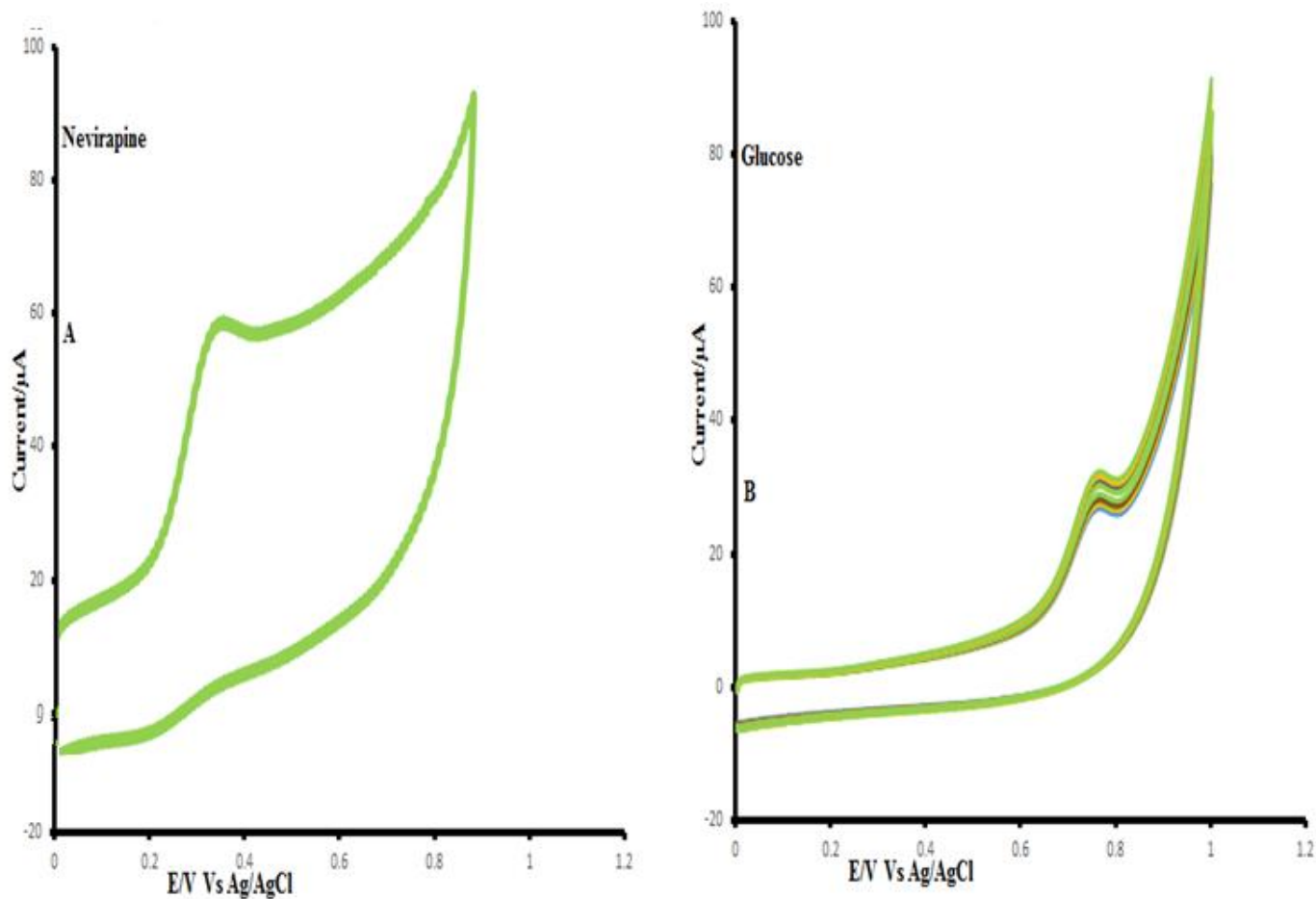


Fig 4.16: Cyclic Voltammograms of the detection of 0.1 mM Nevirapine (A) and Glucose (B) obtained after 5 test runs Scan rate = 100 mV/s in 0.1mM pH 11 PBS.

4.16 Interference studies

Under optimized conditions, the influence of different interferants in the detection of nevirapine was investigated within the voltammetric response of 0.76 μM nevirapine in 0.1 mM PBS. The

tolerance limit was defined as the maximum ratio of interfering to nevirapine was unaffected even in the presence of 5-fold concentration of sodium chloride (NaCl) and ascorbic acid (AA). In this study, the interferants were chosen based on their point sources such as liquid drips (NaCl) and vitamin supplements (AA), which are commonly within reach of HIV patients.

Table 4.3 Effect of possible interfering compounds on nevirapine detection.

Interfering Compound	Mole ratio of NVP: interferant			
	NVP Alone	1:1	5:1	1:5
NaCl	0.650	0.681(4.78)	0.721(10.92)	0.98(3.16)
Ascorbic acid (AA)	0.731	0.828(13.27)	0.923(26.13)	1.07(9.60)

Fig 4.16 shows the peak potential for the oxidation of nevirapine in the presence of NaCl and AA. From this observation (Fig 4.17), there is significantly little effect on the current response of nevirapine even in the presence of 10-fold excess of the interferants (Table 4.3). This revealed the practical applicability of the proposed electrode for the determination of nevirapine in the presence of several other compounds that may be present in clinical samples.

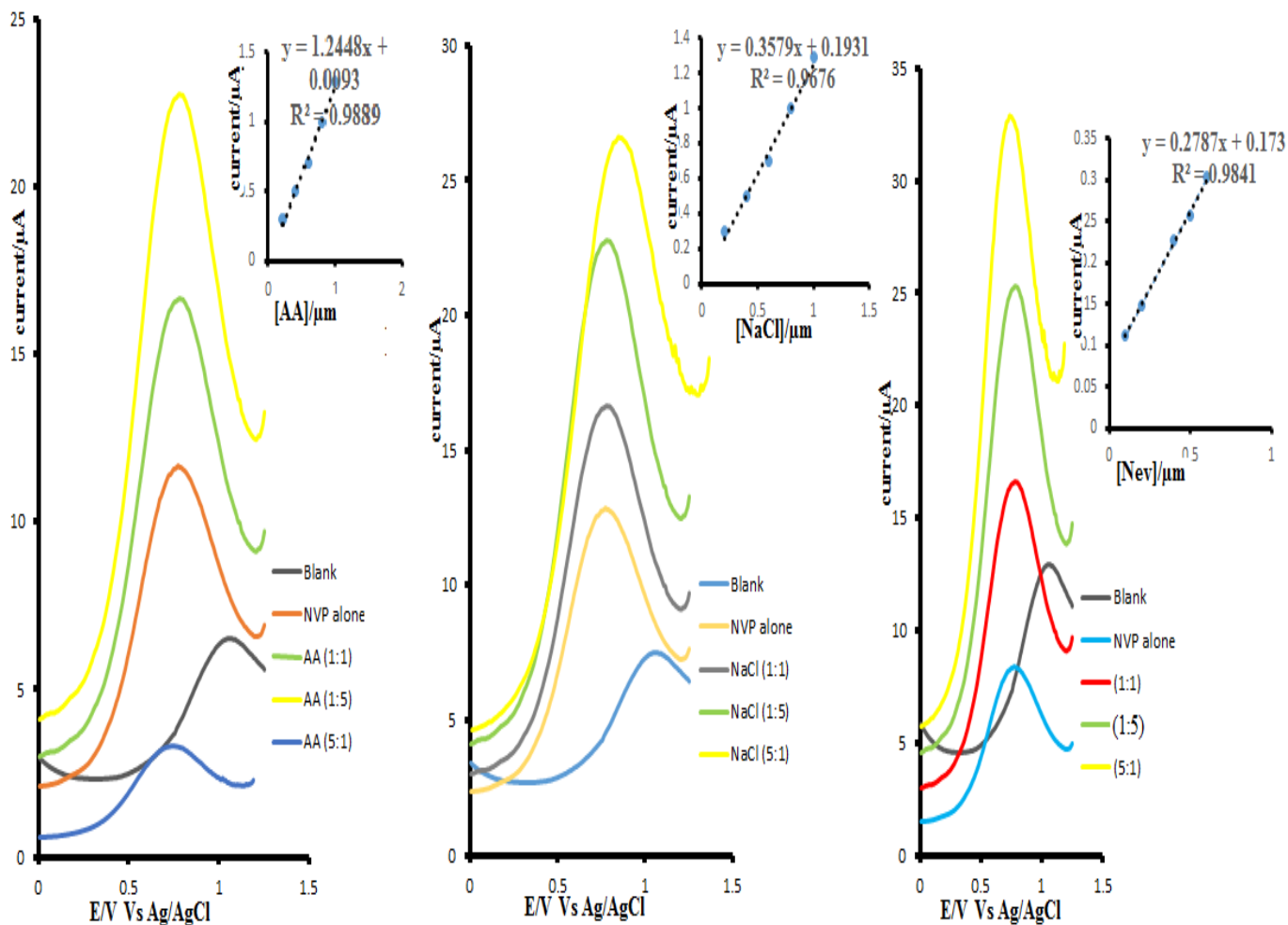


Fig 4.17 Interference plots of AA and NaCl₂ with 0.76 μM nev at various interferants: nevirapine ratios and nevirapine alone.

4.17.0 Real sample analysis

4. 17.1 Determination of nevirapine in urine samples

To prove the applicability of the proposed electrode as a nevirapine voltammetric sensor in real sample, the tablet (200 mg nevirapine per tablet) and human urine were analyzed by the standard addition method using DPV under optimized condition [120]. The proposed method was applied for the detection of nevirapine in urine samples of healthy volunteers, but not to

urine samples of patients treated with nevirapine [120]. In order to validate the proposed electrochemical procedure, GNR/TiO₂/GCE was utilized to detect nevirapine concentration in human urine samples with different amounts of standard nevirapine solutions in the range of 0.76-1.52 μM [121]. The recoveries from the urine samples were measured by drug free with urine with known amounts of nevirapine and differential pulse voltammograms were then recorded [122]. The amounts of nevirapine in the urine samples were then evaluated from the calibration graph [122]. The results obtained are listed in table 2.

It can be observed that the recovery range for nevirapine was between 87 % and 103 %. The average recovery values 95% and RSD values less than 2.57%, which indicate the high accuracy and precision of the proposed method [122]. The percent recovery of nevirapine was determined by comparing the peak currents of the drug in urine with those of pure nevirapine using the calibration curve. These show that the proposed method was readily acceptable for analytical applications. The average recovery values, higher than 94.74 %, and RSD values less than 2.47 %, indicate the high accuracy and precision of the proposed method.

Table 4.4. Results of analysis of nevirapine in spiked milk and human urine samples (n = 3)

	NVP (μM)	Recovery, (μM)	% Recovery	% RSD
urine	0.76	0.81	87%	1.95
samples	1.14	1.17	103%	1.91
	1.52	1.35	95%	2.07

4.17.2 Analysis of NVP in pharmaceutical tablets

The practical analytical application of the DPV method was further established by determining nevirapine concentrations in tablets. The nevirapine tablet was crushed and soaked in methanol for 24 hours. The suspension was filtered, the resulting solution was transferred to a 100 mL volumetric flask and the volume was completed with methanol. It contained 3.57 mg mL⁻¹ of nevirapine and the working solutions were prepared from this solution. Voltammograms of sample solutions were recorded as shown in (Fig4.18) [123]. The results obtained by means of the standard addition method showed that the content of nevirapine tablet was well estimated in the presence of nevirapine. Three standard additions were used of 2.5, 10 and 15 μL on 0.76 μM nevirapine equivalent to 1.14, 2.28 and 3.04 μM respectively [114].

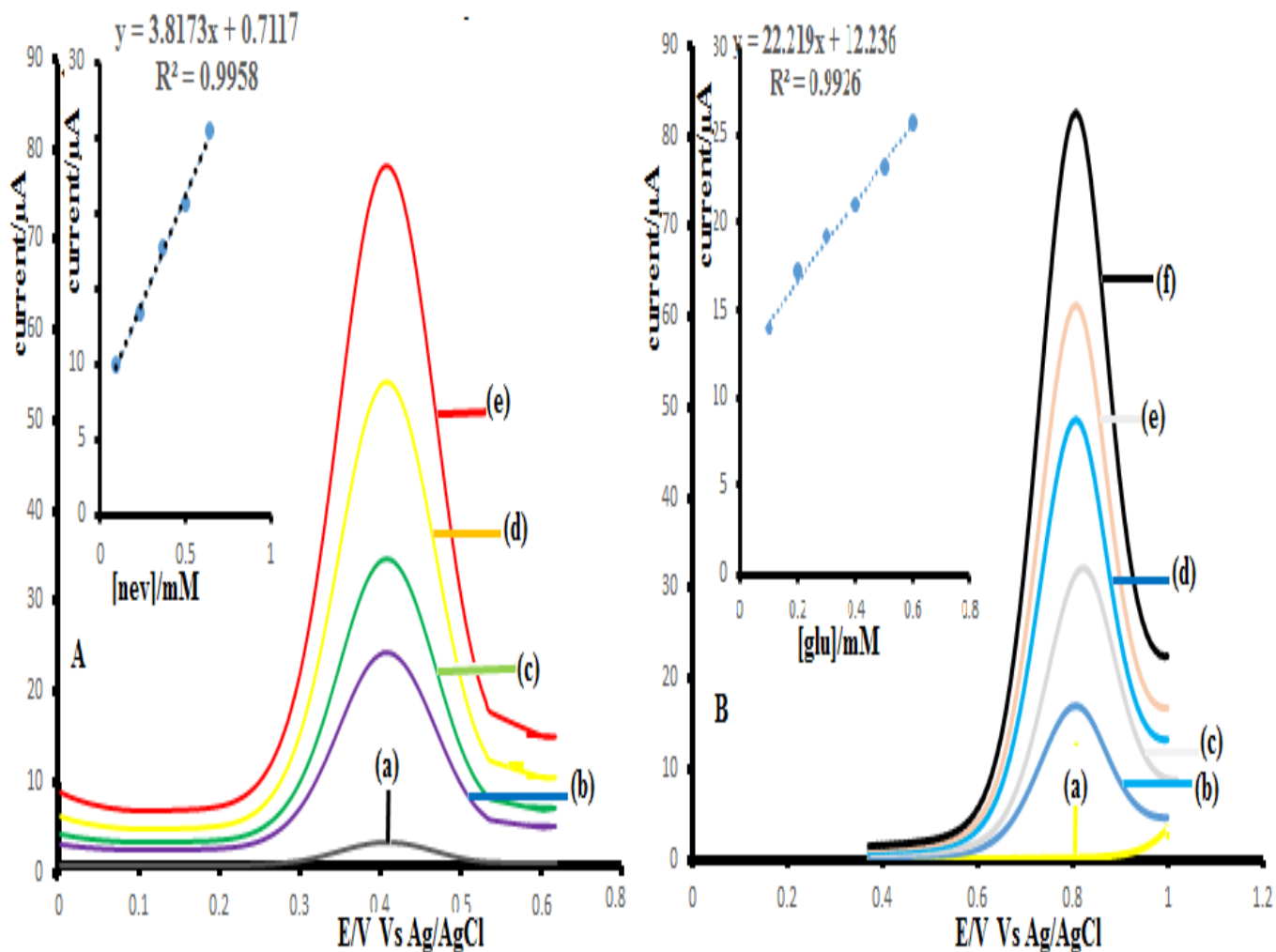


Figure 4.18: DPV plot showing the standard additions methods for nevirapine tablet at 20 mV s⁻¹ (A) and glucose (B) 0.1 mM in 0.1mM pH 11 PBS.

Table 4.5 Determination of nevirapine in pharmaceutical tablet (Nevirapine, 200 mg)

	Standard addition of NVP tablet to NVP		
	Nvp: 5	NVP: 10	NVP: 15
Concentration (μM)	1.26	2.12	2.80
% Recovery	109.2 \pm 2.7	92.8 \pm 1.1	93.1 \pm 0.9
% RSD	4.07	1.43	1.38

The low RSD values highlighted the reproducibility of the results (Table 4.5). Recovery studies were carried out using a standard addition method. Known quantities of pure nevirapine were mixed with defined amounts of pre-analyzed formulations; then the mixtures were analyzed as before. The total amount of the drug was then determined, and the amount of drug added was calculated by the difference. The high percentage of recovery indicates that the commonly encountered excipients in the formulation did not interfere with the proposed method.

4.18 interferants of glucose

Selectivity is one of the most important attributes of a biosensor. In particular, it is very important to use a nonenzymatic glucose biosensor without enzymes such as glucose oxidase, which reacts only to glucose. In general, some oxidizable compounds including ascorbic acid (GA), ascorbic acid (AA) and uric acid (UA) and (0.1 mM each) can interfere with the electrochemical signal of glucose [115, 123]. The physiological level of glucose in normal serum was 0-4 mM and the levels of these interfering species are no more than 0.1 mM, though a ratio between glucose and interferences was even higher in food samples. Since the interfering species have higher electron transfer rates than glucose, their oxidation currents are comparable to that of high concentrated glucose. It was expected that the well-distributed TiO₂ nanoparticles on the GNRs with a high effective surface area would give high sensitivity and selectivity for glucose detection under physiological conditions, because a high real surface area of an electrode favors a kinetically controlled sluggish reaction (the electrooxidation for glucose), while the electrooxidation of the interfering species being diffusion-controlled does not depend significantly on the electrode surface. As shown in (Fig. 4.20), the interference currents by GA, AA and UA were negligible, unlike the strong response by glucose. The current response by GA, AA and UA was only 2.4%, 2.3%, 1.9%, and 0.3% respectively [130]. These results suggest that the GNR/TiO₂/GCE electrode has high selectivity for the detection of glucose [124].

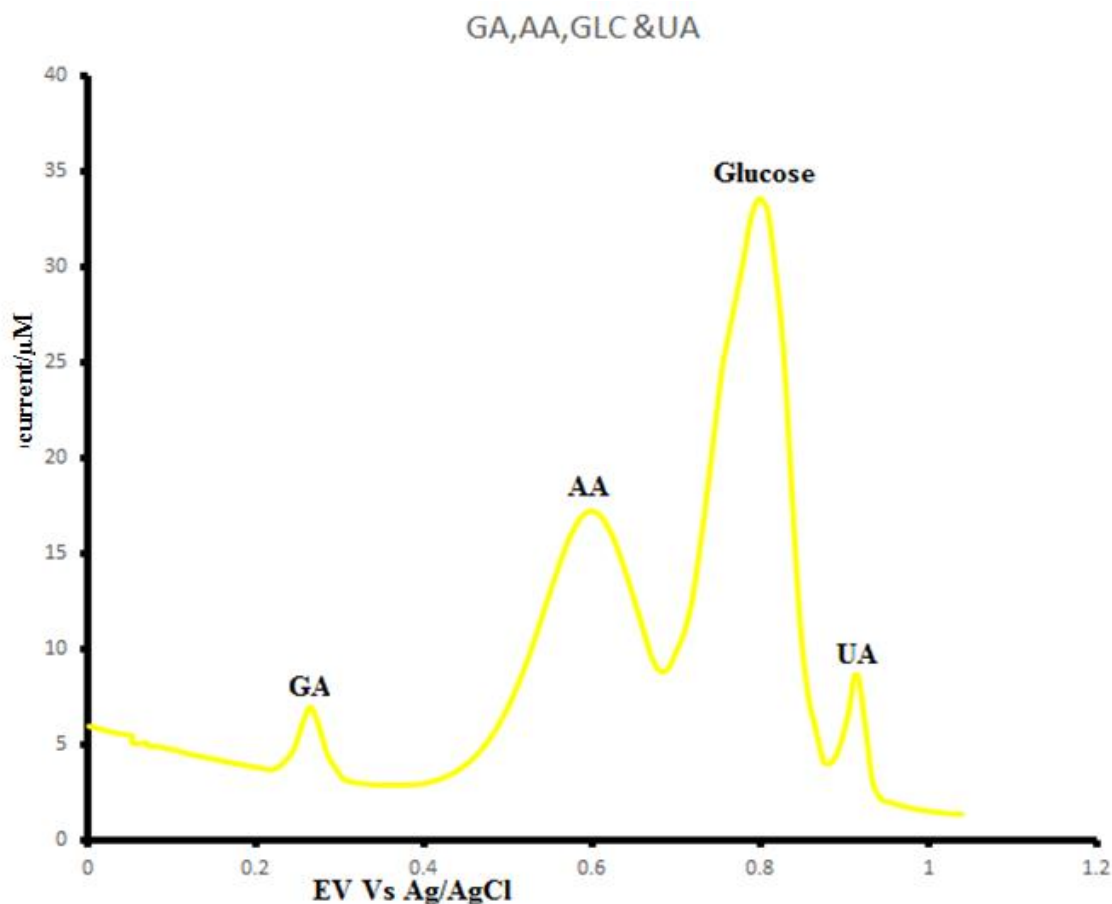


Fig 4.19: DPVs was used for the interferences studies of (i) GA (ii) AA (B) (iii) glucose and (iv) UA in 0.1 PBS at GNR/TiO₂/GCE.

4.19 Real sample detection for glucose.

To evaluate its applicability, the electrode was used for detection of glucose in human urine samples. The recovery measurements were first carried out. Four samples with the known glucose concentrations were sampled and certain amounts of glucose were added. The results were presented in (Table 4.6). The average recoveries for the four different samples are 100.5, 100.3, 100.1, and 99.0%, respectively, and the RSD was 2.37, 2.75, 3.49, and 4.67%, respectively, indicating that the developed electrode has high accuracy in measuring glucose. Five urine samples were analyzed using five independently prepared electrodes (one electrode per sample). Only an

appropriate dilution of the samples with the supporting electrolyte (PBS, pH 11) was needed before the measurements were performed [131]. The determined results were compared with those measured with a commercial blood glucose monitoring system (Table 4.6). It was shown that the values measured by the developed electrode were in good agreement with the data from the commercial monitor, demonstrating the developed nonenzymatic glucose electrode has great potential for practical application for the analysis of glucose in real clinical samples [125].

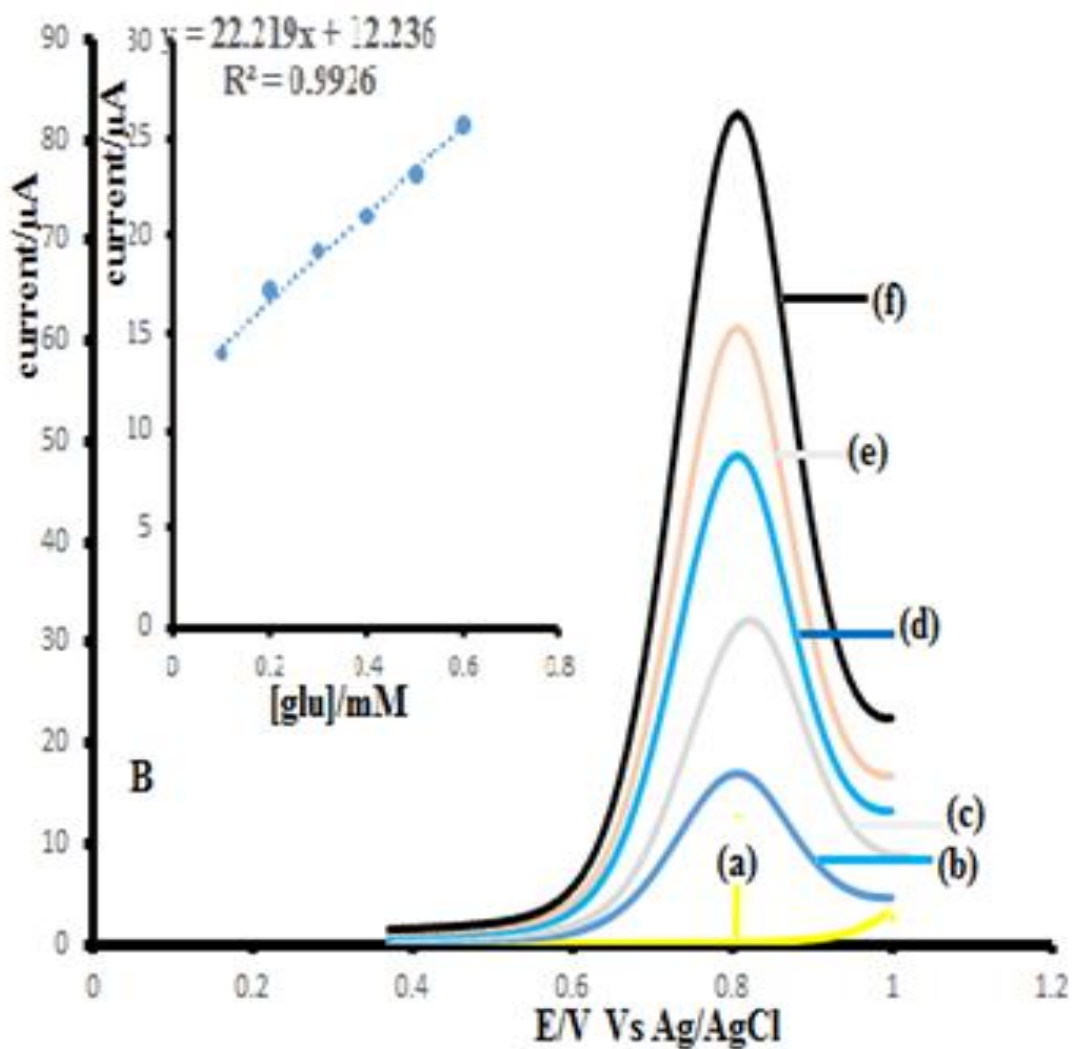


Fig 4.20 differential pulse voltammogram of (a) 0.1 M PBS + human urine (without glucose), (b)

0.1 M PBS + human urine + glucose 0.003 M, (c) 0.1 M PBS + human urine + glucose 0.005 M (d)0.1 M PBS + human urine + glucose 0.007 M (e) 0.1 M PBS [122].

Table 1 shows the results of recovery of determination of glucose in human urine using differential pulse voltammogram at glassy carbon electrode by the 0.1 M PBS electrolyte [126]. Determination of glucose in human urine by differential pulse voltammogram at glassy carbon electrode by 0.1 M PBS electrolyte has very good recovery value that was in the range 95-105%.

Table 4.6: Determination of glucose in human urine.

urine samples	Glucose added (μM)	Glucose founded %	% RSD
Sample 1	3.00	2.99	99.67
Sample 2	5.00	5.12	102.40
Sample 3	7.00	6.79	97.00
Sample 4	9.00	87.8	97.56

CHAPTER FIVE

5.0 Introduction

This chapter concludes the work done in the research and gives recommendations to these work pertaining the future of the study.

5.1 Conclusion

On the basis of good electrochemical activity, an ultra-sensitive reproducible and stable modified electrode GNR/TiO₂/GCE was developed for the detection of nevirapine and glucose. The modifier (GNR, TiO₂ and GNR/TiO₂) were characterized by FT-IR, UV- vis and TGA to show the extent of modification and confirm the incorporation of the TiO₂ into the graphene nanoribbon (GNR) [103]. Cyclic voltammetry and electrochemical impedance spectroscopy (EIS) were further applied in the characterization of the electrode modifier (GNR, TiO₂ and GNR/TiO₂) to study their behavior with respect to charge transfer resistant and electron transfer kinetics. Electrocatalytic detection of nevirapine and glucose were optimized at pH 11.0 in phosphate buffer solution. Differential pulse voltammetry (DPV), Linear sweep voltammetry (LSV), cyclic voltammetry (CV) and chronoamperometry were used in the study of electrocatalytic detection of nevirapine and glucose. Surface area of the modified electrode was determined using variation of scan rate and was obtained to be 0.40 cm² which was about twice the surface area of bare glass carbon electrode which was an indication of a large surface area for catalysis on the hybrid electrode. The developed method was characterized by high sensitivity and was reproducible for the electrocatalytic detection of nevirapine and glucose. These was confirmed by lower over potentials and higher peak current recorded on the composite electrode. Differential pulse voltammetry was utilized in the determination of (LOD) and (LOQ) which were established to be 53.2 μM and 177.5

μM respectively, which is lower than traditional methods and comparable to available literature of electrochemical methods. Chronoamperometry was used in the establishment of the catalytic rate constant, $2.45 \times 10^1 \text{ M}^{-1}\text{s}^{-1}$ for nevirapine and $2.45 \times 10^1 \text{ M}^{-1}\text{s}^{-1}$ for glucose which shows the applicability of the electrode towards the electrocatalytic detection of nevirapine and glucose. The GNR/TiO₂/GCE electrode revealed good reproducibility and stability towards detection of nevirapine and glucose. These methods showed to be simple and less time consuming for determination of nevirapine and glucose. The Interference studies was carried out using DPV and it was established that the presence of AA, CaCl₂ and NaCl in the same matrix as nevirapine. The maximum ratio of interfering to nevirapine was unaffected even in the presence of 5-fold concentration of sodium chloride (NaCl), calcium chloride (CaCl₂) and ascorbic acid (AA). The developed electrochemical sensor offers a simple and fast wide detection range and convenient method for use in research laboratories. For the glucose, ascorbic acid (GA), ascorbic acid (AA) and uric acid (UA) and (0.1 mM each) can interfere with the electrochemical signal of glucose [114,115].

5.2. Recommendations

There is need to enhance the performance of this newly developed sensor by modifying the chemical sensor with a modifier that prevent/reduce polymerization reaction and extensive electrode fouling during the detection of nevirapine and glucose. There is also a need to synthesize porous GNR for easy embedment of titanium oxide nanoparticles. The electrode can be applied in the detection of multiple analytes and an industrial sample. The advantage of this modification process was that it was fast and relatively stable GNR/TiO₂/GCE layer can be formed on the carbon based electrode where the interactions occur between GNR and TiO₂ and the

substrate surface. The disadvantages are that the electrode surfaces are not reproducible and unstable over long periods of time. Further work can be done using different electrode modification techniques so as to promote excellent reproducibility. Therefore, further studies should be carried out to observe the nanoparticles morphologies, different sizes and shapes, and how they affect the electrochemical process.

REFERENCES

- [1] Meng L, Jin J, Yang G, Lu T, Zhang H, Cai C. Nonenzymatic Electrochemical Detection of Glucose Based on Palladium - Single-Walled Carbon Nanotube Hybrid Nanostructures **2009**;81:7271–80.
- [2] Song Y, Zhu C, Li H, Lin Y. RSC Advances A nonenzymatic electrochemical glucose sensor based on mesoporous Au/Pt nanodendrites† **2015**:82617–22. doi:10.1039/C5RA16953D.
- [3] Rahman MM, Ahammad AJS, Jin JH, Ahn SJ, Lee JJ. A comprehensive review of glucose biosensors based on nanostructured metal-oxides. *Sensors* **2010**;10:4855–86. doi:10.3390/s100504855.
- [4] Palanisamy S, Cheemalapati S, Chen SM. Enzymatic glucose biosensor based on multiwalled carbon nanotubes-zinc oxide composite. *Int J Electrochem Sci* **2012**;7:8394–407.
- [5] Muthuchamy N, Gopalan A, Lee K. Highly selective non-enzymatic electrochemical sensor based on a titanium dioxide nanowire–.RSC Adv **2018**;8:2138–47. doi:10.1039/C7RA09097H.
- [6] J. A. Plambeck, *Electroanalytical chemistry, Basic principles and application*, wiley interscience publication, USA (**1982**).
- [7] *Theoretical Background of Electrochemical Analysis* **2013**. doi:10.1007/978-3-642-34252-3.
- [8] Salimi A, Noorbakhash A, Karonian FS. Carbon Based nevirapine and Further Applications. *Int J Electrochem Sci* 2006;1:435–46. **2016**.

- [9] Shahrokhian S, Kohansal R, Ghalkhani M, Amini MK. Electrodeposition of Copper Oxide Nanoparticles on Precasted Carbon Nanoparticles Film for Electrochemical Investigation of anti-HIV Drug Nevirapine **2015**:1989–97. doi:10.1002/elan.201500027.
- [10] Zhang F, Li L, Luo L. Electrochemical oxidation and determination of antiretroviral drug nevirapine based on uracil-modified carbon paste electrode **2013**:263–9. doi:10.1007/s10800-012-0516-z.
- [11] Jing M, Hou Z, Yang H, Li G, Zhou M, Xu W. Zn₂SnO₄ coated reduced graphene oxide nanoribbons with enhanced electrochemical performance for lithium-ion batteries. *J Mater Res* 2016; 31:3666–74. doi:10.1557/jmr.**2016**.431.
- [12] Solís-Fernández P, Bissett MA, Tsuji M, Ago H. Tunable doping of graphene nanoribbon arrays by chemical functionalization. *Nanoscale* 2015;7:3572–80. doi:10.1039/C4NR07007K.
- [13] Ahmad K, Mohammad A, Rajak R, Mobin SM. Construction of TiO₂ nanosheets modified glassy carbon electrode (GCE/TiO₂) for the detection of hydrazine. *Mater Res Express* **2016**;3:74005. doi:10.1088/2053-1591/3/7/074005.
- [14] Benvidi A, Banaei M, Tezerjani MD, Molahosseini H, Jahanbani S. Impedimetric PSA aptasensor based on the use of a glassy carbon electrode modified with titanium oxide nanoparticles and silk fibroin nanofibers **2017**;2.
- [15] Hallaj R, Haghghi N. Photoelectrochemical amperometric sensing of cyanide using a glassy carbon electrode modified with graphene oxide and titanium dioxide nanoparticles. *Microchim Acta* **2017**;184:3581–90. doi:10.1007/s00604-017-2366-1.

- [16] C. Marzolini, A. Beguin, A. Telenti, A. Schreyer, T. Buclin, J. Biollaz, L.L.A. Decosterd, Determination of lopinavir and nevirapine by high-performance liquid chromatography after solid-phase extraction: application for the assessment of their transplacental passageat delivery, *J. Chromatogr. B Anal. Technol. Biomed. Life Sci.* **774** (2002) 127-140.
- [17] Sanghavi BJ, Srivastava AK. Adsorptive stripping voltammetric determination of imipramine, trimipramine and desipramine employing titanium dioxide nanoparticles and an Amberlite XAD-2 modified glassy carbon paste electrode. *Analyst* **2013**;138:1395. doi:10.1039/c2an36330e.
- [18] Dioxide T, Modified N, Paste C. A Sensitive Voltammetric Determination of Anti-Parkinson Drug Pramipexole Using Titanium Dioxide Nanoparticles Modified Carbon Paste Electrode **2016**;0:1–11. doi:10.5935/0103-5053.20160192.
- [19] Teradal NL, Prashanth SN. Electrochemical studies of nevirapine , an anti-HIV drug , and its assay in tablets and biological samples *2012*;2:67–75. doi:10.5599/jese.**2012**.0008.
- [20] Gholivand MB, Ahmadi E, Haseli M. A novel voltammetric sensor for nevirapine, based on modified graphite electrode by MWCNs/poly(methylene blue)/gold nanoparticle. *Anal Biochem* **2017**. doi:10.1016/j.ab.2017.03.018.
- [21] Xiao P, Zhang Y, Garcia BB, Sepehri S, Liu D, Cao G. Nanostructured electrode with titania nanotube arrays: fabrication, electrochemical properties, and applications for biosensing. *J Nanosci Nanotechnol* *2009*;9:2426–36. doi:10.1166/jnn.**2008**.SE21.
- [22] Ortiz B, Park S-M, Doddapaneni N. Electrochemical and spectroelectrochemical studies of graphene nanoribbon. *J Electrochem Soc* **1996**;143:1800–5. doi:10.1149/1.1836907.

- [23] Stelzle M, Wagner R, Nisch W, Ja W, Schaldach M. On the chemical modification of pacemaker electrodes and patterned surface functionalization of planar substrates **1997**;12:853–65.
- [24] Cao N, Zhang Y. Study of Reduced Graphene Oxide Preparation by Hummers ' Method and Related Characterization **2015**;2015.
- [25] Shumba M, Nyokong T. Electrode modification using nanocomposites of boron or nitrogen doped graphene oxide and cobalt (II) tetra aminophenoxy phthalocyanine nanoparticles. *Electrochim Acta* 2016;196:457–69. doi:10.1016/j.electacta.**2016**.02.166.
- [26] Moore RR, Banks CE, Compton RG. Basal plane pyrolytic graphite modified electrodes: Comparison of carbon nanotubes and graphite powder as electrocatalysts. *Anal Chem* **2004**;76:2677–82. doi:10.1021/ac040017q.
- [27] Banks CE, Crossley A, Salter C, Wilkins SJ, Compton RG. Carbon nanotubes contain metal impurities which are responsible for the “electrocatalysis” seen at some nanotube-modified electrodes. *Angew Chemie - Int Ed* **2006**;45:2533–7. doi:10.1002/anie.200600033.
- [28] S. Notari, C. Mancone, T. Alonzi, M. Tripodi, P. Narciso, P. Ascenzi, Determination of abacavir, amprenavir, didanosine, efavirenz, nevirapine, and stavudine concentration in human plasma by MALDI-TOF/TOF, *J. Chromatogr. B. Anal. Technol. Biomed. Life Sci.* 863 (2008) 249-257.
- [29] R.M. Lopez, L. Pou, M.R. Gomez, I. Ruiz, J. Monterde, Simple and rapid determination of nevirapine in human serum by reversed-phase high-performance liquid chromatography, *J. Chromatogr. B Biomed. Sci. Appl.* 751 (**2001**)371- 376.

- [30] N. Kaul, H. Agrawal, A.R. Paradkar, K.R. Mahadik, HPTLC method for determination of nevirapine in pharmaceutical dosage form, *Talanta* 62 (2004) 843-852.
- [31] R. Sekar, S. Azhaguvel, MEKC determination of antiretroviral reverse transcriptase inhibitors lamivudine, stavudine, and nevirapine in pharmaceutical formulations, *Chromatographia* 67 (2008) 389-398.
- [32] Lingappan, N.; Gal, Y.-S.; Lim, K. T. Synthesis of Reduced Graphene Oxide/Polypyrrole Conductive Composites. *Mol. Cryst. Liq. Cryst.* 2013, 585, 60-66. Hu, C., Yang, D.-P., Xu, K., Cao, H., Wu, B., Cui, D., et al. (2012). Ag@BSA core/shell
- [33] microspheres as an electrochemical interface for sensitive detection of urinary retinal-binding protein. *Analytical Chemistry*, 84, 10324–10331
- [34] M.S.M. Ahmed, J.S. Reddy, I.E. Chakravarth, K. Prabhavathi, *J. Chem. Pharm. Res.* 3(4) (2011) 172-176.
- [35]. Lim, Y. S.; Tan, Y. P.; Lim, H. N.; Tan, W. T.; Mahnaz, M.; Talib, Z. A.; Huang, N. M.; Kassim, A.; Yarmo, M. A. Polypyrrole/Graphene Composite Films70 Synthesized via Potentiostatic Deposition. *J. of Appl. Polym. Sci.* 2013, 128, 224-229
- [36] Gomez R, Jolly SJ, Williams T, Vacca JP et al (2011) Design and synthesis of conformationally constrained inhibitors of nonnucleoside reverse transcriptase. *J Med Chem* 54:7920–7933

- [37] T.V. Sreevidya, B. Narayana, Spectrophotometric determination of nevirapine using tetrathiocyanatocobalt(II) ion as a reagent, *Ecletica Quím.* 35 (2010) 93-102.
- [38] L. Li, Y. Cheng, Y. Ding, Y. Lu, F. Zhang, Application of thioglycolic acid capped nano-ZnS as a fluorescence probe for the determination of nevirapine, *Anal. Methods.* 4 (2010) 93-102.
- [39] S. Shahrokhian, R. Kohansal, M. Ghalkhani, M.K. Amini, Electrodeposition of copper oxide nanoparticles on precasted carbon nanoparticles film for electrochemical investigation of anti-HIV drug nevirapine, *Electroanalysis* 27.
- [40] Anderson, J., Kräusslich, H.G. and Bartenschlager, R. (Ed.) 2009. *Handbook of Experimental Pharmacology*, 189: Antiviral strategies. Springer Verlag, Berlin Heidelberg.
- [41] R.N. Rao, D.D. Shinde, *J. Pharm. Biomed. Anal.* 50 (2009) 994-999.
- [42] *Indian Pharmacopoeia 1996: Addendum 2002*. New Delhi: The controller of publications; (2002) 919 - 921.
- [43] D. Rey, M. Partisani, G. Hess-Kempf, V. Krantz, M. Priester, C. Cheneau, C. Bernard Henry, Ede Mautort, L. Decroix, J.M. Lang, *J. Acq. Immun. Def. Synd.* 37 (2004) 1454-1456.
- [44] C.C.J. Carpenter, M.A. Fischl, S.M. Hammer, M.H. Hirsch, D.M. Jacobsen, D.A. Katzenstein, J.S.G. Montaner, D.D. Richman, M.S. Saag, R.T. Schooley, M.A. Thompson, S. Vella, P.G. Yeni, P.A. Volberding, *J. Amer. Med. Assoc.* 277 (1997) 1962-1969.
- [45] R.M. Gulick, J.M. Mellors, D. Havlir, J.J. Eron, C. Gonzalez, D. McMahon, D.D. Richman, F. T. Valentine, L. Jonas, A. Meibohm, E. A. Emini, J. A. Chodakwitz, *New Engl. J. Med.*

337 (1997) 734-739.

- [46] W. Cavert, D.W. Notermans, K. Staskus, S.W. Wietgreffe, M. Zupancic, K. Gebhard, K. Henry, Z.Q. Zhang, R. Mills, H. McDade, C.M. Schuwirth, J. Goudsmit, S.A. Danner, A.T. Haase, *Science* 276 (1997) 960.
- [47] J.R. Huff, P.S. Anderson, D.B. Olsen, S.S. Carroll, S.D. Young, S.F. Britcher, L.E.E.O. Tran, L.S. Payne, W.C. Lumma, T.A. Lyle, J.R. Huff, P.S. Anderson, D.B. Olsen, S.S. Carroll, D.J. Pettibone, J.A.O. Brien, R.G. Ball, S.K. Balani, J.H. Lin, I. Chen, W.A. Schleif, V.V. Sardana, W.J. Long, V.W. Byrnes, E.A. Emini, L- 743,726 (DMP-266): a novel, highly potent nonnucleoside inhibitor of the human immunodeficiency virus type 1 reverse transcriptase, *Antimicrob. Agents Chemother.* 39 (1995). 2602-2605.
- [48] M.J. Murphy RL, Nevirapine: a Review of its Development, Pharmacological Profile and Potential for Clinical Use, vol. 5, 1996, pp. 1183-1199.
- [49] Famigliani, V. and Silvestri, R. 2016. Review Focus on Chirality of HIV-1 Non-Nucleoside Reverse Transcriptase Inhibitors. *Molecules*, 21: 221.
- [50] B. Uslu, S.A. Ozkan, *Comb. Chem. High T. Scr.* 10 (2007) 495-513.
- [51] V.K. Gupta, R. Jain, K. Radhapyari, N. Jadon, S. Agarwal, *Anal. Biochem.* 408 (2011) 179–196.
- [52] Hammam, E. 2004. Behaviour and quantification studies of amiloride drug using cyclic and square-wave adsorptive stripping voltammetry at a mercury electrode. *J. Pharm. Biomed.*

Anal., 34: 1109-1116.

[53] Danaei, G.; Finucane, M. M.; Lu, Y.; Singh, G. M.; Cowan, M. J.; Paciorek, C. J.; Lin, J. K.; Farzadfar, F.; Khang, Y.-H.; Stevens, G. A.; Rao, M.; Ali, M. K.; Riley, L. M.; Robinson, C. A.; Ezzati, M., National, Regional, and Global Trends in Fasting Plasma Glucose and Diabetes Prevalence Since 1980: Systematic Analysis of Health Examination Surveys and Epidemiological Studies with 370 Country-Years and 2.7 Million Participants. *Lancet* **2011**, 378, 31-40.

[54] WHO, Diabetes. August **2011**, Fact sheet No312.

[55] How GTS, Pandikumar A, Ming HN, Ngee LH. Highly exposed {001} facets of titanium dioxide modified with reduced graphene oxide for dopamine sensing. *Sci Rep* 2014;4:2–9. doi:10.1038/srep05044.

[56] Sagu JS, Peiris TAN, Wijayantha KGU. Rapid and simple potentiostatic deposition of copper (II) oxide thin films. *Electrochem Commun* 2014;42:68–71. doi:10.1016/j.elecom.2014.02.014.

[57] Fouladgar M, Mohammadzadeh S. Determination of Methimazole on a Multiwall Carbon Nanotube Titanium Dioxide Nanoparticle Paste Electrode. *Anal Lett* **2014**;47:763–77. doi:10.1080/00032719.2013.855782.

[58] Wilson J. Cyclic Voltammetric Study of ferrocyanide/ferricyanide Redox Couple. vol. 4. Virginia: **2000**.

[59] Periasamy AP, Ting SW, Chen S. Amperometric and Impedimetric H₂O₂ Biosensor Based on Horseradish Peroxidase Covalently Immobilized at Ruthenium Oxide Nanoparticles

- Modified Electrode **2011**;6:2688–709.
- [60] Nicholson RS. Theory and Application of Cyclic Voltammetry for Measurement of Electrode Reaction Kinetics. *Anal Chem* **1965**;37:1351–5. doi:10.1021/ac60230a016.
- [61] Dou KP, Kaun C-C, Zhang R-Q. Selective interface transparency in graphene nanoribbon based molecular junctions. *Nanoscale* **2018**. doi:10.1039/C7NR08564H.
- [62] Song YZ, Yang MJ, Yuan J, Han XL. Determination of norepinephrine tartrate at oxidized graphene nanoribbon modified glassy carbon electrode. *Int J Electrochem Sci* **2016**;11:9030–40. doi:10.20964/2016.11.20.
- [63] DuVall SH, McCreery RL. Control of catechol and hydroquinone electron-transfer kinetics on native and modified glassy carbon electrodes. *Anal Chem* **1999**;71:4594–602. doi:10.1021/ac990399d.
- [64] Kissinger PT, Heineman WR. Cyclic voltammetry. *J Chem Educ* **1983**;60:702. doi:10.1021/ed060p702.
- [65] Brown JH. Development and Use of a Cyclic Voltammetry Simulator To Introduce Undergraduate Students to Electrochemical Simulations. *J Chem Educ* **2015**;92:1490–6. doi:10.1021/acs.jchemed.5b00225.
- [66] B.S. Kappelhoff, H. Rosing, A.D. Huitema, J.H. Beijnen, Simple and rapid method for the simultaneous determination of the non-nucleoside reverse transcriptase inhibitors efavirenz and nevirapine in human plasma using liquid chromatography, *J. Chromatogr. B* 792 (2003) 353-362.
- [67] Settle F a. *Handbook of Instrumental Techniques for Analytical Chemistry*. Prentice Hall

- PTR **1997**:968. doi:10.1109/MEI.1998.730821.
- [68] Bard a, Faulkner L. Allen J. Bard and Larry R. Faulkner, *Electrochemical Methods: Fundamentals and Applications*, New York: Wiley, **2001**. Russ J Electrochem **2002**;38:1505–6. doi:10.1023/A:1021637209564.
- [69] Streeter I, Thompson M, Compton RG. Linear sweep voltammetry at the tubular electrode: Theory of EC2 mechanisms. J Electroanal Chem **2006**;591:133–40. doi:10.1016/j.jelechem.2006.03.043.
- [70] Yuan Y, Wang L, Amemiya S. Chronoamperometry at micropipet electrodes for determination of diffusion coefficients and transferred charges at liquid/liquid interfaces. Anal Chem **2004**;76:5570–8. doi:10.1021/ac0493774.
- [71] Orazem ME, Tribollet B. *Electrochemical Impedance Spectroscopy*. **2008**. doi:10.1002/9780470381588.
- [72] S. Notari, C. Mancone, T. Alonzi, M. Tripodi, P. Narciso, P. Ascenzi, Determination of abacavir, amprenavir, didanosine, efavirenz, nevirapine, and stavudine concentration in human plasma by MALDI-TOF/TOF, J. Chromatogr. B. Anal. Technol. Biomed. Life Sci. **863 (2008)** 249-257.
- [73] Laborda E, Marti F. Electrocatalysis at Modified Microelectrodes: A Theoretical Approach to Cyclic Voltammetry ´ **2010**:14542–51.
- [74] Ates M. Review study of electrochemical impedance spectroscopy and equivalent electrical circuits of conducting polymers on carbon surfaces. Prog Org Coatings **2011**;71:1–10. doi:10.1016/j.porgcoat.2010.12.011.

- [75] Manohar AK, Bretschger O, Nealson KH, Mansfeld F. The use of electrochemical impedance spectroscopy (EIS) in the evaluation of the electrochemical properties of a microbial fuel cell. *Bioelectrochemistry* 2008;72:149–54. doi:10.1016/j.bioelechem.2008.01.004.
- [76] Hasanzadeh M, Karimzadeh A, Shadjou N, Mokhtarzadeh A, Bageri L, Sadeghi S, et al. *SC. Mater Sci Eng C* 2016. doi:10.1016/j.msec.2016.07.026.
- [77] L.A. Zanolli Filho, C.R. Galdez, C.A. Silva, M.F.M. Tavares, D.M. Costa, M.S.A. Prado, J. Brazil. *Chem. Soc.* 22 (2011) 2005-2012.
- [78] Nyoni S, Mugadza T, Nyokong T. Improved l-cysteine electrocatalysis through a sequential drop dry technique using multi-walled carbon nanotubes and cobalt tetraaminophthalocyanine conjugates. *Electrochim Acta* 2013. doi:10.1016/j.electacta.2013.10.023.
- [79] Heli H, Pishahang J. *Electrochimica Acta* Cobalt oxide nanoparticles anchored to multiwalled carbon nanotubes : Synthesis and application for enhanced electrocatalytic reaction and highly sensitive nonenzymatic detection of hydrogen peroxide. *Electrochim Acta* 2014;123:518–26. doi:10.1016/j.electacta.2014.01.032.
- [80] Bachhav SG, Patil DR. Synthesis and Characterization of Polyaniline-Multiwalled Carbon Nanotube Nanocomposites and Its Electrical Percolation Behavior 2015;5:90–5. doi:10.5923/j.materials.20150504.03.
- [81] "NEVIRAPINE" The american society of health-system pharmacists. Archived from the original on 20 december 2016.

- [82] Si, Y.; Samulski, E. T. Synthesis of Water Soluble Graphene. *Nano Lett.* 2008, 8 (6), 1679–1682.
- [83] Mugadza T, Arslano Y, Nyokong T. *Electrochimica Acta (II)*— Single walled carbon nanotube conjugate platforms and their use in electrocatalysis of amitrole 2012;68:44–51. doi: 10.1016/j.electacta.2012.02.041.
- [84] Siangproh W, Leesutthipornchai W, Dungchai W, Chailapakul O. Electrochemical detection for flow-based system: A Review. *J Flow Inject Anal* 2009; 26:5–25.
- [85] Research Journal of Pharmaceutical, Biological and Chemical Sciences for the detection of nevirapine Using GNRs modifiers electrodes. n.d.; 5:2091–105. Hargrave et al. at Boehringer Ingelheim.
- [86] B. Xiao, X. Li, B. Wang, C. Langford, R. Li, X. Sun, Graphene Nanoribbons Derived from the Unzipping of Carbon Nanotubes: Controlled Synthesis and Superior Lithium Storage Performance, *J. Phys. Chem. C* 118 (2014) 881–890.
- [87] B. Xiao, X. Li, B. Wang, C. Langford, R. Li, X. Sun, Graphene Nanoribbons Derived from the Unzipping of Carbon Nanotubes: Controlled Synthesis and Superior Lithium Storage Performance, *J. Phys. Chem. C* 118 (2014) 881-890.
- [88] Recent Advances in Graphene Based TiO₂ Nanocomposites (GNR/TiO₂) for Photocatalytic Degradation of Synthetic Dyes.
- [89] M. Shumba and T. Nyokong, “Electrode modification using nanocomposites of boron or nitrogen doped graphene oxide and cobalt (II) tetra aminophenoxy phthalocyanine

nanoparticles,” *Electrochim. Acta*, 196, 457–469, **2016**.

[90] Johra FT, Lee JW, Jung WG. Facile and safe graphene preparation on solution based platform.

J Ind Eng Chem **2014**;20:2883–7.

[91] Ayad MM, Salahuddin NA, Minisy IM, Amer WA. Chitosan/polyaniline nanofibers coating

on the quartz crystal microbalance electrode for gas sensing. *Sensors Actuators, B Chem*

2014;202:144–53.

[92]. C. Zhong, J. Wang, Z. Chen, and H. Liu: SnO₂–graphene composite synthesized via an

ultrafast and environmentally friendly microwave autoclave method and its use as a superior

anode for lithium-ion batteries. *J. Phys. Chem. C* 115(50), 25115 (2011).

[93] D. V. Kosynkin, A. L. Higginbotham, A. Sinitskii, J. R. Lomeda, A. Dimiev, B. K. Price, J.

M. Tour. *Nature*, 458(2009) 872.

[94] Paredes, J. I., Villar-Rodil, S., Martinez-Alonso, A., & Tascon, J. M. D. (2008).

Graphene oxide dispersions in organic solvents. *Langmuir*, 24(null), 10560.

[95]. J. I. Paredes, S. Villar-Rodil, A. Martinez-Alonso, and J. M. D. Tascon. Graphene oxide

dispersions in organic solvents. *Langmuir*, 2008, 24, 10560.

[96]. S. Saxena, T. A. Tyson, S. Shukla, E. Negusse, H. Chen and J. Bai. Investigation of structural

and electronic properties of graphene oxide. *Appl. Phys. Lett.*, 2011, 99, 013104.

[97] Eda, G., Y.-Y. Lin, C. Mattevi, H. Yamaguchi, H.-A. Chen, I. S. Chen, C.-W. Chen, and M.

Chhowalla, *Advanced Materials* 22, 505 (2010).

[98] G. Ramachandran, A.K. Hemanthkumar, V. Kumaraswami, S. Swaminathan, A simple and

rapid liquid chromatography method for simultaneous determination of zidovudine and nevirapine in plasma, *J. Chromatogr. B Anal. Technol. Biomed. Life Sci.* 843 (2006) 339-344.

[99] Manohar AK, Bretschger O, Neelson KH, Mansfeld F. The use of electrochemical impedance spectroscopy (EIS) in the evaluation of the electrochemical properties of a microbial fuel cell. *Bioelectrochemistry* **2008**; 72:149–54. doi: 10.1016/j.bioelechem.2008.01.004.

[100] Chang BYS, Huang NM, An'amt MN, Marlinda AR, Norazriena Y, Muhamad MR, CH, C. (2012). Facile hydrothermal preparation of titanium dioxide decorated reduced graphene oxide nanocomposite. *International Journal of Nanomedicine*, 7(1), 3379-3387. doi: <http://dx.doi.org/10.2147/IJNS28189>.

[101] M. Shumba and T. Nyokong, “Electrode modification using nanocomposites of boron or nitrogen doped graphene oxide and cobalt (II) tetra aminophenoxy phthalocyanine nanoparticles,” *Electrochim. Acta*, 196, 457–469, **2016**.

[102] Chi, J., Jayewardene, A.L., Stone, J.A., Aweeka, F.T. 2003. An LC-MS-MS method for the determination of nevirapine, a non-nucleoside reverse transcriptase inhibitor, in human plasma. *J. Pharm. Biomed. Anal.*, 31: 953-959.

[103] Eda, G. and M. Chhowalla, *Advanced Materials* 22, 2392 (2010)

[104] M. J. Kianoush Sarhangzadeh, Habib Razmi, Rahim Mohmmad-Rezaei, “Carbon Nanotube Composite Modified Carbon-Ceramic,” *Anal. Lett.*, 1–27, **2014**.

[105] Cui, R., Huang, H., Yin, Z., Gao, D., & Zhu, J. J. (2008). Horseradish peroxidase functionalized gold nanoparticle label for amplified immunoanalysis based on gold nanoparticles/carbon nanotubes hybrids modified biosensor. *Biosensors &*

- Bioelectronics, 23, 1666–1673.
- [106] Cao Q, Zhao H, Zeng L, Wang J, Wang R, Qiu X, He Y (2009) Electrochemical determination of melamine using oligonucleotides modified gold electrodes. *Talanta* 80:484–488.
- [107] Y. Ding, Y. Wang, L. Su, M. Bellagamba, H. Zhang and Y. Lei, *Biosens. Bioelectron.*, 2010, 26, 542–548
- [108] E. Masson, X. X. Ling, R. Joseph, L. Kyeremeh-Mensah, X.Y. Lu, *RSC Advances* 2 (2012) 1213-1247.
- [109] S.S. Kalanur, J. Seetharamappa, *Anal. Lett.* 43 (2010) 618-630.
- [110] S. Yang, R. Yang, G. Li, L. Qu, J. Li and L. Yu, *J. Electroanal. Chem.* 639, 77 (2010). doi:10.1016/j.jelechem.2009.11.025.
- [111] X. Gu, X. Li, S. Wu, J. Shi, G. Jiang, G. Jiang, S. Tian, *RSC Adv.* 2016, 6, 8070–8078.
- [112] C. Xu, F. Sun, H. Gao, J. Ang, *Anal. Chim. Acta.* 2013, 780, 20–27.
- [113] Esteva Guas, A.M., Balbin Tamayo, A.I., Piña Leite-vidal, J.J. 2014. Determination of nevirapine in the presence of cucurbit (7) uril with a gold electrode. *J. Electrochem. Sci. Eng.*, 4(1): 37-44.
- [114] B. Dogan-Topal, S. A. Sibel, B. Uslu, *The Open Chemical and Biomedical Methods Journal* 3 (2010) 56-73
- [115] Laviron, E. **1979**. General expression of the linear potential sweep voltammogram in the

- case of diffusionless electrochemical systems. *J. Electroanal. Chem.*, 101: 19-28.
- [116] Tan L, Zhou KG, Zhang YH, Wang HX, Wang XD, Guo YF, Zhang HL (2010) Nanomolar detection of dopamine in the presence of ascorbic acid at β -cyclodextrin/graphene nanocomposite platform. *Electrochem Commun* 12:557–660.
- [117] Jiang L, Ding Y, Jiang F, Li L, Mo F (2014) Electrodeposited nitrogen-doped graphene/carbon nanotubes nanocomposite as enhancer for simultaneous and sensitive voltammetric determination of caffeine and vanillin. *Anal Chim Acta* 833:22–28.
- [118] Spataru N, Sarada BV, Tryk DA, Fujishima A (2002) Anodic voltammetry of xanthine, theophylline, theobromine and caffeine at conductive diamond electrodes and its analytical application. *Electroanalysis* 14:721–728.
- [119] Hansen BH, Dryhurst G (1971) Electrochemical oxidation of theobromine and caffeine at the pyrolytic graphite electrode. *J Electroanal Chem* 30:407–416.
- [120] C.M.A. Brett, A.M.O. Brett, *Electrochemistry: Principles, Methods and Applications*, Oxford Science University Publications, Oxford 1993.
- [121]. Ma JY, Zhang YS, Zhang XH, Zhu GB, Liu B, Chen JH (2012) Sensitive electrochemical detection of nitrobenzene based on macro-/meso-porous carbon materials modified glassy carbon electrode. *Talanta* 88:696–700.
- [122] Maringa A, Mugadza T, Antunes E, Nyokong T. Characterization and electrocatalytic behaviour of glassy carbon electrode modified with nickel nanoparticles towards amitrole detection. *J Electroanal Chem* 2013; 700:86–92.

- [123] Liu, S., Zhang, C., Yuan, L., Bao, J., Tu, W., Han, M., Dai, Z. 2013. Component-controlled synthesis of small-sized Pd-Ag bimetallic alloy nanocrystals and their application in a nonenzymatic glucose biosensor. *Part. Part. Syst. Charact.*, 30(6): 549-556.
- [124] Shimada, T., Ookubo, K., Komuro, N., Shimizu, T. and Uehara, N. **2007**. Blue-to-red chromatic sensor composed of gold nanoparticles conjugated with thermoresponsive copolymer for Thiol sensing. *Langmuir*, 23(22): 11225-11232.
- [125] Teradal, N.L., Prashanth, S.N., Seetharamappa, J. **2012**. Electrochemical studies of nevirapine, an anti-HIV drug, and its assay in tablets and biological samples. *J. Electrochem.Sci. Eng.*, 2: 67-75.
- [126] Zhang, F., Li, L., Luo, L., Ding, Y. Liu, X. **2013**. Electrochemical oxidation and determination of antiretroviral drug nevirapine based on uracil-modified carbon paste electrode. *J. Appl. Electrochem.*, 43: 263-269.
- [127] Drake KF, Duyne RPVAN, Bond AM. Cyclic differential pulse voltammetry: a versatile instrumental approach using a computerized system 1978;89:231–46.
- [128] F. Zhang, L. Li, L. Luo, Y. Ding, X. Liu, Electrochemical oxidation and determination of antiretroviral drug nevirapine based on uracil-modified carbon paste electrode, *J. Appl. Electrochem.* 43 (2013) 263–269. doi:10.1007/s10800-012-0516-z.
- [129] Van Heeswijk, R.P.G., Hoetelmans, R.M.W., Meenhorst, P.L., Mulder, J.W., Beijnen, J.H. 1998. Rapid determination of nevirapine in human plasma by ion-pair reversed phase highperformance liquid chromatography with ultraviolet detection. *J. Chromatogr. B*, 713: 395-399.

[130] Y. Zhou, J. Zhi, X. Zhang, M. Xu, *Diam. Relat. Mater.* 20 (2011) 18-22.

[131] R.N. Goyal, N. Bachheti, A. Tyagi, A.K. Pandey, *Anal. Chim. Acta* 605 (2007) 34-40.

APPENDIX

APPENDIX A: MATERIALS

List A1: Apparatus used for the study

Volumetric flasks, Beakers, Spatula, Wash bottles, Funnels, Erlenmeyer flask, weighing crucibles, Buchner funnel, water bath, hot plate, measuring cylinders and micropipette.

Reagents and chemical

Name	Chemical formulae	Manufacturer	Concentration/mass
Distilled water	H ₂ O	MSU	10 ⁻⁷ M
Hydrochloric acid	HCl	ACE	0.1 M
Hydrogen peroxide	H ₂ O ₂	ACE	2 ml
Potassium ferricyanide	[Fe(CN) ₆] ^{-3/4-}	ACE	1 Mm
Sodium hydroxide	NaOH	Skylabs	0.1 M
Potassium dihydrogen phosphate	KH ₂ PO ₄ .2H ₂ O	Skylab's	15.604 g
Ethanol	C ₂ H ₅ OH	Skylabs	99 %
di-potassium hydrogen phosphate	K ₂ HPO ₄	Skylabs	14.201 g
Potassium bromide	KBr	ACE	1.0021 g

Potassium chloride	KCl	ACE	1 M
multiwall carbon nanotubes	MWCNT	ACE	100 mg
Sodium nitrate	NaNO ₃	ACE	75 mg
Potassium permanganate	KMnO ₄	ACE	450 mg
Sulphuric acid	H ₂ SO ₄	ACE	60 ml
Glucose	C ₆ H ₁₂ O ₆	ACE	18.0156 g
Nevirapine	(C ₁₅ H ₁₄ N ₄ O)	Skylabs	10693.171 mg

Table A. 2: Instrumentation

Name	Model	Manufacturer	Use
Analytical Balance	GA-110	OHAUS	Weighing
pH meter	Az-8601	OHAUS	pH measurement
PGSTAT	PGSTAT302F	Autolab	Electrocatalysis
Ultra-Sonicator	KQ-250B	China Corp	Ultra-agitation

Treatment of Glassware

Laboratory liquid soap was used for washing all the glassware and they were rinsed using distilled water to remove contaminants and impurities.

APPENDIX B: DATA TREATMENT

B1: Surface area

Constant $R = 8.314$, $T = 273$ K

Randle-sevick equation

$$I_p = (2.69 \times 10^5) n^{3/2} A D^{1/2} V^{1/2} C$$

$D = 7.6 \times 10^{-6} \text{ cm}^2/\text{s}$, $C = 1 \times 10^{-3} \text{ M}$, $m = 1 \times 10^{-5}$ and $A = 0.238 \text{ cm}^2$

Theoretical surface area

B2: Surface Coverage

$$n^2 F^2 R_{ct} A C$$

$$I_p = \frac{\quad}{4RT}$$

Where $R = 8.314 \text{ J mol}^{-1}$, $T = 293 \text{ K}$ (20 °C), $F = 9.6487 \text{ C/mol}$, $A_{\text{eff}} = 0.238$

cm^2 , $n = 2$, $R^2 = 0.67203$, $v = 400 \text{ mV/s}$, $I_{pa} = 2.87 \times 10^{-5}$

$$2.87 \times 10^{-5} = \frac{2 \quad (9.6487)^2 \times 0.238 \times \quad}{4 \times 8.314 \times 293} \times 400 = 1.58 \times 10^{-5} \text{ mol/cm}^2$$

Therefore, surface coverage is $1.58 \times 10^{-5} \text{ mol/cm}^2$.

B3: Tafel slopes

$E_{pa} = \log v + K$ where $b = \text{Tafel slope}$, and $v = \text{scan rate}$ and K is intercept $m = b/2$

Nevirapine, $m = 140$ mV/decade and glucose, $m = 226$ mV/decade

B4: Limit of detection and limit of quantification

Table B.1: Excel Liniest function

<i>Regression Statistics</i>		SE intercept	1.4334E-06				
Multiple R	0.998122314	SD intercept	3.5112E-06				
R Square	0.996248154	LOD	1.9312E-06				
Adjusted R Squar	0.995310192	LOQ	5.852E-06				
Standard Error	1.53977E-06	\sqrt{N}	2.44948974				
Observations	6	SLOPE	6				
ANOVA							
	<i>df</i>	<i>SS</i>	<i>MS</i>	<i>F</i>	<i>Significance F</i>		
Regression	1	2.51822E-09	2.51822E-09	1062.14178	5.28525E-06		
Residual	4	9.48355E-12	2.37089E-12				
Total	5	2.5277E-09					
	<i>Coefficients</i>	<i>Standard Error</i>	<i>t Stat</i>	<i>P-value</i>	<i>Lower 95%</i>	<i>Upper 95%</i>	<i>Lower 95.0%</i> <i>Upper 95.0%</i>
Intercept	3.21884E-05	1.43345E-06	22.45527353	2.3289E-05	2.82085E-05	3.61683E-05	2.82085E-05 3.61683E-05
X Variable 1	5.99788E-05	1.84038E-06	32.5905167	5.2852E-06	5.48691E-05	6.50885E-05	5.48691E-05 6.50885E-05

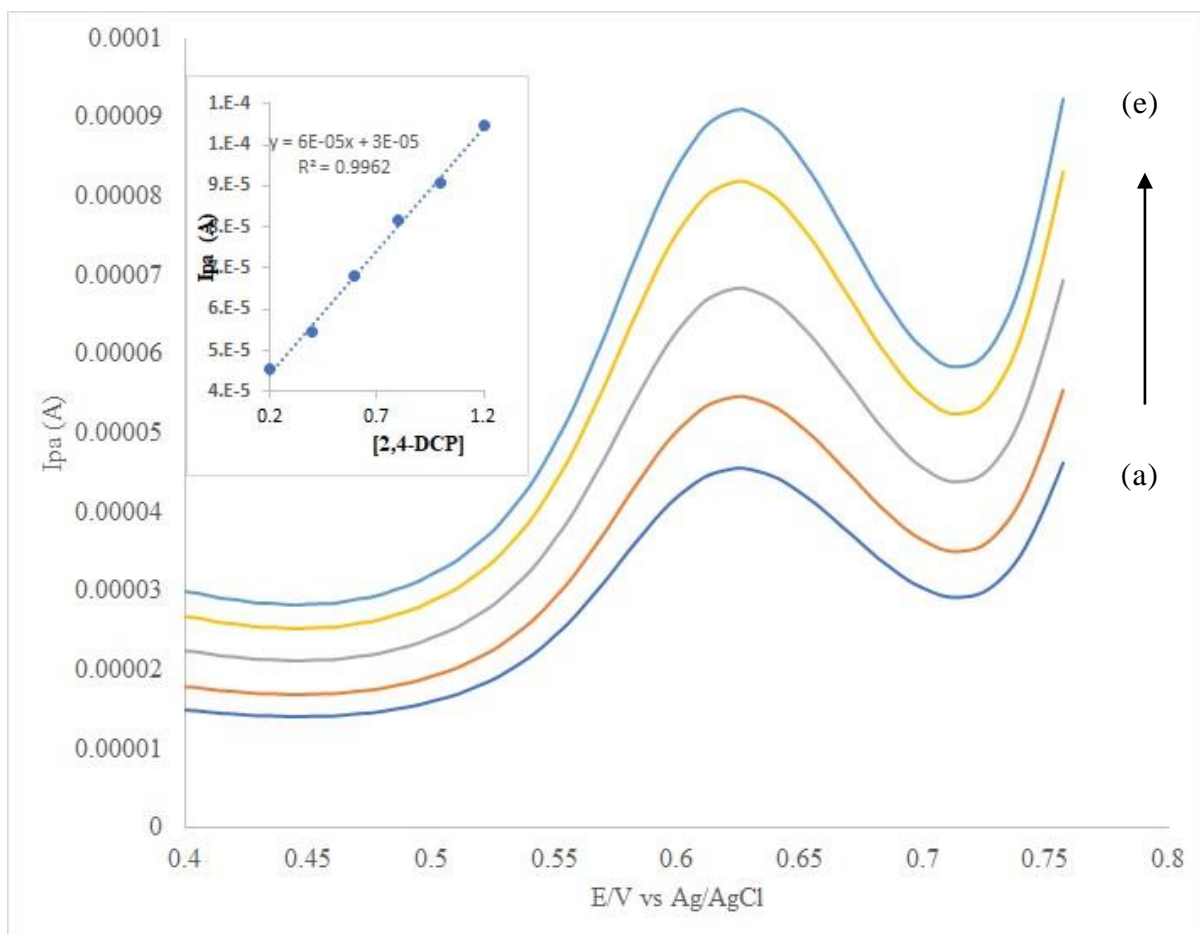
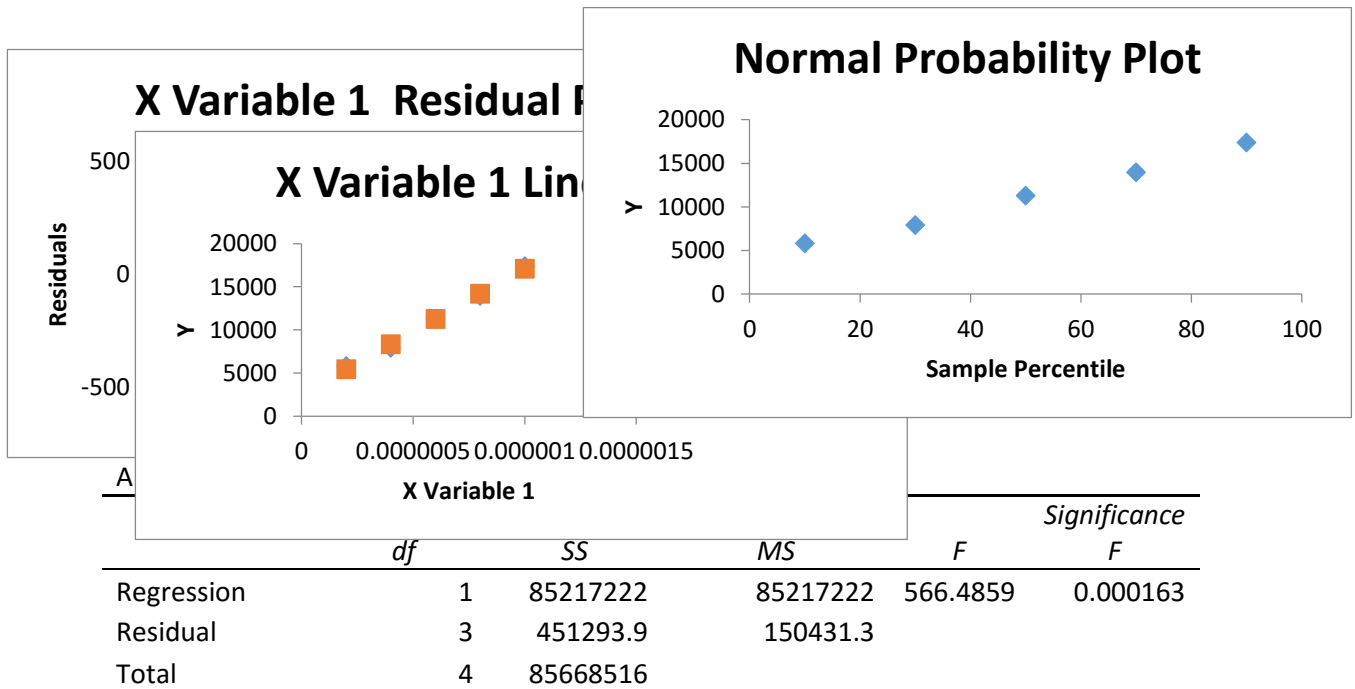
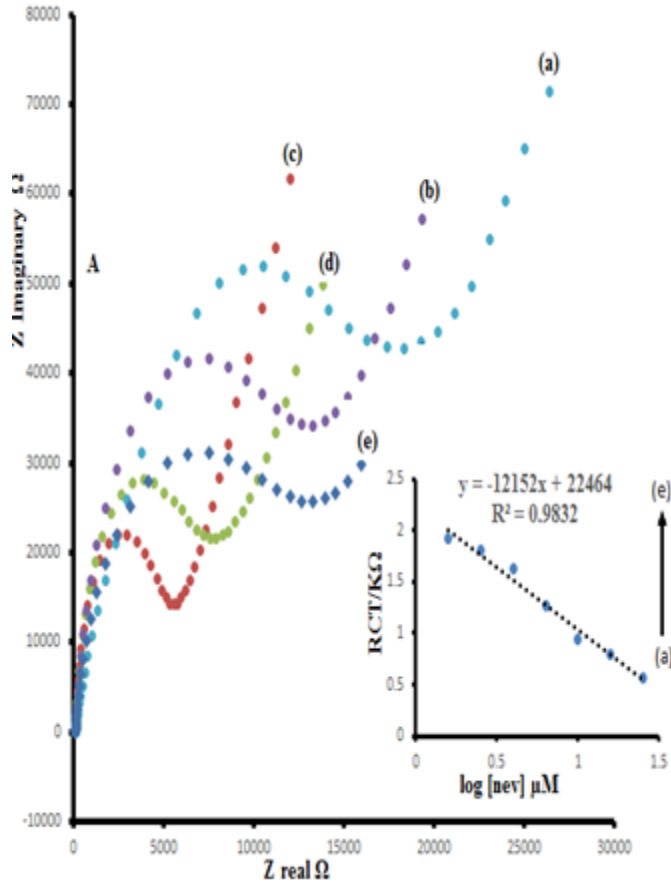


Figure 4.21: DPV for rGO/Mn₂O₃:Co₃O₄GCE in: (a) 0.2 mM, (b) 0.4 mM, (c) 0.6 mM,



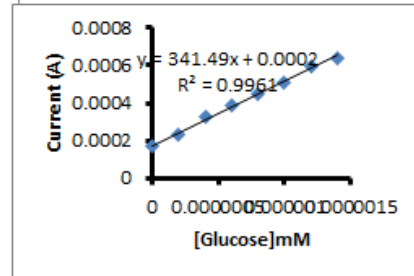
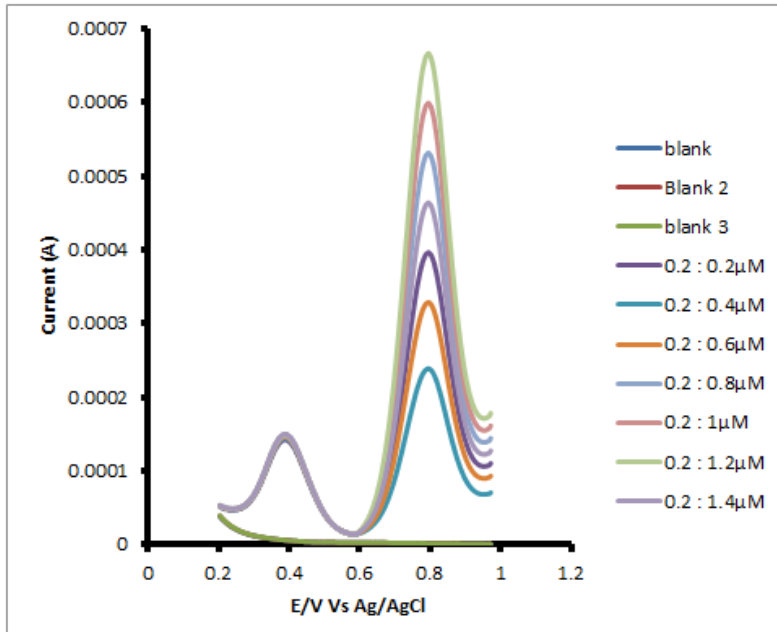
	Coefficients	Standard Error	t Stat	P-value	Lower 95%	Upper 95%
Intercept	2507.215	406.7855	6.163481	0.008596	1212.642	3801.788
X Variable 1	1.46E+10	6.13E+08	23.80097	0.000163	1.26E+10	1.65E+10

RESIDUAL OUTPUT

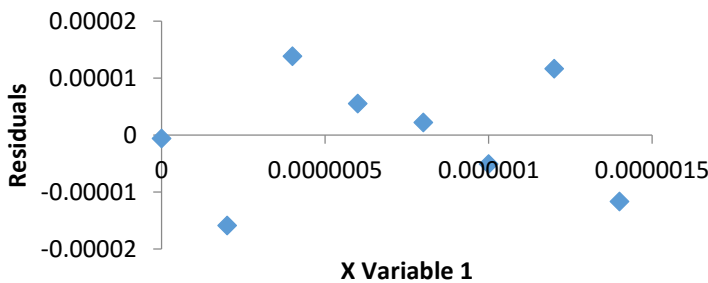
Observation	Predicted Y	Residuals	Standard Residuals
1	5426.414	367.5264	1.09418
2	8345.613	-430.204	-1.28078
3	11264.81	29.2356	0.087039
4	14184.01	-237.963	-0.70845
5	17103.21	271.4058	0.808015

PROBABILITY OUTPUT

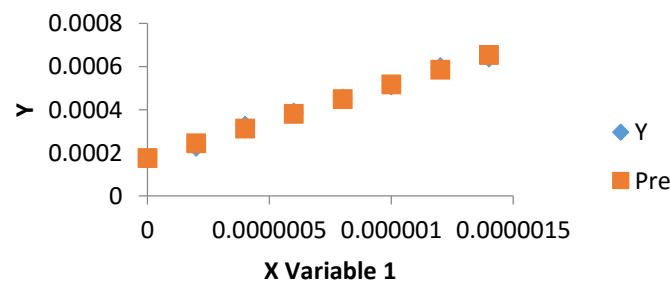
Percentile	Y
10	5793.94
30	7915.408
50	11294.05
70	13946.05
90	17374.62



X Variable 1 Residual Plot



X Variable 1 Line Fit Plot



<i>Regression Statistics</i>	
Multiple R	0.998025
R Square	0.996054
Adjusted R Square	0.995396
Standard Error	1.14E-05
Observations	8

ANOVA

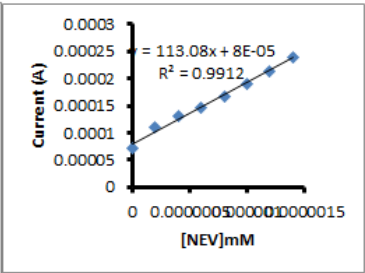
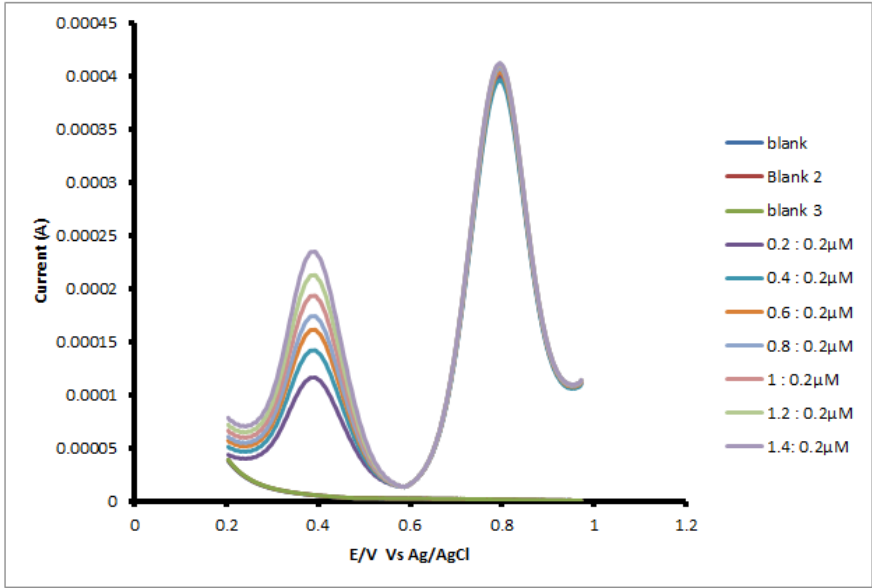
	<i>df</i>	<i>SS</i>	<i>MS</i>	<i>F</i>	<i>Signifi</i>
Regression	1	1.95912E-07	1.96E-07	1514.479	1.9
Residual	6	7.76155E-10	1.29E-10		
Total	7	1.96688E-07			

	<i>Coefficients</i>	<i>Standard Error</i>	<i>t Stat</i>	<i>P-value</i>	<i>Lower</i>
Intercept	0.000176	7.34164E-06	23.9161	3.51E-07	0.0
X Variable 1	341.4881	8.774934777	38.91631	1.92E-08	320

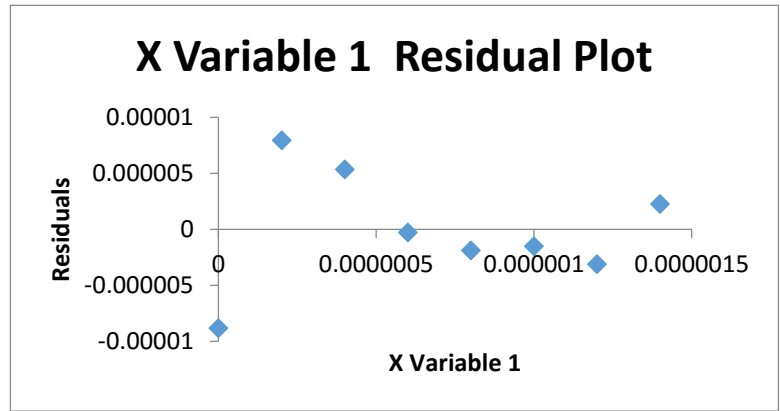
7.09466E-08 LOD
2.1499E-07 LOQ

RESIDUAL OUTPUT

<i>Observation</i>	<i>Predicted Y</i>	<i>Residuals</i>	<i>Standard Residuals</i>
1	0.000176	-5.8333E-07	-0.0554
2	0.000244	-1.5881E-05	-1.50817
3	0.000312	1.38214E-05	1.312586
4	0.00038	5.52381E-06	0.524582
5	0.000449	2.22619E-06	0.211416
6	0.000517	-5.0714E-06	-0.48162
7	0.000585	1.1631E-05	1.104562
8	0.000654	-1.1667E-05	-1.10795



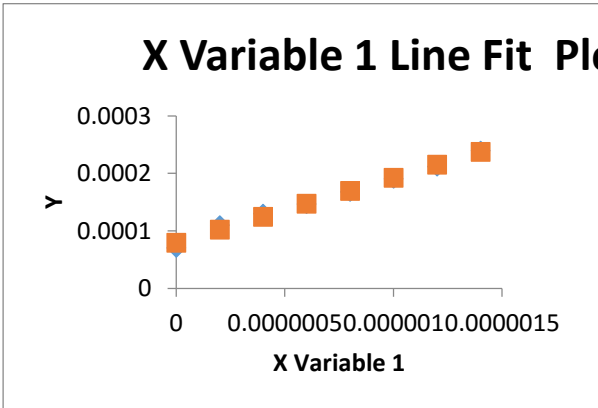
SU



MMARY OUTPUT

<i>Regression Statistics</i>	
Multiple R	0.995595
R Square	0.991209
Adjusted R Square	0.989744
Standard Error	5.64E-06
Observations	8

ANOVA



	<i>df</i>	<i>SS</i>	<i>MS</i>	<i>F</i>	<i>Significa</i> <i>F</i>
Regression	1	2.14836E-08	2.15E-08	676.494	2.13
Residual	6	1.90543E-10	3.18E-11		
Total	7	2.16741E-08			

	<i>Coefficients</i>	<i>Standard</i> <i>Error</i>	<i>t Stat</i>	<i>P-value</i>	<i>Lower</i>
Intercept	7.94E-05	3.63761E-06	21.83213	6.03E-07	7.05
X Variable 1	113.0833	4.347770517	26.0095	2.13E-07	102.4

1.06153E-07 LOD

3.21675E-07 LOQ

RESIDUAL OUTPUT

<i>Observation</i>	<i>Predicted Y</i>	<i>Residuals</i>	<i>Standard</i> <i>Residuals</i>
1	7.94E-05	-8.8167E-06	-1.68988
2	0.000102	7.96667E-06	1.526964
3	0.000125	5.35E-06	1.02543
4	0.000147	-2.6667E-07	-0.05111
5	0.00017	-1.8833E-06	-0.36098
6	0.000193	-1.5E-06	-0.2875
7	0.000215	-3.1167E-06	-0.59737
8	0.000238	2.26667E-06	0.43445